

THREE-DIMENSIONAL ANALYSIS OF A REACTOR FOR  
THE PRODUCTION OF II-VI MATERIALS USING  
CFD COMMERCIAL CODE FLUENT

By

ZELJKO NIKOLIC

Bachelor of Science

Oklahoma State University

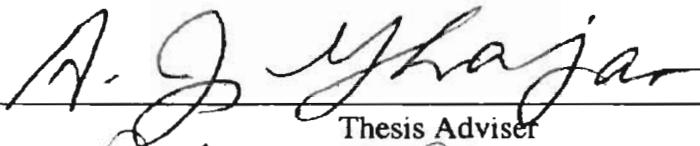
Stillwater, Oklahoma

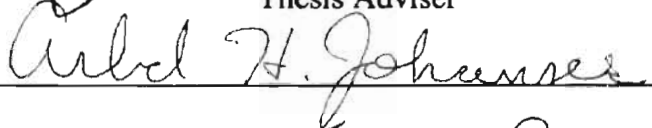
1997

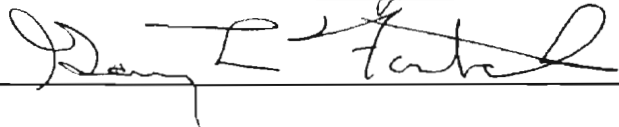
Submitted to the Faculty of the  
Graduate College of the  
Oklahoma State University  
in partial fulfillment of  
the requirements for  
the Degree of  
MASTER OF SCIENCE  
May, 2000

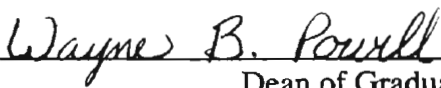
THREE-DIMENSIONAL ANALYSIS OF A REACTOR FOR  
THE PRODUCTION OF II-VI MATERIALS USING  
CFD COMMERCIAL CODE FLUENT

Thesis Approved:

  
\_\_\_\_\_  
Thesis Adviser

  
\_\_\_\_\_

  
\_\_\_\_\_

  
\_\_\_\_\_  
Dean of Graduate College

## ACKNOWLEDGEMENTS

I would like to express very special gratitude and appreciation to my graduate advisor, Dr. Afshin Ghajar. His guidance, patience and dedication were great help in enduring and successfully completing this research. The words of encouragement he provided in difficult moments will never be forgotten. The other professors associated with the research project, Dr. A. H. Johannes and Dr. Gary Foutch, deserve thanks for the guidance and input throughout.

My colleagues and friends enhanced the experience of working on this project. Brent Foster deserves special mention as a colleague and a friend throughout undergraduate and graduate study. His work also represented a basis of the modelling for the research presented in this thesis. I would also like to thank Trey Morrison and Chris Shay for providing insight into the chemistry of reaction as well as helping acquire experimental data used. Derek Ligon and Srdjan Jankovic are special friends who provided social distractions in my life.

I would like to thank Janet Smith for always having a kind word of advice or just time to listen. Tom Potts and others at Eagle Picher Inc. deserve mention for granting the opportunity and help for the duration of the project. Financial assistance provided by Oklahoma State University, The Oklahoma Center for Advancement of Science and Technology, and Eagle-Picher Technologies, Inc. is greatly appreciated.

I am forever grateful to my family for providing the opportunity to come to Oklahoma State University and complete my degree. My parents, Gordana and Laza Nikolic, continuously provided emotional as well as financial help in my life. My grandparents also deserve thanks for always being there for me. Katica and Albin Starc and Mara Nikolic gave unlimited love and support to my decisions. My other family deserves special appreciation for their guidance and encouragement. Bonnie and Don Muegge and their family provided home away from home. They are always going to be special in my heart. My girlfriend, Davorka Vucetic, gave me her unlimited support and love. My brother, Zvonko Nikolic, deserves recognition for words of encouragement and sense of humor that makes life brighter.

## TABLE OF CONTENTS

Chapter	Page
I. INTRODUCTION .....	1
1.1 Semiconductor Industry Background .....	1
1.2 Overview of Eagle-Picher Process.....	3
1.3 Objectives .....	5
II. LITERATURE REVIEW .....	7
2.1 Introduction.....	7
2.2 Chemical Vapor Deposition.....	8
2.3 Production of II-VI Chemicals.....	10
2.4 Applications of II-VI Materials .....	13
2.5 CFD Modeling .....	16
2.5.1 Reactive Flow and Computational Fluid Dynamics .....	19
2.5.2 FLUENT Modeling.....	25
2.5.3 Chemical Vapor Deposition Modeling Using Fluent CFD Package	32
2.5.4 Other CFD Codes.....	33
III. RESEARCH AND OPTIMIZATION OF THE CURRENT SYSTEM.....	36
3.1 Introduction.....	36
3.2 Current Process Description .....	37
3.3 Process Analysis .....	42
3.4 Thermocouple Set Up .....	44
3.5 Design of Experiments and Results .....	51
IV. FLUENT CFD PACKAGE.....	54
4.1 Introduction.....	54
4.2 CFD Package .....	55
4.3 Planning CFD Analysis.....	57
4.4 GeoMesh .....	58

Chapter	Page
4.4.1 DDN .....	59
4.4.2 P-Cube.....	60
4.4.3 Leo .....	61
4.4.4 TGrid.....	61
4.5 FLUENT/UNS .....	63
4.5.1 Mass Conservation Equation .....	63
4.5.2 Momentum Conservation Equation .....	63
4.5.3 Turbulence Modeling.....	64
4.5.4 Energy Equation.....	66
4.5.5 Buoyancy Effects .....	68
4.5.6 Chemical Species Transport .....	69
4.5.7 Mass Diffusion Coefficients .....	70
4.5.8 FLUENT/UNS Numerical Scheme.....	72
4.5.9 Pressure-Velocity Coupling .....	74
4.5.10 Residuals and Convergence .....	76
V. FLUENT 3D MODEL .....	78
5.1 Introduction.....	78
5.2 Fluent 5 Model Development .....	79
5.3 Convergence .....	83
5.4 Presentation and Comparison of Results .....	88
VI. CONCLUSIONS AND RECOMMENDATIONS .....	106
REFERENCES .....	109
APPENDIX A REACTOR DIMENSIONS AND TEMPERATURE DATA.....	116
APPENDIX B FLUENT COMPUTATIONAL FLUID DYNAMICS MODEL DOCUMENTATION .....	123
B.1 Procedure for Creating the Geometry .....	124
B.1.1 Start GeoMesh.....	124
B.1.2 Start DDN.....	125
B.1.3 Create Points .....	125
B.1.4 Create a Line Between Two Points .....	126
B.1.5 Create Cylindrical Surface .....	126
B.1.6 Create Surface at the Entrance of the Tube.....	127
B.1.7 Blank the Points and the Lines.....	127
B.1.8 Convert the Surfaces to B-Splines Surfaces.....	128
B.1.9 Find the Intersection Between the Surfaces .....	128
B.1.10 Create Trimmed Surface .....	129
B.1.11 Save and Exit DDN.....	130

Chapter	Page
B.2 Domain Topology .....	130
B.2.1 Copy the Part and Start P-Cube.....	130
B.2.2 Set the Model Type .....	131
B.2.3 Create the First Face.....	131
B.2.4 Rubberband the Edges to the Cylinder.....	132
B.2.5 Create the Sub-Face Inside the Intersection.....	133
B.2.6 Pre-Selecting Objects .....	135
B.2.7 Specify a Uniform Node Distribution .....	135
B.2.8 Specify the Boundary Types .....	137
B.2.9 Removing Interior Walls.....	139
B.2.10 Interpolate the Grid .....	139
B.2.11 Load the Leo with the Domain Files.....	140
B.2.12 Display a Report of Skewness.....	140
B.2.13 Starting Over in P-Cube .....	141
B.2.14 Mouse Button Functions .....	142
B.2.15 Function Keys .....	143
B.2.16 Write Out the TGrid Grid File.....	144
B.2.17 TGrid .....	144
B.3 GAMBIT Geometry and Topology Procedure.....	148
B.3.1 Geometry Creation Steps in GAMBIT.....	149
B.4 FLUENT 5 Model .....	156
B.4.1 Grid Scale .....	156
B.4.2 FLUENT Settings.....	157
B.4.3 Creating Material Properties .....	164
B.4.3.1 Copying a Material from the Database .....	164
B.4.3.2 Modifying Properties of an Existing Material.....	165
B.4.3.3 Creating a New Material .....	165
B.4.4 Setting Physical Properties.....	165
B.4.5 Initializing and Solving Process.....	171
B.4.6 Save the Case and Data File (run.cas, run.dat).....	173
B.4.7 Postprocessing.....	173
B.4.7.1 Display Velocity Vectors on Cross-Section of the Duct.....	173
B.4.7.2 Display the Vectors at the Desired Cross-Section .....	173
B.5 Transport and Physical Properties.....	174
APPENDIX C COMPUTATIONAL DATA.....	181

## LIST OF TABLES

Table	Page
2-1    Microelectronic Unit Operations .....	8
3-1    Design of Experiments: Factor of Study.....	51
5-1    Default Convergence Criteria used within FLUENT .....	84
5-2    Typical Residual Values for Default and Reduced Under-Relaxation Factors	85
5-3    Yield Results for Various Cases .....	91
5-4    Result Comparison with 2D Pre-exponential Factor Value.....	93
A-1    Tube Dimensions .....	122
B-1    Lennard-Jones Parameters .....	176
B-2    Heat of Formation Properties.....	178
B-3    Specific Heat Values.....	179
B-4    Quartz Properties for FLUENT .....	179
B-5    Thermochemical Data for $\text{Se}_2(\text{g})+2\text{Zn}(\text{g})=2\text{ZnSe}(\text{g})$ .....	180
C-1    Case BA97202 Process Characteristics .....	182
C-2    Case BA97195 Process Characteristics .....	183
C-3    Computational Study Data .....	184



## LIST OF FIGURES

Figure	Page
3-1 Current Eagle-Picher Reactor .....	37
3-2 ZnSe Run Yield (February 1996 through June 1997).....	43
3-3 Cross-Section of the Thermocouple Data Acquisition Set Up .....	47
3-4 Temperature Data Acquisition Set Up.....	48
4-1 Program Interactions for FLUENT/UNS and RAMPANT Software Packages	56
4-2 GeoMesh Session Manager.....	58
4-3 DDN User Interface .....	59
4-4 P-Cube User Interface.....	60
4-5 Overview of the Solution Process.....	73
5-1 Residual Pattern for Baseline Model – Default Under-Relaxation.....	86
5-2 Residual Pattern for Baseline Model – Reduced Under-Relaxation.....	87
5-3 Gravity Effects Excluded.....	89
5-4 Reactor Inlet Affected by Laminar Flow .....	89
5-5 Reactor Inlet Effects (Turbulence Model) .....	90
5-6 Pre-exponential Factor Variation Effects on Yield.....	95
5-7 Pre-exponential Factor Variation Effects on Yield (Flow Rate Case).....	97
5-8 Pre-exponential Factor Variation Effects on Yield (Temperature Case)....	99

Figure	Page
5-9 Velocity Vectors Colored by Concentration of Zn ( $\text{kg/m}^3$ ).....	102
5-10 Velocity Vectors Colored by Concentration of $\text{Se}_2$ ( $\text{kg/m}^3$ ).....	103
5-11 Velocity Vectors Colored by Concentration of ZnSe ( $\text{kg/m}^3$ ).....	104
5-12 Velocity Vectors Colored by Static Temperature.....	105
A-1 Reactor Inlet.....	117
A-2 Thermocouple Collar Readings and Furnace Readings for Reactor Zone 1 ZnSe Synthesis: Experimental Run 1, July 8, 1997.....	118
A-3 Thermocouple Collar Readings and Furnace Readings for Reactor Zone 2 ZnSe Synthesis: Experimental Run 1, July 8, 1997.....	119
A-4 Furnace and Boiler Temperature Profiles ZnSe Synthesis: Experimental Run 2, July 10, 1997.....	120
A-5 Thermocouple Collar Readings and Furnace Readings for Reactor Zone 1 ZnSe Synthesis: Experimental Run 4, July 14, 1997.....	121
B-1 Start Modals Panel .....	131
B-2 Bunch Panel .....	136
B-3 Boundary Conditions Panel .....	138
B-4 Boundary Nodes Panel.....	146
B-5 Init/Mesh Controls Panel .....	146
B-6 GAMBIT Graphical User Interface (GUT) .....	148
B-7 Create Coordinate System Panel.....	150
B-8 Create Real Cylinder Panel.....	151
B-9 Split Volume Panel .....	151

Figure	Page
B-10 Subtract Real Volume Panel .....	152
B-11 Specify Continuum Types Panel .....	153
B-12 Specify Boundary Conditions Panel .....	154
B-13 Mesh Volumes Panel.....	155
B-14 Final Mesh Imported to FLUENT.....	155
B-15 FLUENT Solver .....	156
B-16 Scale Grid Panel .....	157
B-17 Solver Panel.....	158
B-18 Viscous Panel .....	159
B-19 Species Panel.....	160
B-20 Radiation Model Panel .....	160
B-21 Multiphase Model Panel.....	161
B-22 Operating Conditions Panel .....	161
B-23 Outflow Boundary Conditions Panel .....	162
B-24 Zn Velocity Inlet Boundary Condition Panel.....	162
B-25 Se <sub>2</sub> Velocity Inlet Boundary Condition Panel.....	163
B-26 Wall Boundary Condition Panel .....	164
B-27 Species Panel.....	166
B-28 Reaction Setting Panel .....	167
B-29 Polynomial Profile for CP for Se <sub>2</sub> .....	168
B-30 Polynomial Profile for CP for ZnSe.....	169
B-31 Quartz Properties Panel.....	170

Figure	Page
B-32 Residual Monitor Panel.....	172
B-33 Iterate Panel .....	172

## NOMENCLATURE

### English Letters

A	Area, $\text{m}^2$ , or pre-exponential factor, $\text{m}^3/\text{kmol}\cdot\text{s}$
$C_p$	Specific heat at constant pressure, $\text{J}/\text{kg}\cdot\text{K}$
$E_a$	Activation energy, $\text{J}/\text{kmol}$
eV	Electron-volt
g	Acceleration due to gravity, $\text{m}/\text{s}^2$
Gr	Grashof number, dimensionless
H	Enthalpy, kcal, J
$\Delta H_{\text{reaction}}$	Heat of reaction, $\text{J}/\text{kmol}$
k	Rate constant, $\text{m}^3/\text{kmol}\cdot\text{s}$ , or turbulent kinetic energy, $\text{m}^2/\text{s}^2$
$\kappa$	Thermal conductivity, $\text{W}/\text{m}\cdot\text{K}$
Kn	Knudsen number, dimensionless
m	Mass of species, kg
M	Molar weight, $\text{kg}/\text{kmol}$
N	Avogadro's number, $6.022\text{E}+23$ molecules/mol
P	Pressure, Pa
Pr	Prandtl number, dimensionless
R	Ideal gas constant, $8314 \text{ J}/\text{kmol}\cdot\text{K}$

Ra	Reyleigh number, dimensionless
Re	Reynolds number, dimensionless
Sc	Shmidt number, dimensionless
$S_m$	Source Term
T	Temperature, K
$T_m$	Melting temperature, K
$T_{min}$	Minimum temperature, K
$T_{max}$	Maximum temperature, K
V	Velocity, m/s

#### Greek Letters

$\alpha$	Thermal diffusivity, $m^2/s$
$\beta$	Thermal expansion coefficient, $1/K$
$\Delta$	Change in
$\varepsilon$	Maximum energy of interaction between two molecules, erg
$\varepsilon$	Turbulence dissipation rate, $m^2/s^3$
$\nu$	Kinematic viscosity, $m^2/s$
$\kappa$	Boltzmann constant, $1.30E-16$ erg/K
$\mu$	Dynamic viscosity, Pa-s
$\rho$	Density, $kg/m^3$
$\sigma$	Molecule collision diameter, m
$\sigma$	Characteristic diameter, Å
$\Omega_\mu$	Collision integral parameter, dimensionless

## Abbreviations

2D	Two-dimensional
3D	Three-dimensional
CDROM	Compact disc read-only-memory
CFD	Computational Fluid Dynamics
CVD	Chemical Vapor Deposition
CVT	Chemical Vapor Transport
DOE	Design of Experiments
EP	Eagle-Picher Inc.
FIDAP	Fluid Dynamics Analysis Package
g	Gas Phase
LED	Light Emitting Diode
LPCVD	Low Pressure Chemical Vapor Deposition
MBE	Molecular Beam Epitaxy
MOCVD	Metalorganic Chemical Vapor Deposition
PDF	Probability Density Function
PVT	Physical Vapor Transport
RNG	Renormalization Group
s	Solid phase
SIMPLE	Semi-Implicit Method for Pressure-linker Equations
XRD	X-ray diffraction

## **CHAPTER I**

### **INTRODUCTION**

#### **1.1 Semiconductor Industry Background**

Eagle Picher Inc. future needs will consist of placing greater emphasis on understanding large and complex systems of importance, in contrast to studying simpler, well-defined systems that give neater and more intellectually satisfying answers. For example, a basic understanding of chemical synthesis reaction processes currently used at Eagle Picher Inc. requires input from many different fields, such as thermodynamics, chemical kinetics, heat transfer, transport phenomena, atomic and molecular physics, etc. Current reaction process is somewhat of an unknown and great amount of scientific effort has been attracted to design suitable models in such a way that complex phenomena, and the parameters which control it, become available for future experimentation and research.

Semiconductor industry faces increasing pressure to decrease the cost and time of converting a new idea into a marketable product. Long-term development projects may be affected by the changes in economic conditions. For example, a new production process for the large volume chemical may seem very profitable when the idea originates. This profitability may be affected by economic changes during the development period, such as raw materials or demand for the product. In today's economy, as the profitable



lifetime of manufacturing processes becomes shorter, it is more difficult to justify initial over design into increased future capacity, and the premium on precise design becomes higher. Therefore, there is a strong need to bypass or compress the development stages, which is done by using computer simulations and computational fluid dynamics. This type of development is specially emphasized in chemical industry, which used to go through pilot-plant stage before binding decisions on plant design were made. Eagle Picher Inc. and Oklahoma State University chose computational simulations as the mean for achieving short and long term goals of the research project.

Eagle Picher Inc. and Oklahoma State University research team experienced change in demand of the final product during the research project. During initial stages of research, besides gaining knowledge on the present system, new reactor proposal was required in order to build a pilot reactor for prediction of results. Changes in market demand caused the initial pilot reactor plans to be substituted by the computational fluid dynamics design, based on the present reactor improvements.

The data requirements for this type of modeling exercises include broad spectrum, but the most common ones are diffusion, thermal conductivity and viscosity. Since the development of new processes often involves compounds of materials whose properties have not been directly measured, reliable estimation techniques become very important. The accuracy requirements on transport data are still one gray area. Complete data is very important in studying the interrelations, which arise from within the set of transport properties. On the other hand, in some engineering calculations such as presented in this work, the highly accurate data are not essential because the limiting factor is within the model used or purity of materials. It is very important to strive for the best accuracy

possible without unreasonable effort on time consumption. Information on transport properties for this research was completely unknown when the project started.

In the planning of experimental measurement programs, greater emphasis should be placed on accurate, comprehensive measurement on a few key substances. The industrial interests in specific material tend to change fast and chances of finding data needed on a new material are small. The data obtained from key related substances may become adequate for immediate need. Key substances identified in the project were temperature, input flow rates and product yield.

Mixture properties require many measurements and grow rapidly with the number of species involved. Experimental set up to map out all the possibilities would be expensive and time consuming. Usually, the small and accurate set of measurements is sufficient to develop further correlation methods and connect them with the properties of pure species. The correlation methods used to relate mixture properties were available through various options included in the computational commercial code used.

Chemical Vapor Deposition (CVD) is commonly used method to deposit thin films or layers on substrates. This process has wide applications in the microelectronic industry for the fabrication of solid state devices. The production of high quality devices with uniform properties requires efficient control and manipulation of the flow field and associated transport process within the CVD reactor. The understanding of the complex interactions between the flow field, heat and mass transfer and chemical reactions can be significantly enhanced through accurate models.

## **1.2 Overview of Eagle-Picher Process**

Eagle-Picher Inc. (EP) has been operating, for nearly fifty years, a laboratory-scale facility for the production of II-VI materials. As a result of this laboratory-scale operation, basic understanding of the chemistry and the reaction mechanism involved in the production of these compounds were acquired through trial and error process. Reactant flow rate, boiler and reactor temperatures, and loading have been determined by the yield results of the reaction. However, due to the high temperature and long-residence times encountered in the reactor, the specific operating conditions have not been quantified adequately.

EP and Oklahoma State University committed time and resources to analyze, optimize and design a chemical reactor for synthesis of II-VI materials. This type of reactor is an aerosol flow reactor – flow of the vapor phase particles enters the reactor zone where the condensable product is formed. Reactants are introduced to the reactor by the inert carrier gas at low mass flow rates (less than  $1\text{E-}04$  kg/s). The product is mainly deposited on the reactor floor, although part of the product may be in the form of convection rolls created along the reactor ceiling and walls. In the present system, it takes around three days to synthesize the product and prepare the reactor for the next run. This is due to the lengthy steps in the set-up and breakdown process described in Chapter III.

The main drawback of the current reactor system is the lack of reliability and reproduction of the results. Current process has a failure rate of around 25% and cost of waste materials estimated at over \$50000 annually. The cause of unexpected results of low yields (average of 54.2% for successful runs only) and high percent of run failure is

connected to the lack of knowledge about exact values of process parameters, and hence lack of the process control. Operators experience weights heavily on the success of the each process run.

The commercial potential for a full-scale process is very significant. The commercial demand for the product shifted toward more efficient and larger scaled process of production. The demand for these chemicals is growing dramatically, due to advanced technology in microelectronics industry. These II-VI materials are key components in high-tech semiconductor and microelectronics industry.

The optimization process of the current reactor became the primary focus of the research due to the scale back of the estimated market demand of the product. Initially, it was estimated that the market demand could consume 100 times current production of II-VI compounds in innovative research and application. Change in the direction of the semiconductor industry affected this number to fall down from 100 fold to 2, for product used mainly for EP needs. Due to this change of focus, computational fluid dynamics (CFD) became integral part of the optimization process. CFD was carried out using commercial code FLUENT available at the university through the Department of Mechanical and Aerospace Engineering.

Zinc selenide was the material of choice for computational purposes.

### **1.3 Objectives**

The objective of this research was to help understand and explain from the scientific point of view the commercial process for the production of cadmium and zinc selenides and sulfides. The process used for the production of zinc and cadmium

selenides can also be used to make other Group II-VI chemicals. The long term goals were to understand chemical reaction kinetics, mass-transfer limitations and operating parameters, and propose a new chemical reactor design to successfully manufacture significantly larger quantities of these materials. The new design basis would be information received from experimental and numerical parts of the research.

The specific objectives of this work are as follows:

1. Evaluate the operation of the current reactor design through the experimental set up and at the same time obtain information for reference and starting point of computational process.
2. Identify the key heat distribution and temperature control features of the reactor and develop methods to achieve reproducible high-temperature performance. The most important product criterion is that the cadmium selenide and zinc selenide produced meet the required physical and chemical property specifications.
3. Optimize the current chemically reacting system by varying governing parameters in FLUENT commercial code, through a three-dimensional (3D) numerical model and draw a comparison with two-dimensional (2D) model developed by Foster (1999).
4. Document procedures used to simulate the process in FLUENT commercial CFD code, to provide the reference for future chemically reacting flow work.

While the work of Shay (1998) and Morrison (1998) concentrated on the design of the new reactor, Foster (1999) and this study concentrated on simulating phenomena inside the reactor. Foster (1999) concentrated on duplicating experimental results using 2D modeling, meanwhile, using 3D modeling was the focus of this work.

## **CHAPTER II**

### **LITERATURE REVIEW**

#### **2.1 Introduction**

The purpose of this chapter is to relate information on chemical vapor deposition (CVD), production methods of II-VI chemicals and their application. Once the relationship was established, a goal was to describe computational fluid dynamics (CFD) and relate it to chemical vapor deposition. The chemical vapor deposition process was used to produce materials at Eagle-Picher Inc. (EP). The main purpose of this study was to simulate conditions and results studied at EP using CFD.

First part of this chapter contains introduction to chemical vapor deposition and a review of production methods for II-VI materials. The importance of these materials in modern electronics is explained in the following section. Different applications in modern semiconductor industry are also discussed. Fourth section of this chapter introduces computational fluid dynamics. The extensive research was done on importance of CFD, different approaches, as well as FLUENT modelling examples available for reference. The parallel between experimental and numerical parts of the research is drawn. Further, reactive flows were analyzed using various CFD methods. After general CFD application on reactive flows and CVD flows, FLUENT modelling is

described using benchmark problems and applications directly related to the work done for this project. Finally, few other commercial CFD codes are mentioned.

## **2.2 Chemical Vapor Deposition**

Processing of electronic materials from electronic and opto-electronic devices combines a fascinating variety of physical transport processes and chemical reactions that raise new challenges to reaction engineering. Chemical vapor deposition and plasma processing of thin films are emphasized as areas where reaction engineering has significant impact. As a result of the reaction engineering processes, microelectronic industry has undergone an impressive evolution to the current state. Almost all aspects of modern life are based on microelectronic circuits, although the first transistor was introduced less than sixty years ago.

New device structures and high levels of integration are goals met by scientists and engineers, resulting in rapid growth and development of the microelectronic industry. Fabrication of microelectronic components involves a variety of complex chemical processes summarized in Table 2.1.

Table 2-1. Microelectronic Unit Operations (Jensen, 1987)

<u>Unit Operation</u>	<u>Examples</u>
Bulk Crystal Growth	Czochralski, floating zone, Bridgman
Liquid Phase Epitaxy (LPE)	
Physical Vapor Deposition (PVD)	Evaporation, molecular beam epitaxy (MBE), sputtering
Chemical Vapor Deposition (CVD)	Low pressure CVD, organ metallic CVD, laser CVD
Doping	Diffusion, ion implementation
Oxidation	
Resist Processing	Coating, baking, development
Plasma Processing	Plasma enhanced chemical vapor deposition (PECVD), Plasma etching
Packaging	Encapsulation, bonding
Substrate Cleaning	

Chemical reaction engineering theories are important for chemical vapor deposition and plasma processing. These theories are based on the high purity of starting materials, as well as the products. Impurities on the ppm level may drastically affect the performance of devices. This tendency is advantageous for analysis, but has some practical disadvantages.

Chemical vapor deposition is the key process in chemical reaction engineering analysis. In this process, chemically reacting gasses are used to synthesize a thin solid film. Complex flow fields, intricate gas phase chemistry and high temperatures are related to those found in combustion. The type of chemical reactions in CVD distinguishes it from the physical vapor deposition methods like sputtering and evaporation. CVD reactions are usually supplied by thermal energy, although photons and electric discharges (plasmas) can also be used. CVD processes operate under wide range of temperatures and pressures. Atmospheric pressures and slightly reduced pressures ranging from 10 to 100 kPa are used for epitaxial films and single semiconductors. Low pressure CVD (LPCVD) is used for polycrystalline production at approximately 100 Pa.

CVD kinetics is essential to reactor modeling. The objective of reactor modeling is to relate performance measures such as film deposit rates, uniformity and composition, with operating conditions like temperature, pressure and reactant concentration. Due to the high temperatures and low pressures used in CVD, gas rate constants may not be used directly. Wall effects of heat and mass transfer are primary concerns, but pressure dependence may have significant impact. According to the classical Lindemann theory (Laidler, 1965), the rate of formation of products has the following form:



$$rate = \frac{k_1 k_2 P_A^2}{k_1 P_A + k_2} \quad (2-1)$$

where  $P_A$  is the partial pressure of the reactant. From the relation, reaction is first order in the high-pressure limit, but becomes second order at low pressures. Although this theory predicts change of order as pressure is lowered, it cannot be used to estimate rate parameters. Jensen (1987) also suggests other theories as more accurate estimates for the rate of formation.

### **2.3 Production of II-VI Chemicals**

The production of cadmium and zinc selenides falls into the general category of II-VI chemistry. These two are of primary interest for Eagle-Picher Inc. Other reactions of interest in this classification include the production of cadmium and zinc sulfides and tellurides. Kucharczyk and Zabłudowska (1986) present a review of the alternative methods used to make II-VI chemicals.

If a reaction takes a place in a system in which there is only one component material undergoing crystallization, then the growth of crystal under such conditions is called one-component crystallization. The process of the monocrystal growth is a heterogeneous reaction of the following types:

- Solid  $\rightarrow$  crystal (solid, recrystallization, sintering, polymorphous transition)
- Liquid  $\rightarrow$  crystal (Verneul method, zone melting, cooling of nucleus, drawing)
- Gas  $\rightarrow$  crystal (sublimation-condensation, evaporation)

Multi component (there is a large concentration of admixture, crystallizing material arises as a result of chemical reaction) crystallization occurs as following:

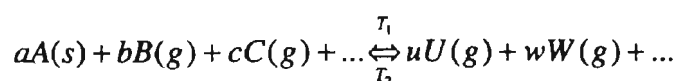
- Growth by reversible reactions due to changes in temperature or concentration

- Growth by irreversible reactions (epitaxial growth)

The single component crystallization methods are used to purify and crystallize existing II-VI compounds. The starting material is in its final compound form, but its physical structure is not in the desired crystalline form. The transport in the gas phase may be either dynamic or static. In the dynamic method, inert gas is used as carrier gas and it was first used by Frerichs (1947) to obtain CdS in the form of platelets and needles. Static method is based on diffusion in the gas phase and was first used by Reynolds and Czyzak (1950). Later, Greene et al. (1958) and Piper and Polich (1961) updated the reaction system. They found that the growth conditions have crucial effect on the quality and size of the crystals. The optimum conditions such as temperature gradient, velocity of moving the ampoule, dimensions and shape of the ampoule, its purity, composition and pressure of gases introduced to the reactor as well as initial substances were selected experimentally. Most important conclusion of their study was that longer residence time and decomposition of vapor in the hot crystallization zone improve the quality of product.

Clark and Woods (1968) compared the monocrystals obtained from the horizontal and vertical position. They noticed defects in the form of empty spaces in the crystals obtained from the vertical furnace. They were associated with large temperature gradients or fast movement of the ampoule. These depended upon the cooling method of the ampoule – fast process by removing the ampoule from the furnace, and slow process by leaving the ampoule in the cooling furnace. The horizontal method was assumed to have more uniform product characteristics due to slow velocity allowing extra diffusion time. Some other experiments were explored for production of ZnSe and they did not show the dependence on the velocity of the ampoule.

Nietsche (1971) used the newest technique for production first. The gas of the solid material is transported using carrier substance from the areas with different temperatures. This is the method of a heterogeneous reversible reaction leading to the formation of gaseous products according to the following reaction:



This chemical transport reaction has temperatures chosen such that at  $T_1$  reaction proceeds at the right, and at  $T_2$  to the left. The most difficult task is choosing a transport substance such that the transporting chemical reaction creates large differences of pressures at low differences of temperatures. The main advantage was that the crystallization took place at considerably lower temperatures. For example, iodine transport method lowered temperature to 750°C from the sublimation temperature of 1300°C.

Bottcher et al. (1996) investigated influence of convection on zinc selenide single crystal growth by chemical vapor transport. It is reported that the crystal quality strongly deteriorated for Rayleigh number values of 4000 and larger. Mackowski et al. (1996) reports that heat transfer in the crystal and deposition on the walls affect the rate and the uniformity of crystal growth.

Murakami et al. (1992) studied compositional profile dependence on the nozzle configuration in  $Hg_{1-x}Cd_xTe$  growth using metal organic chemical vapor deposition (MOCVD) system having multi nozzle injectors. The profile of the epilayer from two nozzles was the same as the summation of the two profiles produced with one nozzle.

Large, high quality HgCdTe wafers are required for the next generation of two-dimensional infrared detector arrays. Takigawa et al. (1992) observed the metal organic chemical vapor deposition (MOCVD) with the use of linearly aligned multi-nozzles.

Bottcher and Hartmann (1995) looked at the wide-bandgap II-VI compounds, which are promising materials for blue-light emitting diodes and laser diodes. ZnSe single crystals have been grown from the vapor phase by dissociative sublimation and chemical vapor transport (CVT) in sealed ampoules. For CVT growth of ZnSe single crystals with iodine transport as an agent, it was found, that crystallographic perfection and morphological stability are strongly related to rate limiting mechanisms for mass and heat transport. In contrast to seeded physical vapor transport ( $T > 1150\text{ }^{\circ}\text{C}$ ) and high-pressure melt grown ( $T > 1580\text{ }^{\circ}\text{C}$ , system pressures up to 100 atm) free growing (without contact to the ampoule wall), relatively large ZnSe crystals have been prepared by low temperature CVT growth. These crystals showed morphological stability, reduced strain, no detectable twinning, grain boundaries, stacking faults, and structural disorder.

## **2.4 Application of II-VI Materials**

Group II-VI materials produced at Eagle-Picher are base materials used by research personnel for the fabrication of green and blue Light Emitting Diodes (LED). A major research effort is underway at Eagle-Picher to commercialize LED's and develop green and blue laser diodes. If successful, this research will develop into valuable market commodity. The market demand would require Eagle-Picher to produce basic II-VI

materials to be used for the fabrication of crystals and wafers. These crystals and wafers are used for production of the electronic devices.

Group II-VI compounds are interesting to the semiconductor industry because of their optical and electrical properties, in particular photoluminescence and electroluminescence (e.g. Leung et al., 1991). Another area of interest is to use these materials for the production of hydrogen gas from solar cells (e.g. Babu et al., 1995). The production is quite complex since even minor changes in the synthesis process can produce a wide range of polycrystalline and monocrystalline compounds. A primary concern in these formulations is the deviation from 1:1 stoichiometric ratio of metal to selenium in crystal composition.

The optical and electrical properties of these materials impacted many research directions. One of those research areas is application of these materials for photoconductive switching utilizing wide-bandgap materials such as diamond and zinc selenide. Photoconductive switching utilizing these materials has the advantage of high power handling capabilities. One of the high voltage photoconductive switches utilizing polycrystalline ZnSe was investigated in the research of Cho et al. (1994). ZnSe is a direct bandgap semiconductor with a relatively large bandgap of 2.67 eV at 300 K. Recent experiments with photoconductive switching in polycrystalline ZnSe showed that this material has the potential for efficient high-power switching in opening and closing modes of operation. Operation of the switches at electric fields up to 100 kV/cm showed that bandgap shifts became important and significantly changed the performance of the photoconductive switch. The ZnSe model switch was capable of duplicating the power gain results obtained from commonly used GaAs switch. ZnSe did not require fast

modulation of the laser pulse, which was necessary for GaAs substrate. Wenisch et al. (1996) also compared different substrate materials for production of LED's. ZnSe multi-quantum-wells in ZnSe grown by the Molecular Beam Epitaxy (MBE) were superior to GaAs substrates based on X-ray diffraction (XRD), transmission electron microscopy (TEM), and electro-optical measurements.

Yu et al. (1992) were the pioneers in observing blue stimulated emission from a semiconductor laser structure. They reported the shortest wavelength ever generated by a semiconductor laser diode to be at 475.4 nm (2.606 eV).

Zinc selenide and its related alloys  $\text{Zn}_{1-x}\text{Cd}_x\text{Se}$ ,  $\text{ZnS}_y\text{Se}_{1-y}$ , and  $\text{Zn}_{1-x}\text{Mg}_x\text{S}_y\text{Se}_{1-y}$  are wide bandgap semiconductors, which are important for application in compact disc read-only-memories (CD ROM's) and high-definition video displays through the use of blue-green light emitting diodes and lasers. In the work of Healy and Ayers (1993), CdZnSe ohmic contact is proposed for use in laser diode structure allowing continuous operation of blue-green lasers at higher temperatures than currently achieved and extending the lifetime of the device. Current market trend is use of blue lasers fabricated by MBE. The major drawbacks of these lasers are their large forward voltage drops (15 – 30 V) and excessive power dissipation.

Huang et al. (1996) reports zinc selenide to be one of the most promising materials for optoelectronic devices due to recent progress in making light emitting and laser diodes. There has also been considerable interest in using this material in the production of high power optical switches and photodetectors. ZnSe exhibits high defect density due to its weak ionic atomic bonding, resulting in a high recombination rate both in the bulk material and at the surface, making difficult production of high quality

switches and photodetectors. They managed to produce a high-quality metal-semiconductor-metal photoconductive detector on ZnSe grown by MBE with low response time (2.3 ms).

In the study done by Min-Yen (1996), ZnSe epilayers have been grown by low pressure photo-enhanced MOCVD. The growth rate, crystallinity, and optical properties were improved by using laser irradiation. In this case the growth rate and quality were improved with increasing laser density. This type of photo-enhanced technique has potential to obtain high-quality epilayer of ZnSe at a lower growth temperature.

ZnSe crystals grown using High Pressure Bridgman technique were used to fabricate solid-state radiation detectors in the work of Eissler and Lynn (1995). From II-VI semiconductors, only cadmium telluride (CdTe) and cadmium zinc telluride (CdZnTe) have been developed as practical, room temperature, solid state radiation detectors. Zinc Selenide (ZnSe), with a band gap of 2.7 eV, compared to CdTe at 1.47 eV should have potential to operate at lower bias currents and higher temperatures ( $25 < T < 160$  °C). The application would find use in x-ray and  $\gamma$ -ray detectors.

## **2.5 CFD Modeling**

Since the processes under consideration have such an overwhelming impact on semiconductor industry and modern day technology, we should be able to deal with them effectively. This ability can result from an understanding of the nature of the processes and from methodology with which to predict them quantitatively. The prediction of behavior in a given physical situation consists of the values of the relevant variables governing the processes of interest.

The most reliable information about a physical process is often given by actual measurement. An experimental investigation involving full-scale equipment can be used to predict how identical copies of the equipment would perform under the same conditions. The actual measurement approach was used for the purpose of gathering data for the modeling of the II-VI chemical reactor during this research.

A theoretical prediction works out the consequences of a mathematical model, rather than those of an actual physical model. For the physical processes of interest here, the mathematical model mainly consists of differential equations. If the methods of classical mathematics were to be used for solving these equations, there would be little hope of predicting many phenomena of practical interest.

Advantages of the numerical simulations are obvious. Some of the most important advantages are:

- Low cost (computer run time vs. experiment; increasing importance as the physical situation to be studied becomes larger and more complicated)
- Speed (may study the implications of hundreds of different configurations and choose the optimum design)
- Complete information (can provide values of all relevant variables: velocity, pressure, temperature, concentration, turbulence intensity throughout the domain of interest)
- Ability to simulate realistic conditions (in theory, it is easy to simulate large or small dimensions, in treating high or low temperatures, following very fast or very slow processes)



- Ability to simulate ideal conditions (prediction method is being used sometimes to study basic phenomenon, in which one wants to focus attention on a few essential parameters and eliminate all irrelevant features).

There are also certain disadvantages associated with modeling process:

- If the prediction has a very limited objective, it may not be cheaper than experiment
- Uncertainty about the extent to which the computed results would agree with reality, in such, the experimental backup is highly desirable.

Based on the listed advantages and disadvantages of the numerical results, the question that one may ask is what is the need for prediction? There is no doubt that experiment is the only method for investigating a new basic phenomenon. In this sense, experiment leads and computation follows. It is in the synthesis of a number of interacting known phenomena that the computation performs more efficiently. Even then, sufficient validation of the computed results by comparison with experimental data is required.

Hilgenstock and Ernst (1996) concluded that the information received by numerical simulation was much more extensive than that in experimental investigation. The same can be said for EP synthesis process and simulations done to verify experiments. Today's CFD codes are relatively easy to use and robust. The field of application ranges from simple two-dimensional isothermal flows to complex three-dimensional unsteady flows with combustion. The advantage of CFD in relation to experiments is that the simulation is in many cases much cheaper. It also yields information on the complete flow field inside the domain of interest.

Hilgenstock and Ernst (1996) raised and answered the following questions:

- What can we learn from CFD that we do not get from experiments?
  1. In contrast to the experiment, CFD predicts flow disturbances in pipe systems and installation effects as a complete three-dimensional flow field.
  2. The phenomenological structure of the flow is clearly visible in the CFD solution.
  3. The decay process of flow disturbances can be investigated in detail.
- Is the accuracy of the numerical solution acceptable?
  1. Numerical data agree very well with experimental findings for advanced turbulence models.
  2. CFD is good and effective basis to investigate installation effects and flow disturbances since the numerical results agree with the accuracy of real testing experiments.
- Is it possible to replace experiments?

In the near future, it will be impossible to replace experiments by CFD simulations, but the experiments and CFD must supplement each other.

### **2.5.1 Reactive Flows and Computational Fluid Dynamics**

According to Cinnela (1996), reactive flows can be defined as fluid flows that are significantly affected by chemical reactions (e.g., combustion, dissociation, and biochemical processes) and/or thermodynamic nonequilibrium (e.g., vibrational excitation). Reaction kinetics has strong impact on the flow fields inside EP chemical reactor for production of II-VI chemicals. Practical applications of reactive fluid flows can be found easily in every day life, from car engines to heating systems to blood circulation in living beings. Common to all these applications is the intermediate

coupling between fluid dynamics, chemistry, and physics. The “computer age” has affected the way engineers and scientists approach these problems, including a third investigative tool, computer simulation, in addition to the traditional means of theoretical and experimental studies.

Significant progress has been made towards accurately simulating reactive flows due to the dramatic increase in computational capabilities in recent years. This task is particularly complicated because it requires major advances in two areas, computational fluid dynamics and physical modeling. Each area has own challenges, and must be closely coupled to reproduce the physical reality. Using very simple physics (incompressible fluids or ideal gases), CFD researchers have been able to simulate fluid flows over or inside extremely complicated geometries. On the other side, by using very simple geometries, many complex physical problems have been investigated. The present challenge is to combine geometrical and physical complexity to achieve realistic simulations that can improve the basic understanding of reactive, nonequilibrium fluid flows.

The accurate simulation of reactive flows has benefited from significant advances in the quality of CFD simulations. Some of the useful developments are preconditioning schemes for the efficient simulation of low-speed reactive flows and adaptive gridding, which allows the major flow features to be accurately detected and tracked with significantly smaller computational resources than more traditional approaches. FLUENT/UNS encompasses these developments.

Gobbert et al. (1997) discusses the simulation of semiconductor manufacturing processes and its importance in recent years. It is considered to be an integral tool in

development and evaluation of processes and equipment. The traditional simulation models include:

- reactor scale simulators, which solve the equations that govern the species and energy transport with chemical reactions throughout the reactor chamber.
- feature scale simulators, which solve the equations that govern the species transport and reaction inside one or more features in order to predict the surface growth due to the surface reactions.

Reactor scale models have been used to evaluate proposed reactor geometries in order to reduce the number of prototypes needed. Feature scale models on the other hand have been used successfully to predict the evolution of the film profiles and compositions inside features as functions of operating conditions, thus narrowing the operating window before test runs are performed. In general, reactor scale and feature scale have been used independently. Feature scale models require information regarding local species fluxes and temperature, which are generally inaccessible to measurement. One way to supply them is to use a reactor scale simulator to first predict the conditions throughout the reactor chamber based on macroscopic quantities like reactor set points. In this approach, a feature scale model could be used at each boundary node of the reactor model, which is assumed to lie inside a patterned region of the wafer. This two-scale approach makes the assumption that the reactor scale simulator is able to compute conditions above a particular feature entrance, though its mesh is coarse compared to the typical dimension of a feature scale simulator.

A mesoscopic scale model and corresponding simulator have been introduced in order to model transport and reaction in the small region above the wafer surface to the

scale of few millimeters. The mesoscopic scale model has been designed to provide information on a length scale models as well as an enhanced interface between those traditional models. This three-scale simulator couples numerical meshes whose typical mesh sizes are separated by fewer orders of magnitude than in two scale models.

Tehver et al. (1998) discusses thermal walls in computer simulations. The physical effects associated with the two different types of thermal walls used in numerical simulations are considered. Two types of surfaces considered for walls were a perfectly smooth surface and a highly uneven, low-density granular surface. When the molecule strikes the perfectly smooth surface, it is specularly reflected. When a molecule strikes granular surface, it undergoes a series of collisions within the surface with different surface molecules, and therefore its escape velocity is uncorrelated with its initial velocity. The velocity of these molecules was calculated using the temperature of the wall. This type of wall is called thermal type in literature. Two types of walls found in literature are reflective and thermal walls. The reflective boundaries assign reversed normal component of the molecule, while the tangential component remains the same. In general, the importance of wall effects is great within one mean free path of molecules. Therefore, use of correct boundary conditions is more important for systems whose characteristic size is small when compared to the mean free path (the Knudsen number  $Kn \geq 1$ ).

The chemical vapor deposition of polycrystalline zinc selenide in a vertical rectangular reactor is numerically simulated on the basis of the three-dimensional transport equations for low Mach number flows and reported by Garibin et al. (1996). The results obtained suggest two different regimes of mass transfer. Also, the influence

of carrier gas flow rate on the process efficiency and the uniformity of deposited layers are analyzed. The properties of CVD-layers are highly dependent on process conditions such as pressure, gas flow and susceptor temperature. The variation in temperature presented a need to take into account change of gas properties with temperature (density, viscosity, thermal conductivity, and specific heat). As a result of varying the flow rate of the carrier gas (Ar), conclusion was that among the process parameters considered in the flow pattern, it is mostly controlled by the flow rate of Ar. There were two different regimes depending upon the magnitude of parameters. The first one is characterized by the formation of the reverse flow in the vicinity of the susceptor, while the recirculation takes place in the second case around the central inlet. Also, the most uniform distribution of mass flux to the susceptor surface is likely at the flow rate values within narrow limits. The transfer coefficients were calculated through the application of kinetic theory using the values of Lennard Jones parameters ( $\sigma$ , collision diameter, and  $\epsilon/k$ , molecule interaction energy). Same method is used within FLUENT/UNS for work done in this thesis.

The effects of radiative heat transfer on the upper wall temperature in a horizontal CVD reactor is studied in detail by Kadinski et al. (1995). Numerical simulations of heat transfer in the horizontal reactor have shown that the upper wall temperature varies about 40-70 K depending on the type of the wall and emissivity of the susceptor. Even such small temperature variations can significantly affect the wall deposition, and consequently highly accurate heat transfer calculations are required for an optimization of the process. Quartz walls are characterized by a specular reflection of radiation and the emittance of specular and diffusive walls can differ essentially. The formation of

deposits on the reactor walls is another factor, which could cause the diffuse character of reflection.

Kobayashi and Yoda (1987) discuss modified  $k$ - $\varepsilon$  model in a straight pipe. Their modified model included reconsideration of eddy viscosity, revaluation of the  $\varepsilon$  equation and consideration of the assumption of isotropic turbulence.

Low-speed flow in pipes with varying cross-sections were analyzed by Uehigashi et al. (1992). They used central finite differencing with explicit method of lines generated by Runge-Kutta scheme to simulate three-dimensional compressible Navier-Stokes equations in cartesian coordinates.

Krishnan and Zhou (1995) developed a computational model for CVD in complex reactor configurations. The general features of the model include comprehensive sub models for component transport based on kinetic theory of gases, provisions for arbitrary number of finite gas phase and surface reactions and full coupling of the physical models with general purpose multi-block CFD code based on Body-Fitted-Coordinates formulation.

The unsplit explicit and implicit-explicit methodologies have been successfully extended to treat stiff, nonequilibrium, chemically reacting flow fields in the paper of Krispin and Glaz (1996). The results of the study show that the extended implicit-explicit method has the capability of producing high-resolution computations, the convergence was satisfactory, and new stiff solver handled more difficult problems than nonstiff solver.

Several other authors modeled chemical vapor deposition processes. Durst et al. (1995) used a multigrid numerical method to study radiation heat transfer and epitaxial

growth in metal organic CVD reactors. The mathematical model implemented was used for two dimensional laminar low Mach number flows and mass transfer. Liu et al. (1991) analyzed effects of substrate temperature and inlet pressure on growth rate in the organometallic vapor-phase epitaxy of cadmium telluride. The effects of change in growth rates for different substrates were discussed. Angermeier et al. (1997) investigated horizontal rapid thermal chemical deposition reactor. Three-dimensional numerical simulation was used to determine growth rates under mass transport limitations in terms of gas phase supersaturation and the impact it may have on surface morphology.

### **2.5.2 FLUENT Modeling**

FLUENT capabilities have been documented through various benchmark problems and actual numerical solutions. While examples of different problems are presented in this section, Chapter IV is dedicated to explaining the code itself. From personal experience, trial and error method worked exceptionally well in working out small problems faced within the solver. Choudhury (1993) uses two problems as candidate benchmark problems for validating CFD codes. One of them was three-dimensional forced convection in an array of protruding elements. Both laminar and turbulent flows are encountered in this problem, similar to the flow inside EP reactor that is mostly laminar, but has few turbulent regions. This problem is solved using Fluent, which has sophisticated turbulence models (e.g.  $k-\epsilon$ , Reynolds Stress and renormalization group models); multiphase models, chemical reaction models, and radiation heat transfer calculation methods. These are accessible to users through an interactive, menu driven interface for problem definition, computation, and post processing. The complete form



of the Navier-Stokes or Reynolds-averaged Navier-Stokes equations is discretized using a finite volume scheme in which the conservation equations are integrated in each control volume. Convective terms are discretized using the power law scheme of Patankar (1980). Central differencing is used for the diffusion terms. Backward-Euler differencing is adopted for the temporal discretization. The Boussinesq approximation is invoked to evaluate the variation of fluid density with temperature, where density is assumed to vary linearly with temperature. Note that Boussinesq approximation can not be used with species calculation, combustion or reacting flows. The equivalent conductivity,  $k_{eq}$ , is simply a measure of enhanced heat transfer due to natural convection, relative to heat conduction. Thus,  $k_{eq}$  is directly proportional to the heat removal rate.

Two unique features of FLUENT were utilized in this benchmark problem. First, a streamwise periodic boundary condition is used in which the flow pattern and scaled temperature field is assumed to repeat from module to module. The second feature of FLUENT utilized is the renormalization group (RNG) turbulence model. The RNG model is suitable for accurately modeling transitional and separated turbulent flows as well as turbulent flows with heat transfer. This turbulence method has been shown to be capable of superior predictions of flow fields, temperature fields and localized transfer phenomena compared with standard turbulence models. For instance, prediction of hot spots and local heat transfer coefficients can be made reliably with the RNG model. RNG method was used for modeling in this work.

Choudhury (1995) continued to work with Fluent, and concluded that variable viscosity flows are commonly encountered in many practical situations. Turbulent flows can have large effective viscosity variations, sometime with several orders of magnitude

change. Large variations of viscosity can pose problems to a CFD code, both in terms of convergence difficulties due to additional non-linearity and large property variations as well as reduced accuracy due to improper interpolation schemes. There are three things considered. First, finite volume schemes are known to suffer from stability problems when large body forces (such as buoyancy) are encountered. Special techniques are employed in FLUENT that guarantee stability and accuracy comparable to the best-staggered schemes. Second, a special algorithm is used to handle the body forces implicitly, ensuring that convergence rates are enhanced for large Rayleigh numbers. Third, special care is taken in handling variable viscosity elements. The variation of viscosity with temperature is expressed as a sequence of three linear functions of temperature for each Rayleigh number.

Hilgenstock and Ernst (1996), using standard turbulence models, reached reasonable agreement with experimental data. The use of advanced turbulence model improves the agreement drastically but needs far more computer resources. Today's CFD codes are relatively easy to use and robust. Within FLUENT, different turbulence models are available with various advantages and disadvantages. The most widely used turbulence method is the  $k-\epsilon$  model, which is robust and requires few additional computer resources. On the other hand it is well known that the  $k-\epsilon$  model is inappropriate at least for separated and vortical flows. The more sophisticated models like the RNG models or the Reynolds stress models are much more complex and CPU-time consuming, but have several advantages compared to the  $k-\epsilon$  model in predicting separated and vortical flow phenomenon. When solving partial differential equations, boundary conditions of different types are needed. For pipe flows these are the wall boundary conditions, which

are easy to define, and the inlet and outlet conditions. The inlet condition is of major importance for the flow simulation because the inlet profile determines the flow inside the pipe completely. There are several possibilities to define the inlet profile in the pipe. The easiest way is to define a constant velocity, but this will not necessarily represent the flow situation in the pipe. Defining a fully developed profile is a better choice, but still there may be differences between the experimental setup and numerical inlet condition. If the objective is to compare experimentally collected data with numerical simulation data, the best way to define the inlet velocity in a pipe is to use an experimental result. Based on the experimental results obtained for the composition of the inlet flow, inlet conditions were assigned in the modeling process of this research.

Authors conclude that CFD is a powerful tool to investigate installation effects. The agreement with experimental data is very good when using fine meshes and advanced turbulence models. On the other hand, basic flow phenomena can be calculated on coarse meshes and with the help of simple turbulence models in an overnight computer run.

Oseid et al. (1994) presented a benchmark backward facing step for the fluid flow and heat transfer. According to the authors, turbulence modeling determines the quality of numerical solutions. Most popularly used turbulence models are two equation models using turbulent kinetic energy ( $k$ ) and its dissipation rate ( $\epsilon$ ) incorporated with various wall functions. Also discussed is a new approach of turbulence modeling called Renormalization Group (RNG) method. This method allows a new  $k$ - $\epsilon$  model to be derived, and it has become accepted practical engineering turbulence model. The RNG based  $k$ - $\epsilon$  modeling is superior because its constants are obtained explicitly from theory.

Also, derived  $k$ - $\epsilon$  method includes an extra term in the  $\epsilon$  equation, which is a function of the mean rate of strain. Finally, it provides a differential relationship between turbulent Reynolds number ( $k/(\nu_0 \epsilon)^{0.5}$ ) and the ratio of effective viscosity to molecular viscosity, which account for low Reynolds number effects. RNG also relates turbulent and effective viscosities.

Brasoveanu and Gupta (1994) examine fuel and air mixing resulting from turbulence caused by different inlet configurations in an axisymmetric combustor with axial inlets. Radial velocity turbulent intensity was the most important factor affecting fuel and air mixing. Radial velocity turbulent intensity should have high values in the inlet area in order to promote the mixing. Important conclusion was that fluctuation in the axial velocity had negligible impact on the mixing inside the combustor. This is very important information for the modeling of EP reactor because one of the goals is to promote the mixing inside the reactor, and it was assumed that increasing flow rates would be the logical answer. In reality, slightly decreasing flow rates provided improved mixing conditions and longer residence time.

Saul and Svejksky (1994) simulated velocity distribution within the vortex combined sewer overflow chamber using 3D mathematical model FLUENT. As a result of their analysis, they suggested improvements in the free surface flow and use of body fitted coordinates to better represent geometry. They discovered small, but significant changes to the flow pattern.

Three dimensional simulation model representing geometry and domain of the furnace using FLUENT may also be found in Jones (1997). Author simulated the sequence of reactions used to represent the combustion of the biomass fuel. Among other

things, he varied diameter and location of the nozzles, changed the walls on which the nozzles were installed, and the relative proportions of air injected by the over fire system. Similar case study of the inlet configuration was done by Shay (1998), using 2D model.

Computations using FLUENT/UNS were carried out with the objective of understanding the turbulent flow field and convective heat transfer in gas turbine disk cavities in the work of Roy et al. (1997). This is an example of 2D axisymmetric calculation mode.

For the development of a new Particle Image Velocimetry technique for three-dimensional flows, the results from the experimental investigation were compared with the numerical simulation obtained using FLUENT. Kurada et al. (1997) reports the development process. In order to have a better understanding of different types of complex flow fields, knowledge of the instantaneous spatial distribution of all three components of velocity is critical and may easily be obtained from FLUENT output. Such information is very important in providing benchmark data for the validation of other experiments and numerical techniques.

Vakikilainen et al. (1998) applied three-dimensional simulation to analyze the high solids firing processes in a recovery boiler. The flow field, combustion and heat transfer were modeled using FLUENT/UNS. This flow field is very complex due to the intense reaction modeling – 250 reactions between 50 chemical species take place inside the boiler.

Some other FLUENT applications follow. Grace et al. (1998) used FLUENT for validation of CFD based recovery furnace models predicted by the University of British Columbia code. Halloin and Wajc (1996) used FLUENT to numerically simulate

creeping flow and heat transfer in forehearths. Particular interests were in the complexity of the flow pattern and secondary currents induced due to the non-uniformity of temperature and density. In their research, 3D model was a necessity. Kolpatzik et al. (1998) needed detailed profiles of temperature and velocity fields surrounding the thermowell inside natural gas pipe flows. CFD is a valuable tool in investigating non-isothermal flows. The accuracy of CFD results easily matches the precision of the experiments and has advantage of evaluating interactions between the different parameters. Although, the numerical simulations can provide complex results faster and in greater detail, need for measurement data will always exist, simply to verify and validate assumptions used in the process.

Hung and Kim (1996) analyzed the effects valve disk angle has on the incompressible fluid flow through the butterfly valves. Hamad and Khan (1998) investigated natural convection in a cylindrical annulus to study the effects of angle of inclination and diameter ratio on heat transfer. The annulus diameter ratio and Rayleigh number have more impact on natural convection heat transfer than the angle of inclination.

Waliszewski et al. (1994) analyzed medical instrumentation. They used FLUENT for a three-dimensional analysis of the velocity fields and corresponding shear stresses in an organ support system to validate their findings.

There are many other Fluent application examples in the literature. Mentioned modeling problems should inform the reader of the scope and variety of applications this CFD package is capable of solving.

### **2.5.3 Chemical Vapor Deposition Modeling Using Fluent CFD Package**

Several CVD processes have been modeled using Fluent CFD package. Alam and Graham (1996) carried out a simulation to study Chemical Vapor Deposition using FLUENT. Simulation of the SiC deposition was observed in a fiber coating CVD reactor. The results of the simulation for a hot wall reactor compared extremely well to the experimental data. As the direct result of the simulation, it was concluded that the temperature profiles tend to be uniform in the radial direction while the reaction kinetics dominates the deposition process. The effects of the reactant flow rates, diffusivity of the reacting species and temperature were examined. It also states that the solution for FLUENT becomes acceptable when residuals of velocity and pressure terms are less than  $10^{-3}$ , the species residuals are less than  $10^{-4}$ , and the enthalpy residuals become less than  $10^{-6}$ . The residual values may have an important role in the solution convergence.

Collins et al. (1994) developed a CFD model for the plasma-enhanced chemical vapor deposition of silicon nitride. Authors in this research paper state that empirical models have inability to completely predict the process responses outside the limited-range multidimensional experimental design space in which they were originally developed. Typically, strongly coupled nonlinear functions occur in physical models, but are approximated by low-order polynomial expressions. This usually results in the models with poor extrapolation properties. These insufficiencies are overcome by the use of the more complex physical models called mechanistic models. These models are based on the fundamental principles of the physical process and equipment design. These numerical methods are capable of solving systems of stiff differential equations that describe the chemical reactions, fluid mechanics, and heat transfer that occur within the

equipment. FLUENT has the capability of solving mechanistic equipment modeling coupled with discretized numerical solver.

Nami et al. (1997) used a 3D model to explain experimentally observed off-axis deposition of grown films during metal organic CVD. The work done by the authors includes all the steps this thesis intends to do. After initial numerical results, the model is used to find the control mechanism for different process conditions. Finally, simulations were compared to the experimental results, and excellent agreement was reached.

Kelkar et al. (1996) analyzed vertical metal organic CVD reactor using Fluid Dynamics Analysis Package (FIDAP). This transient model included property variation and thermo-diffusion effects. Statistical Design of Experiment (DOE) methodology was used to limit the number of simulations for combination of processes. Note that this methodology was used to limit the number of experiments used to acquire data and talked about in Chapter III and in the work of Shay (1998).

#### **2.5.4 Other CFD Codes**

Many computer applications have been used for different types of numerical solutions. Following paragraphs mention couple of examples found in the literature for chemically reacting flows using different CFD codes.

The yield of the popular industry reactor was improved for semiconductor manufacturers by SEMATECH (SEmiconductor MANufacturing TECHnology) researchers and reported by Geyling et al. (1996). CFD was used to analyze the flow pattern inside the reactor. The method made it possible to determine the operating conditions that would eliminate recirculation zones, which were believed to cause



contaminants to be deposited on the wafer. CFD-ACE commercial software was used. It was concluded that CFD-ACE was able to model stiff chemical reactions in complex processes, such as chemical vapor deposition. The software clearly showed the recirculation regions that were responsible for contamination inside the reactor, and the patterns that various experiments with amount of reactants, flow rates and different handling methods could not detect.

Detemmerman and Froment (1998) discussed three-dimensional simulation of furnaces and reactor tubes for the thermal cracking of hydrocarbons. Full 3D CFD model containing transport equations for mass, momentum and energy has been implemented in the software code FLOWSIM, together with the  $k$ - $\epsilon$  turbulence model. It has been coupled with the appropriate kinetic models – radical reaction scheme CRACKSIM for the reactor and combustion kinetics for the furnace. The simulation revealed that no large recirculation patterns occur in the flue gas, which were assumed by the designers. By assuming these recirculation patterns, the designers overestimated efficiency of the firebox, explaining the industrial problems observed with these units. Another example was presented in the work of Wendel et al. (1996). Authors demonstrated a useful role for CFD in large 3D problems, where some experimental data are available for calibrating key parameters. A computational 3D fluid dynamics (CFD) model has been developed using CFDS-FLOW3D to model aerosol products passing out of the process building during the hypothetical accident. The results were global – total time-integrated aerosol flow rates across a few boundary surfaces, as opposed to local velocities, temperatures, or heat transfer coefficients.

This concludes the literature review. The main focus of this review was on computational fluid dynamics. Further literature review on aerosol reactors and chemical vapor deposition may be found in Foster (1999), Morrison (1998) and Shay (1999). While there was little information available on the initial EP process, lot of information collected was used for similar cases and processes. Based on the knowledge and information compiled from these sources, small ray of light shined on the complex and artistic process from EP.

Due to many difficulties experienced in the experimental part of this research, discussed in the following chapter, assessing process characteristics was extremely treacherous. These characteristics were modeled using FLUENT/UNS to the best of capabilities to further understand the occurrences inside the reactor. This particular research shall add more insight to previously done 2D analysis by Foster (1999).

## **CHAPTER III**

### **RESEARCH AND OPTIMIZATION OF THE CURRENT SYSTEM**

#### **3.1 Introduction**

The process of synthesis of II-VI compounds has been applied at Eagle-Picher Inc. (EP) for the last fifty years without major changes. The fast paced developments in microelectronic industry have caused current production of these materials to become insufficient and the need for improvements and redesign was inevitable in order to remain competitive. The focus of the research was to obtain more knowledge about the current process, model the reactor via CFD and propose immediate improvements as well as a new design.

Therefore, first part of the summer 1997 work was to become familiar with the current concepts and parameters. Also, better knowledge of the temperature distributions had to be obtained during the preliminary period of gaining better understanding of the process. The thermocouple set up was designed to provide significant information about temperature profiles. Finally, the key parameters affecting the current process of synthesis reaction were identified and statistical Design of Experiments (DOE) created to assist in obtaining data for comparison with the numerical simulations. As a result, important information was gained about process parameters and applied toward improvements on the current reactor. Acquired knowledge had immediate impact on the current reactor, resulting in increased production. Based on the comparison of

experimental data and numerical models, a new design was suggested in the thesis of Shay (1998) and Morrison (1998).

This chapter will cover the description of the current process, temperature data set up used to gather information, and a brief description of Design of Experiments. Detailed analysis can be found in the work of Shay (1998). Appendix A contains figures and tables to support the information presented in this chapter.

### **3.2 Current Process Description**

The Eagle-Picher designed current process during the late 1940's to produce quantities of II-VI compounds for research purposes. Eagle-Picher has generated sulfides and selenides of cadmium and zinc in the reaction furnace shown below in Figure 3-1.

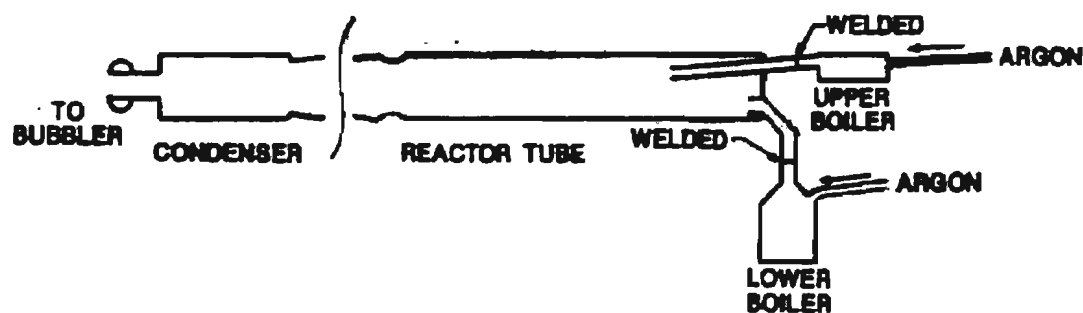


Figure 3-1. Current Eagle-Picher Reactor (Ghajar et al., 1996)

The furnace itself consisted of four independent quartz pieces put together during the reaction process. The boilers for the synthesis materials are welded to the main reactor tube prior to the reaction. The entrance region may be seen in Figure A-1. The water-cooled condenser is glued also to the main reactor tube in such a manner that the vacuum should be formed if plugged from the bubbler end of the reactor. The synthesis

takes place inside a horizontal tubular reactor, where the materials are carried from the boilers using carrier gas. Inside the reactor tube, mixing and particle growth take place allowing the fine powder to be collected after the cool-down process. The tubular reactor part is placed inside the round furnace after the boilers have been welded on. This furnace is used as the heat source to the reaction tube and consists of three different heating zones. This three zone tube furnace manufactured by EP has front and back heating zones roughly half the size of the center zone where the synthesis takes place as postulated. Each heating zone is monitored by several thermocouples, which descend through the top of the shell and firebrick, until they are placed in touch with the inner surface of the furnace lining. These thermocouples are read at the digital readout as well as fed to the digital controller. The boilers used for the synthesis materials are also placed inside two boiler heaters. The lower boiler is used for either gaseous selenium or sulfur, while the upper boiler contains gaseous zinc or cadmium. The smaller heaters are monitored by several thermocouples, which read the output to the digital thermometer.

It takes three full days to conduct a successful synthesis of II-VI compound. On the first day, the main part of the set up takes place. The thoroughly cleaned and dried reactor tube is placed inside the furnace. The condenser is greased with the stopcock grease on the standard taper fitting, which is then connected to the mating fitting of the reactor tube. Next, the lower boiler is loaded with pre-measured amount of selenium and placed inside the heater resting on the jack. This amount is usually equal to 700 g (8.87 moles) of selenide for the 95 mm inside diameter tube. Selenium was included in excess under the assumption that Se-rich conditions favored high conversion of zinc and therefore increased capacity. This jack is then adjusted so that the boiler entrance is in level with the entrance into the tube reactor for this particular material. This is the lower

of the two inlets into the tubular reactor. After the argon tube is attached to the boiler and the slow flow has been established, the operator welds the two together. The exact argon flow rate is not important during the preparation of the reactor, but becomes crucially important once the chemical reactants reach the boiling point and are carried inside the reaction tube. The hydrogen/oxygen welding torch is used for the welding process. After successful weld has been made, the lower heater is slightly dropped so that the boiler is hanging from the tube. The thermocouple is placed in such a manner that contact is made with the quartz boiler approximately half way up from the bottom.

The pre-cleaned upper boiler is loaded with zinc and placed inside the heater, which is resting on an adjustable position rack. The amount of zinc load for the same size tube as mentioned above is typically 500 g (7.65 moles). The outlet of the zinc boiler is adjusted so that it is aligned with the top entrance into the reactor tube using the adjustable jack. Again, after the argon flow is attached to the front of this boiler, and after flow through the boiler has been established, boiler is welded to the reactor tube. Next, the heater is slightly lowered so that the boiler hangs from the top of the main reactor tube. Just like for the lower boiler, the thermocouple is inserted inside the heater until contact is made with the boiler itself somewhere in the center area.

After the boilers have been welded and thermocouple placed to monitor the reaction process, the bubbler is attached to the condenser with amber latex tubing. This assembly is checked for leaks by placing the plug on the bubbler end of the condenser and observing the backpressure rise. Following the successful leak check, the connection between the reactor tube and condenser is wrapped with FiberFrax insulating material. Same material is used to cover the inlets from the boilers into the reactor tube as well as to tightly pack the reactor tube wall outside the furnace to prevent heat loss during the

synthesis. The system is then left with argon flow on until the day two to remove any air deposits from inside the reactor since it is believed that air affects the purity of the final product.

At the start of the second day, condenser's cooling water flow is started and the reaction furnace heaters are turned on. After around two hours, the boiler heaters are turned on at a predetermined heat rate. These predetermined rates raise the temperature inside the boilers slightly above the boiling temperatures of the materials used. This is done in such a manner that the Se boiler reaches this temperature several minutes before the Zn boiler. The vaporized reactants are now carried inside the reactor. The mixing of the chemicals takes place inside the reactor tube once the boiling takes place as they are carried with argon. Mixing results in the reaction that lasts until reactants are emptied from the boilers. The result of the reaction are small crystallites and platelets deposited inside the reactor. Unreacted and excess reactants settled in a water-cooled condenser at the back of the system. Once the end of reaction is reached, the reactor is left to cool with the argon flow intact and the condenser water flow turned off. The FiberFrax insulation is removed and the fan is placed pointing inside the furnace to aid the cooling process.

Finally, the last day, argon flow is stopped and the removing of the parts begins with the condenser. Usually, the condenser is full of the hazardous waste material, which must be carefully scraped into a waste collector. The argon connections and the heaters are carefully removed from the boilers in the front of the reactor tube. Next, the reactor tube, together with still attached boilers is placed onto a special rack where the product is scraped from the inside of the reactor. After scraping the entire product powder from the walls of the reactor tube, the product is collected and weighed. During the collection

process, visualization is used to classify quality of the product as “good” or “bad”. The “bad” product is disposed in the same manner as other waste products of the synthesis.

ZnSe has a form of yellow powder. The variation of colors ranged from bright yellow to tinted variety of red. This latter variety was attributed to the excess amount of selenium in the product. Product consistency differed from very fine powder, to grainy, to coarse. No relationship was established between composition of the product and operating conditions. Currently, II-VI materials produced have 99.999 purity.

Before the boilers and the reactor tube can be cleaned, they are cut apart using abrasive water-cooled saw. Cleaning protocol as well as more detailed process description may be found in Divis (1997).

Each operator develops his/her own feel for the operating set points and timing. Usually a successful run will yield between 500 and 1200 grams of the product, which corresponds to 50-90% zinc molar based theoretical yield.

Zinc based molar yield was calculated from the following equation:

$$YIELD(\%) = \frac{m_{ZnSe}}{\frac{m_{Zn}}{M_{Zn}} \times (M_{Zn} + M_{Se})} \times 100 \quad (3-1)$$

where  $m_{ZnSe}$  is the amount of product,  $m_{Zn}$  is the amount of the reactant used, and  $M_{Zn}$  and  $M_{Se}$  are the molecular weights of zinc and selenium.

The fact that the synthesis results depend on the experience of the operator suggests that the process is not controlled through the monitoring of the key elements, but by the “best guess” available at the time of the reaction. As a result of the insufficient data availability, the primary goal at EP facilities was to obtain information necessary for numerical simulations.



### **3.3 Process Analysis**

T. Morrison, C. Shay and myself conducted the analysis of the process at EP during the summer of 1997. Considering the limited knowledge of the process prior to the time spent at EP, first goal was to understand the “art” of the process using time and resources available. By understanding better the “art” of the process, key parameters such as flow rates, deposition patterns, temperature and flow profiles and product purity would be realized and in depth study designed. By the time all of the parameters that had direct impact on the results of the reaction were acknowledged, we faced limited time to conduct the parameter study with already limited resources. At the same time, there was place for modifications and improvements that could improve the process immediately.

Reactor synthesis was based on the use of pure raw materials, which come at the high cost for 99.9999 purity levels. During seventeen-month period, 48 runs were attempted and roughly one fourth of them did not yield any product at all. This high rate of failure lead to a significant waste of raw materials. Even the “successful” runs, which was basically any run with collectible product, yielded an average of 54.2%, which still does not have the efficiency desired for such a high cost process. The results of production in the past time period are shown in Figure 3-2. Morrison (1998) estimated the cost of unused material to be about \$50000.

Erratic results of the production suggested several suspect areas. One of the areas was control of mass transfer into the reactor tube. Elements are heated to near boiling point and then brought to temperatures above their boiling temperatures. Excess amounts of selenium early in the reaction time could cause convection roles called “warmholes”, which generally resulted in the failure of the run because majority of the reactants were channeled into the condenser. Another byproduct of the excess selenium early in the

reaction is total plugging of the reactor and failure to yield any product. While the geometry creation could not be detected until after the reactor tube is pulled from the reactor, plugging had to be closely monitored because it resulted in the build up of

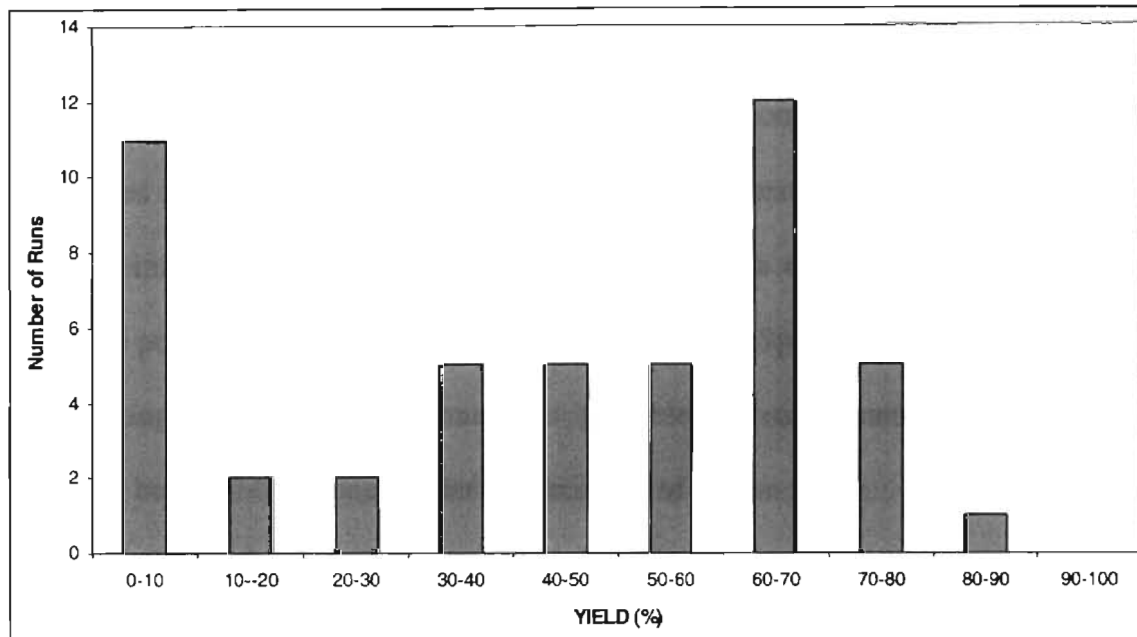


Figure 3-2. ZnSe Run Yield (February 1996 through June 1997)

backpressure with possible devastating consequences.

Reaction results showed lack of consistency, leading to believe that the sensitivity of parameters is crucial for success. Even the smallest subjective factor may have a huge impact on the final product.

Initially, survey of the existing equipment was taken into account. The question faced was what can be learned from existing system knowing how many things are totally subjective and impossible to duplicate. For example, before each run, the operator was in charge of minimizing the heat loss by packing the insulating materials around the reactor. This was totally subjected to the operator. Change of the insulating material had changed

the operating conditions in the past. Also, prior to the student arrival at the site, flow rates were estimated based on the reading of the bubble meter and not actual flow. The meters have not been calibrated in a two-year period. Constant welding and removal of the boilers from the reactor affected the inlet configuration for each run. Thermocouples used to control the temperature of the reactor were not properly positioned and the output given was not detecting actual temperature at desired location. Excessive handling of the reactor tubes caused damage and losses throughout the testing period. These reactor tubes were manufactured in house at EP, but each had its own specifics. These were some of the problems faced throughout the testing period. Special attention was attended to eliminating these factors as much as possible by using same elements, same procedures, but it all functioned under the presence of human factor.

### **3.4 Thermocouple Set Up**

The information obtained from EP concerning temperature distribution provided a good start, but more accurate and detailed data was needed. The thermocouples used to control the temperature of the three zones inside the furnace were not calibrated and monitored often enough, therefore decreasing the accuracy of the data due to the Se that congregated on them. Long time intervals these thermocouples experienced under high temperatures had serious effect on their lifetime, causing brittleness and breaking. Also, these thermocouples were not in direct contact with the reactor tube, which was of great interest in order to have capability of modeling the synthesis on FLUENT/UNS. The thermocouples used were measuring the temperature distribution along the inner furnace wall, but the furnace itself was not in contact with the reactor tube. Temperature of the reactor tube was not known. According to the operator, temperature inside the reactor

could have been anywhere from 950 to 1100 °C. The current temperature limits of the reactor are believed to be around 1300 °C. Another unknown was the effect of the reaction inside the reactor on the temperature distribution during the process. It was important to know the increase in temperature if there was any to estimate the heat transfer inside the reactor tube. Without this type of information, the accuracy of the FLUENT/UNS model would be greatly reduced by the assumptions necessary to estimate the flow and therefore reduce the understanding of the entire process and future design. Also, it was unknown whether there was difference in the temperatures along the same cross-section of the reactor tube and the effect buoyancy force might have on the flow inside the reactor. Most of the times, during the runs that resulted with large amounts of reactants in the condenser, the worm-holes were located along the top of the reactor tube, causing the belief that the buoyancy force had effect on the flow inside the reactor. Another reason for the location of the wormholes was possible concentration of selenium inside the reactor when zinc started boiling and entering the tube. When the flow rate was not high enough, reaction would take place as soon as the material entered the reaction tube and begin forming the tunnel from the inlet nozzle made of the products of the reaction.

One of the attempts to keep the product inside the reactor was placement of the baffles for product collection. The collection of product was related to the flow rate of the carrier gas. The difficulty was in removing the baffles from the reactor due to the fusing created inside the furnace. Breakage during this handling process and unaffected yield stopped the use of this process. One of the observations was that the increased purity of the product was inversely related to the yield. Extra purity level decreased the yield roughly in a half.

Finally, the reactor tube was not centered inside the furnace. The belief was that by centering the tube, heating would be more uniform and maybe it would reduce the number of runs, which ended plugged without quality product to be collected. Before the actual design and use of the thermocouple rings, which were designed to center the tube, quartz stands were placed inside the furnace to aid the centering of the reactor tube. Due to this modification of the EP process, number of runs that resulted with wormholes was reduced, but it was not eliminated.

Temperature data acquisition was based on the experimental design that was first created before arrival at Eagle-Picher and without much knowledge of the process. As it turned out, only a few minor modifications had to be made once on site at Eagle-Picher to enable to collect desired data.

First problem faced was the choice of material for the thermocouple rings that could withstand high temperatures but would be relatively easy to manufacture. The final choice was same type of quartz that was used for the reactor tube due to its unchanged properties at high temperatures, as well as sturdiness that would hold the thermocouples in place during the setup phase as well as during the reaction. It was more difficult to taper the holes on this type of material, but the skilled EP hands did an excellent job of preparing them.

The original design consisted of four quartz rings, which had thermocouples attached to them and was placed along the reactor tube to acquire temperature data. The cross-section of the initial set up is shown in Figure 3-3.

The thermocouple ring is actually shown without tapered holes. The inner circle represents the reactor tube, surrounded by the thermocouple quartz ring, which are located inside the round furnace. Interior part of the furnace is made out of polymer

called mullite. The advantage of this design was that once the thermocouples were cemented onto the rings, they were used as offset device to keep the reactor tube centered inside the furnace.

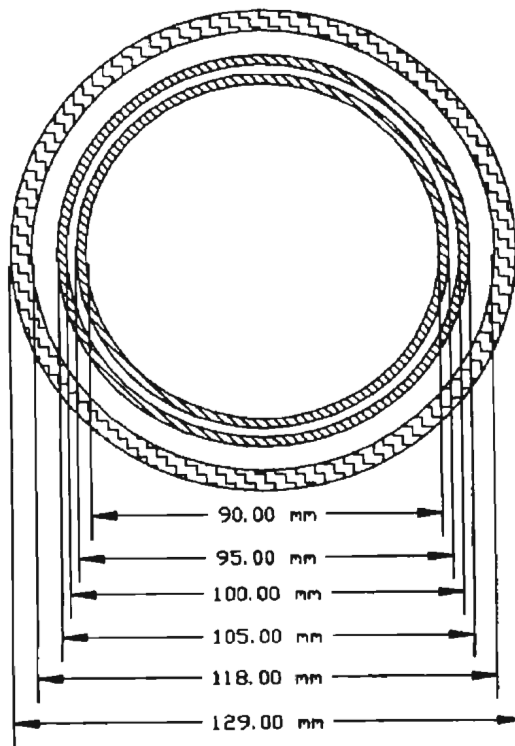


Figure 3-3. Cross-Section of the Temperature Data Acquisition Set Up

Design called for the information from inside the entire furnace and all of its heating zones. As a result, one of the rings was placed in the front and rear heating zones, while the remaining two rings were located along middle heating zone. The set up shown in Figure 3-4 demonstrates the initial locations chosen for the thermocouple rings. These locations were slightly modified once the better knowledge of the process was acquired on site. The individual rings were made of the 5 mm thick 105 mm outside

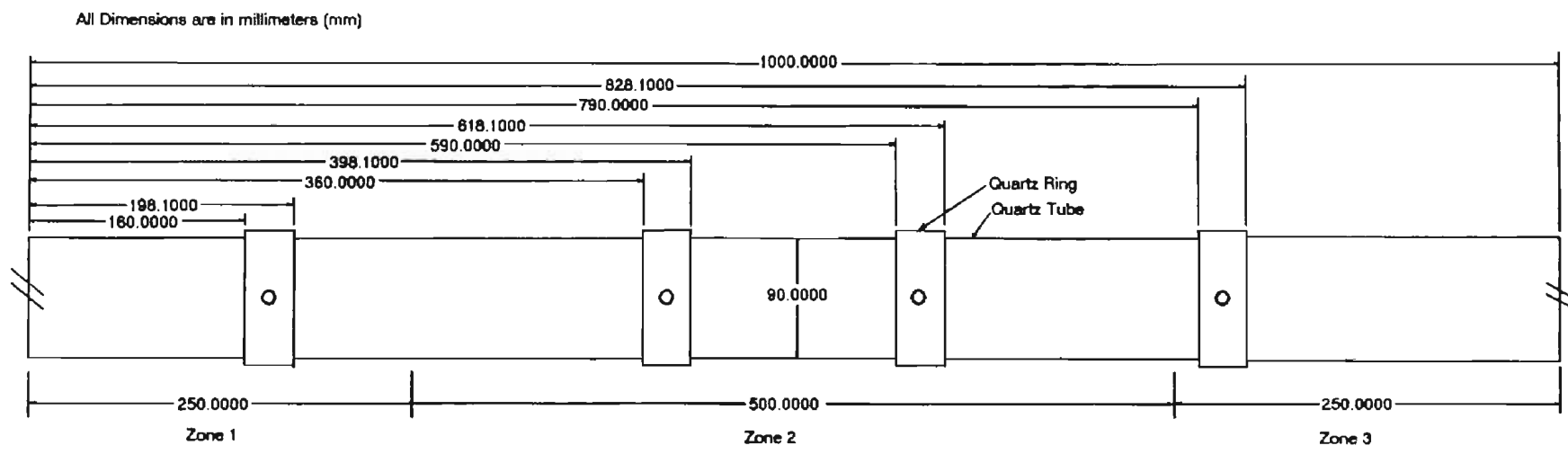


Figure 3-4. Temperature Data Acquisition Set Up

diameter tube that provided just enough space to have the thermocouple beads placed in contact with the reactor tube.

Each quartz ring had four tapered holes located 90° apart in which the thermocouples were placed. Due to the symmetry that existed in temperature profiles with respect to the vertical axis of the reactor, only the data from the top and bottom of the tube were used. On-site experience showed that any irregularities and asymmetries were located along the vertical axes supporting the belief that symmetric conditions existed along the sides. Therefore, the temperature difference between the top and the bottom has impact on flow patterns and deposition inside the reactor.

K-type thermocouples were used for the data acquisition and were protected with high temperature Nextel type ceramic insulation. Initially, the cement Omegabond 400 was used to hold the thermocouples in the tapered holes, but 24 hours curing time and weak bonding became liabilities. The cement also increasingly damaged the quartz rings for each successive run. As a simpler alternative, the thermocouples were taped to the rings and then the rings were taped to the reactor tube to stabilize them during the reaction set-up process. The tape would simply burn off during the furnace warm-up. This simpler and quicker process had to be repeated before every run, but the turnaround time was still faster than with use of the cement. The only downside to this method was that the set up was not as stable as with cement, and extreme care had to be applied during the set-up phase to maintain all components in place and in contact with the reactor tube. Although the thermocouples and ceramic Nextel insulation were rated for the high operating temperatures, due to the long reaction and data acquisition time, they had to be replaced often, sometimes after every run.



The data acquired from the data logger was plotted and analyzed after each reaction run. From the observations of these plots, some immediate conclusions were reached:

- Temperature on the surface of the reactor tube was actually about 30 degrees higher than the temperature measured on the surface of the furnace wall. Figure A-2 shows sample temperature data profile from one of the experimental runs, clearly showing this tendency.
- Non-uniform heating of the reactor tube prior to the start of the reaction - toward the front of the furnace, top of the reactor tube was at a higher temperature than bottom, while in the middle and toward the back of the furnace, bottom was at the higher temperature. These observations may be seen in Figures A-2 and A-3.
- Opinion was formed that the reaction time can be predicted from the temperature change along the reactor tube, which occurred as a result of the exothermic reaction taking place inside the reactor (formation of convection roles might have had an impact). This change of temperature may be seen in Figures A-2 and A-3 as a drop in the profile.
- Prior to peaks, a temperature drop exists toward the rear of the reactor, for which there is no scientific explanation at this time. Instability of the temperature profiles can clearly be seen in Figure A-5.
- Wormholes formed at the top of the reactor matched with the increased temperature readings of the top thermocouple.
- Temperature difference between the top and bottom of the reactor did exist, causing the possible existence of secondary flows.

- Approximate time before the completion of reaction was around 3 hours. Sudden temperature drop may be seen in Figure A-4.

### **3.5 Design of Experiments and Results**

Objective of Design of Experiments was to conduct a factor screening study with the intent of discerning and evaluating the main parameters affecting the Physical Vapor Transport (PVT) synthesis of ZnSe. The effects, relative effects, and interactions of seven parameters on the product quality and yield are to be studied. Design of Experiments was conducted using a  $2^{7-4}$  matrix where 2 represents number of levels of each factor to be studied and 7-4 exponent is the part of the full matrix to be run. This type of study reduces number of runs to 8 from 256 possible combinations in the full matrix. Detailed explanation of Design of Experiments and interactions among the factors is described in the work of Shay (1998).

Factors under study are given in Table 3-1.

Table 3-1. Design of Experiments: Factors of Study

FACTORS		LOW LEVEL	HIGH LEVEL	CURRENT SETTINGS
Argon Flow	ml/min Se	225	265	245
	ml/min Zn	219	305	262
Boiling Rates (final set points)	deg. C Se	718	724	721
	deg. C Zn	950	956	953
Furnace Temperature (front and center zones)	deg. C	975	1075	1000
Reactor Tube *		Tube A	Tube B	
Boiler Ramp Time	hrs:min Se	2:00	1:00	1:30
	hrs:min Zn	2:03	1:03	1:33
Amount of Excess Selenium	Excess moles Se	1.00	2.00	1.22
	total g of Se	683.0	762.0	700
Cooldown Rate		One Fan	Three Fans	One Fan

\* Two different tubes were used to carry out the study. Tube dimensions are shown in Table A-1.

Factors column represents process variables used in the experimental study. Only valuable response variable was molar percent yield based on zinc. It is important to note

that the successful runs (greater than 60% yield) had the product distributed along the bottom of the reactor in a form of a powder, while most of the other runs formed convective rolls. This observation was common for the experiment runs, as well as for the preliminary study. The formation of convection rolls is direct result of the effect flow rate has on the reaction. Lower incoming flow rates allow reactants to congregate around the inlet region and allow creation of the rolls. The most successful runs had product deposited on the floor of the reactor and toward and past midpoint. Another possibility is that due to geometry of the reactor tube, dead flow regions may exist behind inlet nozzles. According to the report from EP, these dead zones exist because of the non-uniform heating. The front of the reactor is cooler than the rest of the reactor and is more likely to experience temperature fluctuations. Initially, both tube inlets extended into this hot zone, but constant plugging was a problem. Current design resulted when a record yield was obtained during a run which resulted in a broken Se tube inlet.

During the experiment study yield results varied from 26.8 to 67.7%, and although main focus was to learn more about possible relationships among parameters, this type of development agreed with the past performance of the system.

As the result of the experiment runs, it was shown that the opinion regarding excess of Se was misleading. It is common feature of II-VI reactions that if 1:1 ratio is used, product contains excess of the metal. The subsequent processes at EP required excess of Se in the product. The excess amount of Se actually affected the rate of the reaction and therefore mixing of the reactants inside the reactor, causing formation of the product in the form of the wormholes. Creation of the wormholes reduces yield of the product and efficiency of the reactor. More favorable setting and design would allow the two reactants to enter the reactor at the same time in such a way that mixing is promoted,

causing the area of contact to increase the reaction of elements. The wormhole product formation had the greatest impact on yield of the product due to the “channeled” reactant outflow to the condenser. The optimum flow would be the one high enough to prevent plugging or wormholes formation in the entry region, but low enough to provide sufficient residence time inside the reactor for reaction to take place.

Another important result of this kind of study was definite connection between the boiling rates of reactants and yield of the product. Premature boiling of Se may cause its congregation in inlet area and cause premature reaction and hence unwanted formations inside. It is very important to bring the elements to their boiling points slowly and to prevent selenium from saturating inlet area prior to entrance of zinc.

Having completed the analysis of the experimental results a confirmation run was completed in order to validate the conclusions drawn from the data with respect to yield. All levels for the confirmation run were chosen from within ranges already experimentally varied with exception of Se. Amount of elemental excess selenium was decreased to 0.5 moles.

The confirmation run resulted in a ZnSe yield of only 35% with a large wormhole. Lack of capability to reproduce any kind of consistency would indicate the results of each individual run to be unique and not specific for the conditions used, leading to inaccurate analysis. Inability to reproduce data may be attributed to possible “hidden” factor, not used in analysis. The unpredictability of the process had to be eliminated via modeling the reaction using CFD.

## **CHAPTER IV**

### **FLUENT CFD PACKAGE**

#### **4.1 Introduction**

Lesser cost and shorter time are factors that drive industry development in our time. These factors influenced rapid development of commercial CFD packages in last quarter of the century. Development of the computer systems also impacted development of these software packages. Variety of problems are approached and solved by the use of modern computer technology and CFD applications.

Oklahoma State University has access to several commercial CFD codes, one of which is Fluent CFD package. Students have taken advantage of available tools to prepare and specialize themselves for competitive marketability to potential employers through the use of these programs. Software companies realize potential of educational institutions and offer the codes at discounted prices to make them available to students.

In this chapter, Fluent CFD package is introduced. Software structure is described for FLUENT/UNS and RAMPANT, concentrating on FLUENT/UNS. Specific components related to this research were described in following sections.

## **4.2 CFD Package**

This section discusses briefly the composition of the Fluent CFD package. The purpose is to introduce to the user names of the subprograms and preprocessing tools. For detailed information on these topics, one should look in Fluent literature available. Literature available is sufficient to get anyone started using the package. Fluent CFD package consists of following components:

- FLUENT/UNS, FLUENT, NEKTON and RAMPANT are all solvers.
- GeoMesh and preBFC, preprocessors for geometry modeling and mesh generation.
- PrePDF, preprocessor for modeling PDF combustion in FLUENT/UNS.
- TGrid, triangular and tetrahedral mesh generator.
- Grid filters for CAD/CAE packages.

Individual components within the package are grouped into smaller packages based on the application capabilities. For example, FLUENT package consists of FLUENT solver and GeoMesh preprocessor, and is used for simple geometries. NEKTON package consists of NEKTON solver and GeoMesh preprocessor, and is used for simulating laminar flow in complex and/or deforming geometries.

FLUENT/UNS and RAMPANT are packages made of three components. Two of the components, GeoMesh and TGrid, are used to generate geometry, domain topology and grid. Once these steps have been completed, the preprocessing is finished and the grid is imported into third and final part of the package – solver, which are FLUENT/UNS and RAMPANT. The interactions between these parts may be seen in Figure 4-1. Everything starts from GeoMesh. The initial geometry is either imported or created into unstructured or structured grid domain. Depending on the type of the mesh,

interior mesh is generated in TGrid for triangular and tetrahedral meshes. For hexahedral meshes, grid is directly imported into the solvers, where the real modeling process takes place.

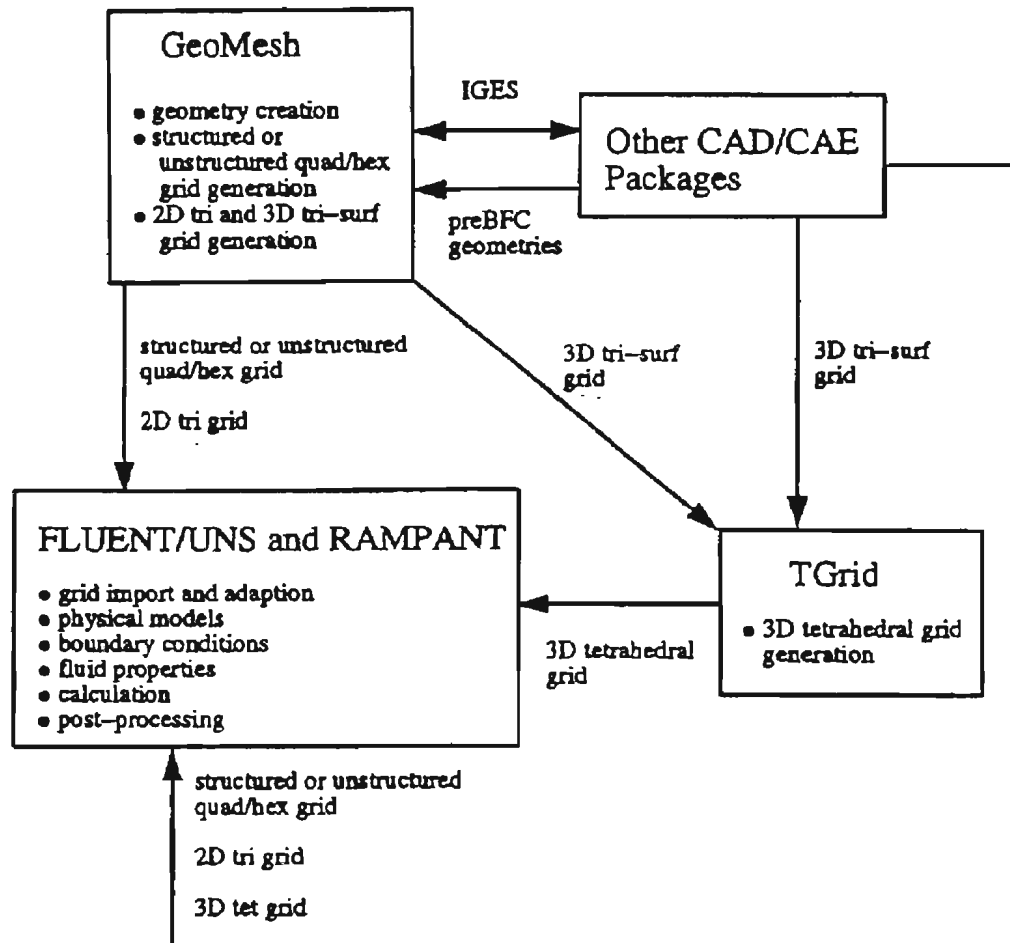


Figure 4-1. Program Interactions for FLUENT/UNS and RAMPANT Software Packages (Fluent Inc., 1996a)

FLUENT/UNS is well suited for modeling incompressible and mildly compressible flows, while for compressible, transonic and supersonic flows RAMPANT is used.

### **4.3 Planning CFD Analysis**

When considering a CFD analysis and before setting up the geometry and grid, the following issues should be considered first according to Fluent Inc. (1996a):

- *Definition of the Modeling Goals:* What specific results are required from the CFD model, and how will they be used? What degree of accuracy is required from the model?
- *Choice of the Computational Model:* How will you isolate the area of interest from the complete physical system to be modeled? Where will the computational domain begin and end? What boundary conditions will be used at the boundaries of the model? Can the problem be modeled in two dimensions, or is a three-dimensional model required? Can you take advantage of symmetry or periodic boundaries to reduce the computational domain?
- *Choice of Solver:* What physical models are required? Is the flow laminar or turbulent? Is the flow compressible or incompressible? Is heat transfer important? Does the solver you choose have necessary models for your problem?
- *Choice of Grid Type:* What type of grid (structured or unstructured quadrilateral/hexahedral or triangular/tetrahedral) is best suited for this problem? Is the geometry very complicated? Do large geometric scale discrepancies exist in your model? Does the solver you choose support the chosen grid type?
- *Design Your Grid:* What degree of accuracy do you need in each region of the domain? Will you need to adapt the grid later? How many cells will you need? Do you have sufficient computer memory?



## 4.4 GeoMesh

GeoMesh Session Manager is shown in Figure 4-2. It prepares domain topologies for the applications used within Fluent CFD package by the use of transfer pull down menu. All applications compatible with GeoMesh may be initialized from the “Applications” pull down menu. It is definitely the central office of the Fluent CFD package firm. It contains options regarding import and export of files, organizing the configuration related services. Although GeoMesh offers variety of options, its main purpose is to assist in geometry and topology creation process. Steps used in this work related to GeoMesh are listed in Appendix B.

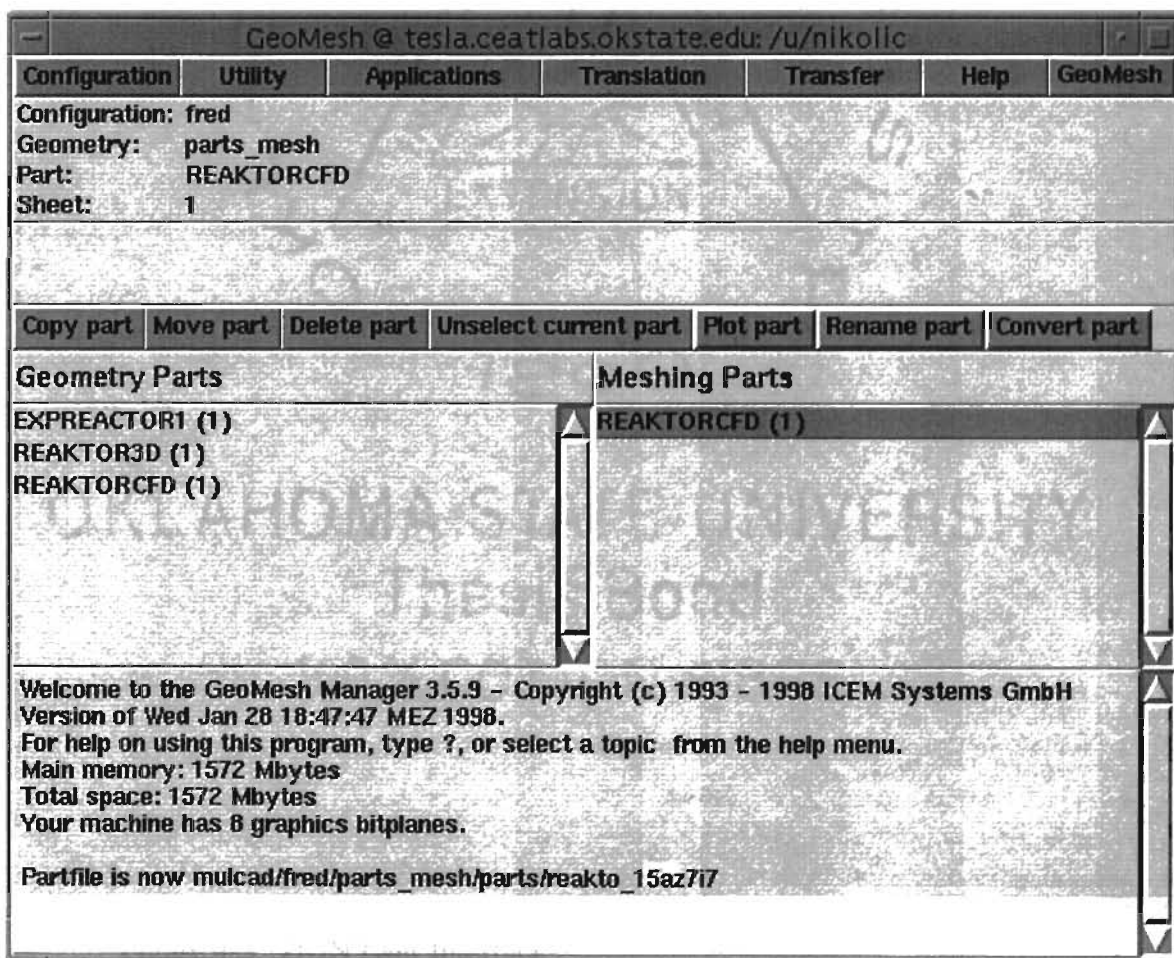


Figure 4-2. GeoMesh Session Manager

#### **4.4.1 DDN**

GeoMesh has a geometry generator part called DDN. DDN is where geometries can be created and modified, or in case of already existing geometry, imported from another CAD system. DDN user interface is shown in Figure 4-3. Typical use consists of creating simple geometric features such as points, which are used to create lines, and then the lines can be used to create surfaces. Detailed information regarding commands and options in DDN may be found in Fluent Inc. (1996a). Steps used to create geometry for this research are listed in Appendix B.

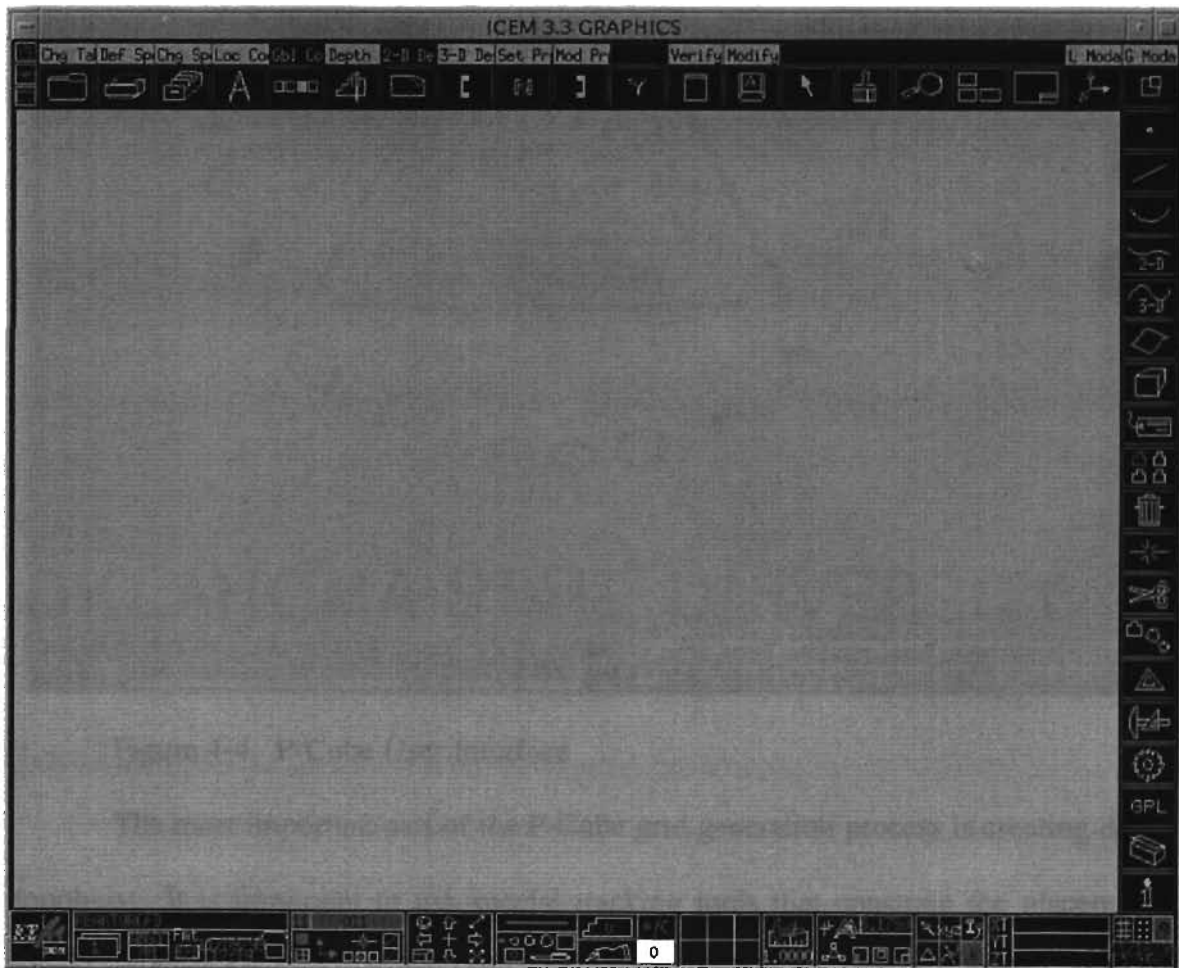


Figure 4-3. DDN User Interface

#### 4.4.2 P-Cube

P-Cube generates grid within the GeoMesh. Within the P-Cube, domain topology is defined, boundary types are assigned, node distribution is specified and grid interpolation is done. P-Cube user interface is shown in Figure 4-4.

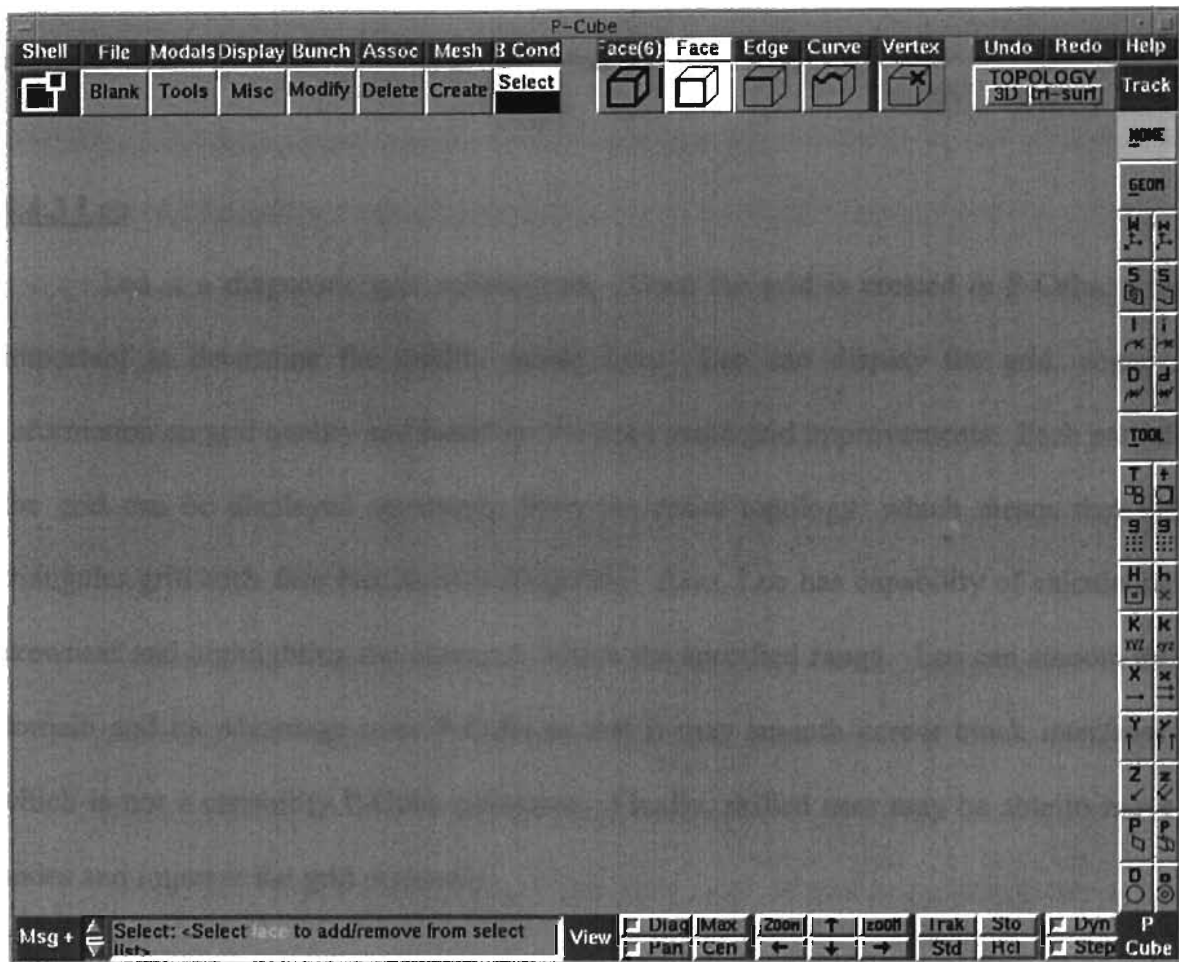


Figure 4-4. P-Cube User Interface

The most important part of the P-Cube grid generation process is creating domain topology. It is important to use special tracking tools that constrain the placement of blocks or faces to the geometry. This allows a body-fitted grid to be created within the domain topology. Faces are interconnected mesh areas that constitute domain topology. Faces may contain quadrilateral or triangular grids. For hexahedral grids, the domain

topology consists of blocks – interconnected mesh volumes. Domain is either a block that contains a hexahedral grid, or a face with triangular or quadrilateral grid. A topology is the way these faces or blocks are connected together and that is what dictates whether the grid is structured or unstructured (for triangular type, it is always unstructured). After the domain topology creation process is complete, node distribution, boundary types assignment and grid interpolation are performed.

#### **4.4.3 Leo**

Leo is a diagnostic grid subprogram. Once the grid is created in P-Cube, it is important to determine the quality inside Leo. Leo can display the grid, acquire information on grid quality and based on the need make grid improvements. Each part of the grid can be displayed separately from the entire topology, which means that for triangular grid each face has its own diagnosis. Also, Leo has capability of calculating skewness and highlighting the elements within the specified range. Leo can smooth the domain and its advantage over P-Cube is that it may smooth across block interfaces, which is not a capability P-Cube possesses. Finally, skilled user may be able to move nodes and improve the grid manually.

#### **4.4.4 TGrid**

TGrid is related to the other products in Fluent Inc. suite as shown in Figure 4-1. It generates grids of virtually any size and complexity for unstructured triangular/tetrahedral grids. TGrid is constructed in such a way that interior mesh generation is processed from the discretized boundary mesh. TGrid requires either a 2D

boundary mesh consisting of nodes and edges, or 3D boundary mesh consisting of nodes and triangular faces. It also gives an option to the user whether to generate complete mesh automatically or through the manual control. There are many tools available to correct and improve the mesh generation manually. It is important to note that TGrid generates unstructured type meshes, which can be used in conjunction with unstructured solvers. The basic steps for using TGrid are given in Fluent Inc. (1996c). They are as follows:

- Read a boundary mesh file into TGrid.
- Examine the boundary mesh for topological problems such as free edges and duplicate nodes. Once the boundary is topologically correct, a 3D surface mesh can be checked for poor face quality. Many grid quality related problems can be solved easily with edge swapping, but more difficult problems may require direct manipulation of the faces and nodes.
- Generate the volume mesh. This can be easily done automatically or by proceeding through a series of steps. The basic steps consist of selecting the cell zones, refining the cell zones, and performing face swapping and smoothing.
- Check the mesh for problems. The cells with skewness problems can cause problem depending on their location. Poor cell structure in critical areas may cause serious accuracy and convergence problems.
- Write the mesh to a new file for input to the solver.

## **4.5 FLUENT/UNS**

FLUENT/UNS is the solver within Fluent CFD package. It was chosen for the modeling in this work because of its applicability to accurately predict laminar, transitional and turbulent flows, various modes of heat transfer, chemical reactions, multiphase flows and other complex phenomena. FLUENT/UNS allows user to choose the structure type of the grid, as well as the ability to modify it within the solver. Many different options within the solver allow straightforward modeling and post processing. In following sections, physical model applied to the simulations within the solver is discussed. Detailed explanation of material presented in this section may be found in Fluent Inc. manuals, which discuss other solution methods and approaches beside ones used for the fork in this research.

### **4.5.1 Mass Conservation Equation**

Continuity equation as conservation of mass equation is usually called is:

$$\frac{\partial \rho}{\partial t} + \frac{\partial}{\partial x_i}(\rho u_i) = S_m \quad (4-1)$$

This general form of continuity equation is valid for compressible and incompressible flows.  $S_m$  is the source term and can be represented by mass added to the continuous phase or from any other source defined by the user.

### **4.5.2 Momentum Conservation Equation**

Conservation of momentum may be written in the following form:

$$\frac{\partial}{\partial t}(\rho u_i) + \frac{\partial}{\partial x_j}(\rho u_i u_j) = -\frac{\partial p}{\partial x_i} + \frac{\partial \tau_{ij}}{\partial x_j} + \rho g_i + F_i \quad (4-2)$$

where  $p$  is the static pressure,  $\tau_{ij}$  is the stress tensor, and  $\rho g_i$  and  $F_i$  are gravitational body force and external body force, respectively. The stress tensor is:

$$\tau_{ij} = \left[ \mu \left( \frac{\partial u_i}{\partial x_j} + \frac{\partial u_j}{\partial x_i} \right) \right] - \frac{2}{3} \mu \frac{\partial u_l}{\partial x_l} \delta_{ij} \quad (4-3)$$

where  $\mu$  is the molecular viscosity and  $\delta_{ij}$  is Kronecker delta function.

### **4.5.3 Turbulence Models**

Understanding the features of the flow analyzed is very important for the selection of the turbulence model. FLUENT/UNS uses the so-called “two-equation” turbulence models. The Renormalization Group (RNG)  $k$ - $\epsilon$  model and standard  $k$ - $\epsilon$  model are two options offered within the code for the solution method. Main differences between the two models are listed in Fluent Inc. (1996b) as following:

- RNG model is derived by a strict statistical technique, while standard  $k$ - $\epsilon$  model is based on the commonly used Reynolds-averaging technique.
- RNG model has an extra term in  $\epsilon$  equation to improve the accuracy of the solution.
- Swirl effects are included in RNG model.
- Standard  $k$ - $\epsilon$  method allows user to specify Prandtl number for analysis, while RNG method uses analytical formula to calculate it.
- Standard  $k$ - $\epsilon$  model is used mainly for Reynolds number modeling, where RNG method accounts more for low Reynolds number effects.

RNG  $k$ - $\varepsilon$  method is the turbulence model of choice for the purpose of this work due to its accuracy and applicability in low Reynolds number flows. The momentum equation for RNG  $k$ - $\varepsilon$  model has following form:

$$\frac{\partial}{\partial t}(\rho u_i) + \frac{\partial}{\partial x_j}(\rho u_i u_j) = \frac{\partial}{\partial x_j} \left[ \mu_{eff} \left( \frac{\partial u_i}{\partial x_j} + \frac{\partial u_j}{\partial x_i} \right) \right] - \frac{\partial p}{\partial x_i} \quad (4-4)$$

where effective viscosity  $\mu_{eff}$  is

$$\mu_{eff} = \mu_{mol} \left[ 1 + \sqrt{\frac{C_\mu}{\mu_{mol}}} \frac{k}{\sqrt{\varepsilon}} \right]^2 \quad (4-5)$$

where  $C_\mu$  is a constant 0.0845 (standard  $k$ - $\varepsilon$  model has this constant at 0.09) and  $\mu_{mol}$  is molecular viscosity.

Transport equations for turbulent kinetic energy and the rate of dissipation are given by RNG theory. The kinetic energy equation is:

$$\frac{\partial}{\partial t}(\rho k) + \frac{\partial}{\partial x_i}(\rho u_i k) = \frac{\partial}{\partial x_i} \left( \alpha_k \mu_{eff} \frac{\partial k}{\partial x_i} \right) + \mu_t S^2 - \rho \varepsilon \quad (4-6)$$

and for the rate of dissipation is

$$\frac{\partial}{\partial t}(\rho \varepsilon) + \frac{\partial}{\partial x_i}(\rho u_i \varepsilon) = \frac{\partial}{\partial x_i} \left( \alpha_\varepsilon \mu_{eff} \frac{\partial \varepsilon}{\partial x_i} \right) + C_{1\varepsilon} \frac{\varepsilon}{k} \mu_t S^2 + C_{2\varepsilon} \rho \frac{\varepsilon^2}{k} - R \quad (4-7)$$

where  $\alpha_k$  and  $\alpha_\varepsilon$  are the inverse effective Prandtl numbers for  $k$  and  $\varepsilon$ , respectively, and  $\mu_t$  is turbulent viscosity. An analytical formula was derived by the RNG theory to compute the inverse Prandtl numbers by:

$$\left| \frac{\alpha - 1.3929}{\alpha_0 - 1.3929} \right|^{0.6321} \left| \frac{\alpha + 2.3929}{\alpha_0 + 2.3929} \right|^{0.3679} = \frac{\mu_{mol}}{\mu_{eff}} \quad (4-8)$$



where  $\alpha_0$  is 1.0. For high Reynolds numbers ( $\mu_{mol}/\mu_{eff} \ll 1$ ),  $\alpha_k$  and  $\alpha_\varepsilon$  become constant with the values of 1.393. The modulus of mean rate-of-strain tensor,  $S_{ij}$ , is  $S$  and is given by:

$$S \equiv \sqrt{2S_{ij}S_{ij}} \quad (4-9)$$

$R$  in Equation (4-7) is given by

$$R = \frac{C_\mu \rho \eta^3 (1 - \eta/\eta_0) \varepsilon^2}{1 + \beta \eta^3} \frac{1}{k} \quad (4-10)$$

where  $\eta \equiv Sk/\varepsilon$ ,  $\eta_0 \approx 4.38$ ,  $\beta = 0.012$ . RNG theory derived model constants  $C_{1\varepsilon}$  and  $C_{2\varepsilon}$  to be 1.42 and 1.68, respectively.

The main difference between standard  $k$ - $\varepsilon$  model and RNG model is in use of  $R$  source term in  $\varepsilon$  Equation (4-7). The turbulent quantities  $k$  and  $\varepsilon$  are calculated based on formulas

$$k = \frac{3}{2} (\mu_{avg} I)^2 \quad (4-11)$$

and

$$\varepsilon = C_\mu^{\frac{3}{4}} \frac{k^{\frac{3}{2}}}{\ell} \quad (4-12)$$

where  $k$  is the turbulent kinetic energy,  $I$  is the turbulent intensity,  $\varepsilon$  is turbulent kinetic energy dissipation rate, and  $\ell$  is the turbulence length scale.

#### **4.5.4 Energy Equation**

In FLUENT/UNS energy equation is written in terms of sensible enthalpy  $h$  as

$$\frac{\partial}{\partial t}(\rho h) + \frac{\partial}{\partial x_i}(\rho u_i h) = \frac{\partial}{\partial x_i} (k + k_t) \frac{\partial T}{\partial x_i} - \frac{\partial}{\partial x_i} \sum_j h_j J_j + \frac{Dp}{Dt} + (\tau_{ik})_{eff} \frac{\partial u_i}{\partial x_k} + S_h \quad (4-13)$$

where  $k$  is molecular conductivity,  $k_t$  is the conductivity due to turbulent transport ( $k_t = \mu_t/Pr_t$ ),  $J_{j'}$  is the diffusion flux of species  $j'$ , and the source term  $S_h$  includes chemical reaction and any other heat source terms that may exist.

Sensible enthalpy is defined as

$$h = \sum_{j'} m_{j'} h_{j'} \quad (4-14)$$

where  $m_{j'}$  is the mass fraction of species  $j'$  and

$$h_{j'} = \int_{T_{ref}}^T c_{p,j'} dT \quad (4-15)$$

where  $T_{ref} = 298.15$  K.

Source of energy due to the reaction is

$$S_{h, reaction} = \sum_{j'} \left[ \frac{h_{j'}^0}{M_{j'}} + \int_{T_{ref,j'}}^{T_{ref}} c_{p,j'} dT \right] R_{j'} \quad (4-16)$$

where  $h_{j'}^0$  is the enthalpy of species  $j'$  and  $R_{j'}$  is the volumetric rate of creation of species  $j'$ . For the reactive flow, inputs given for the formation enthalpy  $h_{j'}^0$  for each species  $j'$  are used to define the mixture enthalpy as

$$H = \sum_{j'} m_{j'} \left[ \int_{T_{ref}}^T c_{p,j'} dT + h_{j'}^0 + \int_{T_{ref,j'}}^{T_{ref}} c_{p,j'} dT \right] \quad (4-17)$$

In conducting solid regions, simple conduction equation is used. The equation contains heat flux due to conduction and volumetric heat sources within the solid

$$\frac{\partial}{\partial t} \rho h = \frac{\partial}{\partial x_i} \left( k \frac{\partial T}{\partial x_i} \right) + \dot{q} \quad (4-18)$$

where  $\dot{q}$  is volumetric heat source and  $h$  is sensible enthalpy given by equation (4-14).

Underrelaxation of the energy equation is controlled by the temperature underrelaxation controls the convergence of energy equation solution except for the nonadiabatic case, where enthalpy underrelaxation factor becomes important. For the case where we have temperature dependent properties or buoyancy, the underrelaxation factor should be in the range of 0.8-1.0. In this case, temperature/enthalpy field impacts the fluid flow. Default value of unity should be kept for flow field which does not contain temperature dependant properties or buoyancy.

#### **4.5.5 Buoyancy Effects**

During a process in which heat is added to the fluid and density of the fluid depends on the temperature, a flow may be induced due to gravity force acting on the variation of density. The importance of this type of convection may be measured by the ratio of the Grashof and Reynolds numbers:

$$\frac{Gr}{Re^2} = \frac{\Delta\rho gh}{\rho\nu^2} \quad (4-19)$$

The effects of bouynacy become important part of the simulation process when this ratio approaches or exceeds unity. If the ratio is very small, buoyancy affects may be neglected in the calculation process. In cases where pure natural convection dominates, the strength of this type of the flow is presented by the magnitude of Reyleigh number:

$$Ra = \frac{g\beta\Delta TL^3 \rho}{\mu\alpha} \quad (4-20)$$

where  $\beta$  is thermal expansion coefficient and is given by following:

$$\beta = -\frac{1}{\rho} \frac{\partial \rho}{\partial T} \quad (4-21)$$

and where  $\alpha$  is thermal diffusivity given by:

$$\alpha = \frac{k}{\rho c_p} \quad (4-22)$$

Rayleigh numbers in range of less than  $10^8$  represent buoyancy induced laminar flows, while the transition to turbulence occurs over the range of  $10^8 < Ra < 10^{10}$ .

#### **4.5.6 Chemical Species Transport**

FLUENT/UNS has the capability to model chemically reacting flows and chemical species transport. There are two different reactions models that the code offers. They are generalized finite rate formulation and mixture fraction/PDF formulation. Generalized finite rate formulation allows user to define the mechanism of the reactions and calculate species transport equations for reactants and product concentrations. Fluent uses Arrhenius rate expression to calculate the reaction rates, which appear as source terms in the species transport equations. Mixture fraction/PDF formulation does not solve individual species transport equations. This method is mainly used for combustion calculations. Chemical species transport and reacting flow in this work will be modeled using generalized finite rate formation.

Species transport equation has the following form:

$$\frac{\partial}{\partial t}(\rho m_i) + \frac{\partial}{\partial x_i}(\rho u_i m_i) = -\frac{\partial}{\partial x_i} J_{i,i} + R_i + S_i \quad (4-23)$$

When conservation equations have to be solved for chemical species, FLUENT/UNS predicts local mass fraction of each species,  $m_i$ , through the solution of a convection-diffusion equation for the  $i$ 'th species.

#### **4.5.7 Mass Diffusion Coefficients**

##### **Fick's Law of Diffusion in Laminar Flows**

Mass diffusion coefficients are required whenever you are solving species transport equations in the multi-component flow. Mass diffusion coefficients are used to compute the diffusion flux of a chemical species as

$$J_{i'} = -\rho D_{i',m} \frac{\partial m_i}{\partial x_i} \quad (4-24)$$

where  $D_{i',m}$  is the diffusion coefficient for species  $i'$  in the mixture. Above equation is strictly valid when the mixture composition is not changing, i.e., for  $D_{i',m}$  independent of composition. This occurs in dilute mixtures when  $m_{i'} \ll 1$ . FLUENT/UNS allows one to specify  $D_{i',m}$  in a variety of ways, including  $D_{i'j'}$ , the binary mass diffusion coefficient of component  $i'$  in component  $j'$ .  $D_{i'j'}$  is not used directly, the diffusion coefficient in the mixture,  $D_{i',m}$ , is computed as

$$D_{i',m} = \frac{1 - X_{i'}}{\sum_{j', j' \neq i'} \frac{X_{j'}}{D_{i'j'}}} \quad (4-25)$$

where  $D_{i'j'}$  is the binary mass diffusion coefficient for species  $i'$  in species  $j'$ , and  $X_{i'}$  is the mole fraction of species  $i'$ .  $D_{i'j'}$  and  $D_{i',m}$  can be inputted for each species.

##### **Diffusion Calculation in Turbulent Flows**

In turbulent flows, governing equation is

$$J_{i'} = -\left( \rho D_{i',m} + \frac{\mu_t}{Sc_t} \right) \frac{\partial m_i}{\partial x_i} \quad (4-26)$$

where  $Sc_t$  is the effective Schmidt number for the turbulent flow given by:

$$Sc_t = \frac{\rho D_t}{\mu_t} \quad (4-27)$$

and  $D_t$  is the effective mass diffusion coefficient due to turbulence. In turbulent flows mass diffusion coefficient inputs consist of defining the molecular contribution to diffusion  $D_{i,m}$  using the same method available for laminar case, with the added option to alter the default settings for the turbulent Schmidt number. Default for Schmidt number is 0.7.

Enthalpy transport due to species diffusion becomes significant when the Lewis number is not unity. The advantage of this part of the solution is that FLUENT/UNS will include this term by default. Enthalpy contribution to the energy is given by

$$\nabla \cdot \left[ \sum_{i'=1}^n (h_{i'}) J_{i'} \right] \quad (4-28)$$

and Lewis number being

$$Le = \frac{\rho D}{k/c_p} \quad (4-29)$$

Reaction rate is defined as the sum of reaction sources over the  $k$  reactions that the species may participate:

$$R_{i'} = \sum_k R_{i',k} \quad (4-30)$$

where  $R_{i',k}$  is the rate of creation/destruction of species  $i'$  in reaction  $k$ . The reaction rate  $R_{i',k}$  is controlled by Arrhenius kinetic rate expression, given by

$$R_{i',k} = \Gamma \left( \nu'_{i',k} M_{i'} T^{\beta_k} A_k \prod_{j' \text{ reactants + products}} C_{j'}^{\nu'_{j',k}} \exp(E_k/RT) \right) \quad (4-31)$$

where  $\nu'_{i',k}$  is molar stoichiometric coefficient for species  $i'$  in reaction  $k$ ,  $M_{i'}$  is molecular weight,  $\beta_k$  is dimensionless temperature exponent,  $A_k$  pre-exponential factor,  $C_{j'}$  molar

concentration of each reactant or product species  $j'$ ,  $\nu_{j'k}$  exponent on the concentration of species  $j'$  in reaction  $k$  and  $E_k$  activation energy for the reaction.

Finally,

$$\Gamma = \sum_{j'=allspecies} C_{j'} \gamma_{j'k} \quad (4-32)$$

where  $\gamma_{j'k}$  is the third body efficiency of the  $j'$ th species in the  $k$ th reaction.

FLUENT/UNS does not include third-body efficiencies in the reaction rate calculation.

#### **4.5.8 FLUENT/UNS Numerical Scheme**

Partial differential equations for conservation of mass, momentum and some scalar quantities (such as chemical species) are solved in FLUENT/UNS. A control volume approach used consists of domain divided into control volumes through the use of computational grid. Discretized equations are created from the governing equations on each control volume and solved for unknowns (velocity, pressure and scalars). The governing equations are solved sequentially and convergence of the solution is not obtained until several iterations are performed. The overview of the solution process is shown in Figure 4-5. Each iteration during solution process consists of the following steps:

1. Velocity field is updated using current values for pressure in  $u$ ,  $v$ , and  $w$  momentum equations.
2. Solutions obtained in step one may not satisfy continuity equation and pressure correction equation is derived from continuity and linearized momentum equation. This pressure correction equation is then solved for necessary corrections such that continuity is achieved.

3. Updated velocity field is used to solve  $k$  and  $\varepsilon$  equations.
4. Energy, species and radiation equations are solved using updated values of other variables.
5. Fluid properties are updated.
6. In the case of interphase coupling, the source term in the appropriate continuous phase equations may be updated with a discrete phase trajectory calculation.
7. Convergence check is made.

These steps are repeated until convergence criteria are made. Detailed description of the discretization process can be found in Fluent Inc. (1996b).

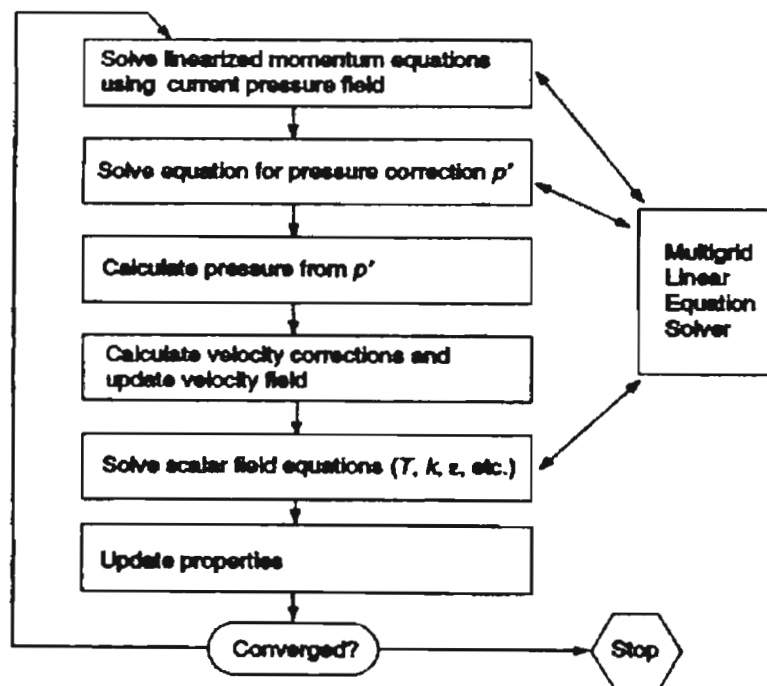


Figure 4-5. Overview of the Solution Process (Fluent Inc., 1996b)



#### 4.5.9 Pressure–Velocity Coupling

Coupling of velocity and pressure represents important part of the solution process. Continuity and momentum equations used to demonstrate this coupling were written in one-dimensional form, as follows

$$\text{Continuity:} \quad \frac{\partial}{\partial x}(\rho u) = 0 \quad (4-33)$$

$$\text{Momentum:} \quad \frac{\partial}{\partial x}(\rho u u) = -\frac{\partial p}{\partial x} + \frac{\partial}{\partial x} \left[ \mu \left( \frac{\partial u}{\partial x} \right) \right] + F \quad (4-34)$$

The one-dimensional momentum equation can be discretized using the procedure described in Fluent Inc. (1996b) to the following form

$$a_p u_p = \sum_{nb} a_{nb} u_{nb} + (p_w - p_c)A + S \quad (4-35)$$

while continuity equation may be discretized to the following form

$$J_e - J_w = 0 \quad (4-36)$$

where  $J$  is the mass flow rate,  $\rho u A$ . Substituting for  $J$ , we get

$$(\rho u A)_c - (\rho u A)_w = 0 \quad (4-37)$$

In order for the calculation process to continue, the velocities in Equation (4-37) must be related to the stored values. This is done through the momentum-weighted average, using factors from Equation (4-35). Therefore, the face flow rate,  $J_e$  may be written in the following form

$$J_e = \hat{J}_e + d_e (p_p - p_w) \quad (4-38)$$

where  $\hat{J}_e$  is impacted by velocities  $u_p$  and  $u_w$ , and  $d_e$  is given by

$$d_e = \frac{\rho_e A_e^2}{a_p} \quad (4-39)$$

The Semi-Implicit Method for Pressure-Linked Equations (SIMPLE) algorithm is used to resolve a problem of solving for pressure field from the continuity equation. Continuity equation does not relate density with pressure for incompressible flow, and that is the purpose of SIMPLE algorithm – to introduce pressure into continuity equation. The algorithm uses pressure and velocity corrections to enforce mass conservation and obtain pressure field. Using the result obtained for the face flux  $J_e^*$  in Equation (4-38)

$$J_e^* = \hat{J}_e + d_e (p_p^* - p_w^*) \quad (4-40)$$

for the initial estimate of the pressure field  $p^*$ , which is used to solve momentum equation. If Equation (4-40) does not satisfy continuity, correction factor is introduced such that the corrected value  $J_e$  satisfies continuity equation. The corrected value  $J_e$  is

$$J_e = J_e^* + J_e' \quad (4-41)$$

The algorithm defines  $J_e'$  as

$$J_e' = d_e (p_p' - p_w') \quad (4-42)$$

where  $p'$  is the cell pressure correction. The flux correction equations may be substituted into discrete continuity equation to obtain pressure correction discrete equation at point  $P$ :

$$a_p p_p' = \sum_{nb} a_{nb} p_{nb}' + b \quad (4-43)$$

where the net flow rate into the cell is defined as source term  $b$  and is given by:

$$b = J_w^* - J_e^* \quad (4-44)$$

Once the pressure field is obtained, pressure correction factor is used to correct cell pressure and the cell flow rate to following:

$$p_e = p_e^* + \alpha_p p_e' \quad (4-45)$$

$$J_e = J_e^* + d_e (p_p' - p_w') \quad (4-46)$$

where  $\alpha_p$  is the underrelaxation factor for pressure. The highlight of this algorithm is that the corrected face flow rate  $J_e$  satisfies the discrete continuity equation for each iteration in exactly the same manner.

#### **4.5.10 Residuals and Convergence**

At the end of each iteration during the solution process, the residual sum for each of the conserved variables is calculated and saved. As the solution converges, these residuals will become very small and approach zero. To define residual, lets look at the conservation equation for a general variable  $\phi$  at a cell  $P$ :

$$a_P \phi_P = \sum_{nb} a_{nb} \phi_{nb} + b \quad (4-47)$$

where  $a_P$  is the center coefficient,  $a_{nb}$  are the coefficients from the neighboring cells that affect the result, and  $b$  is the contribution of the constant part of the source term  $S_c$  in  $S = S_c + S_P \phi$  and of the boundary conditions. The coefficient  $a_P$  can be expressed as follows:

$$a_P = \sum_{nb} a_{nb} - S_P \quad (4-48)$$

The residual  $R^\phi$  is equal to the sum of inequalities over all computational cells and is calculated by FLUENT/UNS and referred to as “unscaled” residual. It is

$$R^\phi = \sum_{cells P} \left| \sum_{nb} a_{nb} \phi_{nb} + b - a_P \phi_P \right| \quad (4-49)$$

Since there is not any scaling involved with the use of already mentioned residual, it is difficult to judge whether the convergence is satisfactory. Therefore, the “scaled” residual is used to represent the flow rate of  $\phi$  through the domain and is represented by

$$R^{\phi} = \frac{\sum_{cellsP} \left| \sum_{nb} a_{nb} \phi_{nb} + b - a_p \phi_p \right|}{\sum_{cellsP} |a_p \phi_p|} \quad (4-50)$$

FLUENT/UNS allows user to monitor residuals and control the solution process by doing so. It is a powerful tool to supplement control and correct results.

This concludes the review of Fluent CFD package. Detailed guide on setup procedures used to establish the variety of computational domains and available methods of solution may be found in Fluent Inc. (1996b). This chapter reviewed only parts of the Fluent physical model, code requirements and capabilities utilized in this research.

## **CHAPTER V**

### **FLUENT 3D MODEL**

#### **5.1 Introduction**

When considering CFD analysis and before setting up the geometry and grid several choices have to be made regarding the modeling goals, choice of the computational model, solver, grid type and design. This chapter describes the development of the model based on the results required from CFD model, convergence criteria and feasibility of the model, which is followed by the discussion of the results obtained. Results obtained were related to the experimental data and previous work done using 2D geometry. Computational inputs and results from Fluent are placed in Appendix C. Initially, a substantial amount of time was spent learning the basic operations of the mesh generator and Fluent solver. More features were added to the problem as computational techniques and their advantages were learned through experience with simpler models. Boundary conditions were calculated based on the experimental data, while thermophysical properties were calculated mostly through the versatility of the solver where available. This chapter discusses techniques applicable to 3D model and is meant to supplement the discussion on the 2D model development found in Foster (1999).

## **5.2 Fluent 5 Model Development**

This section describes the development of the 3D model used in the analysis of the II-VI elements chemical reactor. Basis of the model developed were obtained together with Foster (1999) and used in order to draw a measurable comparison of 2D vs 3D modeling. Documentation regarding the development of the 3D model is included in Appendix B, starting with the geometry creation process, through meshing and finally to the physical model development.

After modeling goals were established, creation of the model geometry was initiated through the use of GeoMesh discussed in chapter IV. Within GeoMesh, the geometry generator part called DDN was used to create and modify geometry, before P-Cube was used to assign domain topology and boundary conditions. After the creation of surface mesh in P-Cube, TGrid was used to complete the meshing process by generating volume mesh inside the geometry. Steps used to complete this process are documented in Appendix B. Initially, FLUENT/UNS was the solver intended for final results, but the changes from Fluent Inc. and their development of a new, improved version of the solver, demanded some flexibility at the researchers end of the process. FLUENT 5 is used instead of FLUENT/UNS due to the modifications made within the solver from Fluent Inc. Fluent Inc. also developed its own geometry preprocessor for geometry setup and mesh generation called GAMBIT. Due to the complications resulting from the licensing and registration agreements regarding GeoMesh, this new geometry preprocessor was used to generate final mesh used in the writing of this thesis. The generation process of the mesh in GAMBIT is also referenced in Appendix B. FLUENT 5 is ideally suited for incompressible and compressible fluid flow simulations in complex geometries

combining solvers known as Rampant, Fluent/UNS and Fluent into one. Besides FLUENT 5, additional programs from Fluent Inc. include NEKTON, FIDAP, POLYFLOW, IcePak, and MixSim. FLUENT 5 graphical user interface (GUI) is made up of four main components: a console window, control panels, dialog boxes, and graphics window, similar to the components each solver had before they were combined. FLUENT 5 uses two types of numerical methods: segregated and coupled solver. Segregated solver is the solution algorithm previously used by FLUENT/UNS and described in section 4.5.8. The coupled solver is the solution algorithm previously used by RAMPANT. In the segregated solution method each discrete governing equation is linearized implicitly with respect to the dependent variable. In other words, each unknown value in the cell is calculated from the relation that includes both unknown and existing values from the neighboring cells. These equations must be solved simultaneously to compute unknown values.

Boundary conditions used to model the reactor were representative of the conditions encountered at Eagle-Picher Inc. They were assigned before the mesh was generated in GAMBIT and their physical values described in Appendix B. It is important to note that although the boundary conditions are assigned in geometry preprocessor, FLUENT has the capability of assigning and changing boundary conditions within the solver. This feature is very useful during experimenting part because it is time saving. Velocity inlets dictate basically what happens inside the reactor in this simulation. Fluent uses the boundary condition inputs at velocity inlets to compute the mass flow into the domain through the inlet and to compute the fluxes of momentum, energy, and species through the inlet. Note also, that outflow boundary condition is used for modeling flow

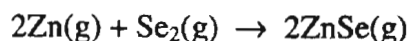
exits where the details of flow velocity and pressure are not known prior to the solution of the problem, as is the case here. For this boundary condition, FLUENT extrapolates the required information from the interior as a result of outflow boundary condition assigning zero diffusion flux for all flow variables and not having any impact on the upstream flow.

Chemical reaction is characterized by the strong rate (mass in moles of a product produced or reactant consumed per unit time) dependence on the temperature presented by the relation dating back to the nineteenth century in the following form:

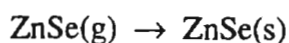
$$k(T) = Ae^{\frac{E_a}{RT}} \quad (5-1)$$

where  $E_a$  was first interpreted as an activation energy by Arrhenius in 1887 (Jordan, 1979). Version represented in the FLUENT reaction mechanism is given by the Equation 4-31.

Reaction mechanism, or a sequence of individual chemical events whose observed results produce the observed reaction, most likely takes the form of a second order reaction between two gaseous materials forming a solid. Due to the complexity of the phase change modeling only gaseous product is considered for this work. Modeling phase change may be a good step for the future work regarding this particular process. Therefore, reaction itself has the following form:



with the subsequent phase change taking place as



since the  $\text{ZnSe(g)}$  compound is very unstable. The heat of reaction is defined as the energy absorbed by the system when the products after reaction are restored to the same



temperature as reactants. Under the assumption that the pressure is the same for reactants and products, heat of reaction is equal to the enthalpy change. Using the output obtained from HSC Chemistry program located in Table B-6, enthalpy change was evaluated at 1000°C to be 66.52kJ for gaseous product. This value played a vital role in determining activation energy due to the assumption given by Laidler (1965) that relates enthalpy and activation energy as:

$$\Delta H_{reaction} = E_a - RT \approx E_a \quad (5-2)$$

Using the assumption stated above, change in enthalpy was converted to appropriate units for the input into FLUENT, resulting in activation energy of 6.65E+07 J/kmol. This value is somewhere in the middle of the range of activation energies calculated or estimated by Shay (1998) and Morrison (1998), which range from 1.90E+07 to 3.00E+08 J/kmol.

Pre-exponential factor A in the Arrhenius rate equation was obtained from the iterative procedure done by Foster (1999). Although, the predetermined value of this factor is used, it is important to note that it may be calculated according to the collision theory given by Smith (1970):

$$A = \sigma_{ZnSe_2}^2 \left( 8\pi R_g T \frac{M_{Zn} + M_{Se_2}}{M_{Zn} M_{Se_2}} \right)^{\frac{1}{2}} \quad (5-3)$$

where  $\sigma_{ZnSe_2}$  is effective diameter of Zn plus  $Se_2$  upon collision and  $R_g$  is product of Boltzmann's constant  $k$ , and Avogadro's number  $N$ . Using values from Table B-1 for effective diameters, value of 1.240E+08 m<sup>3</sup>/kmol-s was calculated and would be a good starting point for iteration process. Note that the value obtained through the iteration

process from Foster (1999) is much lower than the calculated starting value since the effects of inert carrier gas are excluded in collision theory.

For easier use of the available information for every run calculated in the application, a sequence of FLUENT commands called a journal file was used. Commands are arranged in the same order as they would be typed into the program or entered through the GUI, as in this case.

### **5.3 Convergence**

Satisfactory solution convergence is an important part of any computational problem. It is significant to know when the convergence has taken place and when further iteration is unnecessary. FLUENT 5 has its own means of suggesting when the solution reaches steady state through the monitoring of scaled residuals for energy and momentum equations. These residuals indicate the range of change for parameters calculated within each of the governing equations and offer a criterion for interrupting the iteration process once all of the criteria have been satisfied. These criteria vary for different modeling purposes, but default values offered in FLUENT are adequate for majority of applications (Fluent, Inc. 1998c). Default convergence criteria are shown in Table 5-1.

Fluent Inc. (1998c) recommends that the most popular approach is to require unscaled residuals to drop three orders of magnitude with the exception of several cases. One of the cases is where the initial guess used is very good, especially for a nearly isothermal flow where the initial guess is close to the final solution. Although the flow is

not isothermal, there are only small temperature variations inside the reactor if the inlet nozzles are excluded.

Table 5-1. Default Convergence Criteria used within FLUENT

Residuals	Convergence Criteria
Continuity	1.000E-03
x-velocity	1.000E-03
y-velocity	1.000E-03
z-velocity	1.000E-03
energy	1.000E-06
k	1.000E-03
epsilon	1.000E-03
Zn	1.000E-03
Se <sub>2</sub>	1.000E-03
ZnSe	1.000E-03

Segregated solver uses under-relaxation to control the update during each iteration for computed variables. This means that under-relaxation factors are associated with all equations solved. The default values for under-relaxation are set to values that are near optimal for many cases, but in case of increasing residuals they should be reduced. For instance, under-relaxation factor for the energy equation should be in the range 0.8 - 1.0 in the problems where the energy field impacts the fluid flow (via temperature dependant properties or buoyancy), as is the case in this research. Default value of energy under-relaxation factor is 1.0. Simulations using default under-relaxation factors were carried out and the results for residuals are presented in Table 5-2. Following default values, energy under-relaxation factor was reduced to 0.8 to improve solution convergence. To further improve the convergence, under-relaxation factors for pressure, momentum,  $k$ ,

and  $\epsilon$  are also reduced to the values of 0.2, 0.5, 0.5 and 0.5 respectively, resulting in slightly improved values, but not as nearly as expected along the lines of one order of magnitude. The default values are 0.3, 0.7, 0.8 and 0.8, respectively.

Similar to the results obtained by Foster (1999), residuals reach steady values with slight variation after roughly one hundred and twenty iterations, where satisfactory temperature and species distributions were attained without any significant changes in the profiles. Although the changes were not evident, iterations were carried out to the total number of 200 simply to eliminate possibility of unpredicted occurrences taking place. Residuals have larger oscillations during the 3D solution process than for the 2D cases, especially for the default under-relaxation factors, although the magnitude of the residuals is roughly the same as for 2D cases. Some typical residual values are shown in Table 5-2 comparing the effect gravity and under-relaxation factors have.

Table 5-2. Typical Residual Values for Default and Reduced Under-Relaxation Factors

Residual	Baseline Model Residuals	Gravity Effects Excluded Residuals	Baseline Model Residuals (reduced under-relaxation)	Gravity Effects Excluded Residuals (reduced under-relaxation)
Continuity	6.9440E-02	1.1045E-02	1.2677E-02	7.5525E-03
x-velocity	1.3087E-02	4.2410E-03	5.8698E-04	7.2526E-04
y-velocity	2.3556E-02	1.9184E-03	1.8520E-03	4.9547E-04
z-velocity	1.1391E-02	1.9289E-03	3.8396E-04	4.8747E-04
energy	4.3914E-04	1.8593E-03	2.1233E-05	1.4185E-04
k	5.3832E-03	4.9794E-04	2.3756E-04	2.7662E-04
epsilon	4.4693E-03	4.4394E-04	1.1029E-04	1.9265E-04
Zn	1.3996E-03	1.1049E-03	1.1446E-04	4.5089E-04
Se <sub>2</sub>	3.6990E-03	2.5009E-04	1.3576E-04	1.5070E-04
ZnSe	5.9416E-04	1.5355E-04	4.4279E-05	2.2369E-04

Residuals are approximately smaller one order of magnitude when there are no gravitational forces acting on the model. Gravitational force is the main reason final solution reaches oscillatory pattern documented in Figure 5-1. The values of residuals definitively vary more than for the 2D cases in the work by Foster (1999). Once the under-relaxation factors are reduced to previously mentioned values, excellent improvement in convergence is evident, as well as reduced variation. These new improved profiles may be seen in Figure 5-2.

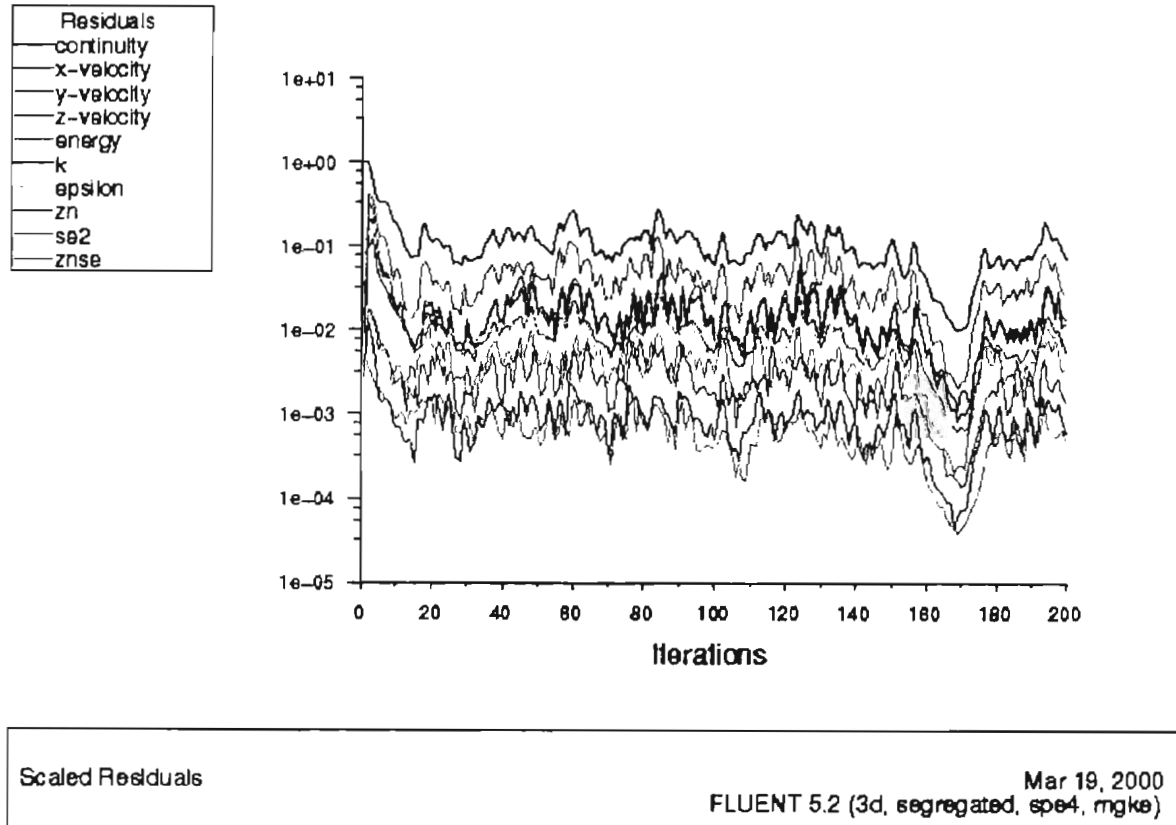


Figure 5-1. Residual Pattern for Baseline Model – Default Under-Relaxation

Mesh used for the development of the model was developed using unstructured grid with 39058 nodes. Unstructured solver uses internal data structures to maintain

contact with neighboring cells, faces, and grid points, does not force an overall structure or topology on the grid and does not use indexing to located neighboring cells. FLUENT 5 unstructured flow solver is usually used in cases of physical models for turbulence heat transfer, reacting flow, and chemical mixing (Fluent Inc., 1996).

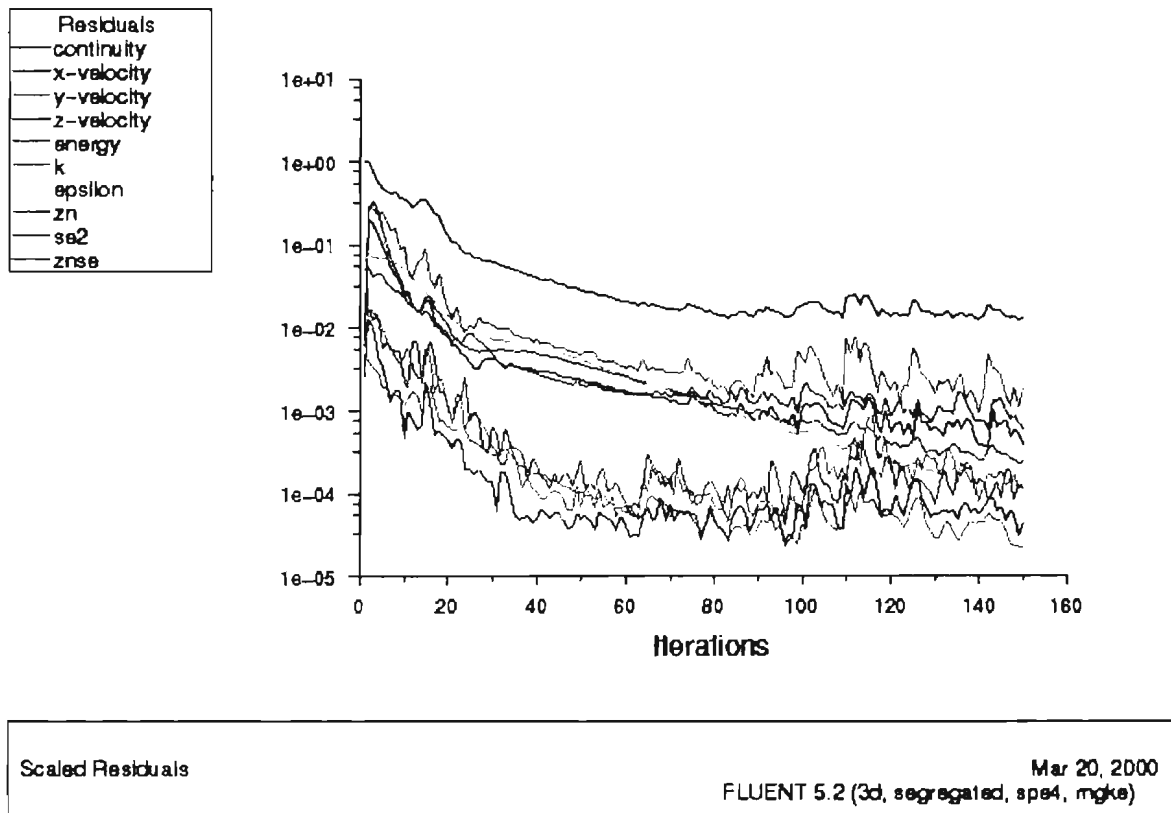


Figure 5-2. Residual Pattern for Baseline Model – Reduced Under-Relaxation

The advantage of unstructured grids over structured grids as given by Bathe (1998) is that structured grid is very effective when relatively simple geometries are considered. However, this approach is also used in mesh generation for the complex geometries using multiblock methods, in which the complete geometry is considered to be an assemblage of blocks, which is not the case in this research. The major difficulty is

to set up the connection between the blocks for complex geometries and varying grid-point spacing.

#### **5.4 Presentation and Comparison of Results**

In the development stages of the model, various options offered by the solver were considered and analyzed in order to obtain the best possible presentation of the reaction process and flow patterns inside the reactor. The model was best represented by RNG turbulence model due to its capabilities to represent buoyant effects on the flow. Turbulence effects on the flow are shown in the following three figures. First, Figure 5-3 shows the case with no gravity effects included in the model. The flow coming through the inlet nozzles does not experience buoyancy effects and continues unobstructed flow in the same direction with diffusion taking place in front of the zinc inlet. For this particular case product was formed only in the region of the reactor past the inlet nozzles due to the lack of recirculating zinc flow in the front of the reactor. Second case considered was considering laminar flow effects in the inlet region since the Reynolds number values indicate this type of behavior. Laminar flow shows the motion of the flow upward for the zinc inlet and downward for the selenium inlet due to the differences in the temperatures of the incoming flows and surroundings inside the reactor. Higher temperatures inside the reactor produce lower density regions with respect to the incoming flow, which promote diffusion effects once the flow enters the interior of the reactor. The question may rise why is zinc diffusion not directed toward the bottom of the reactor as is the case with selenium? Selenium flow enters the reactor in the bottom half and lowers the temperature inside the reactor resulting in the stronger diffusion force

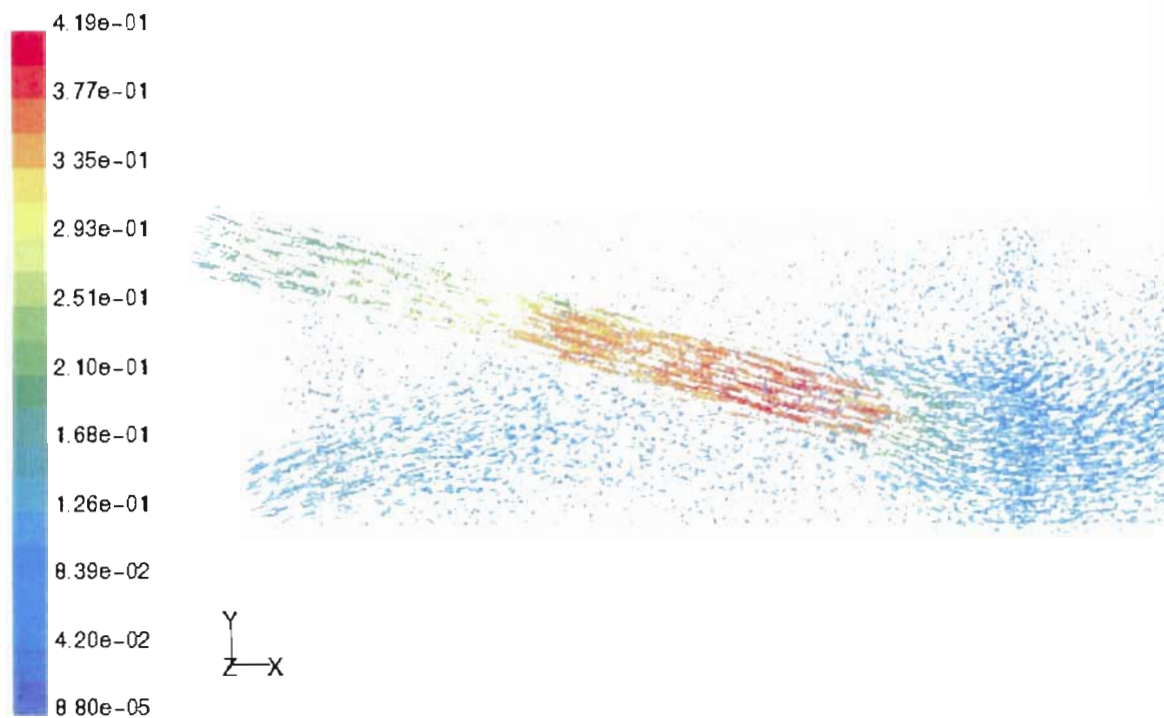


Figure 5-3. Gravity Effects Excluded (Velocity Magnitude, m/s)

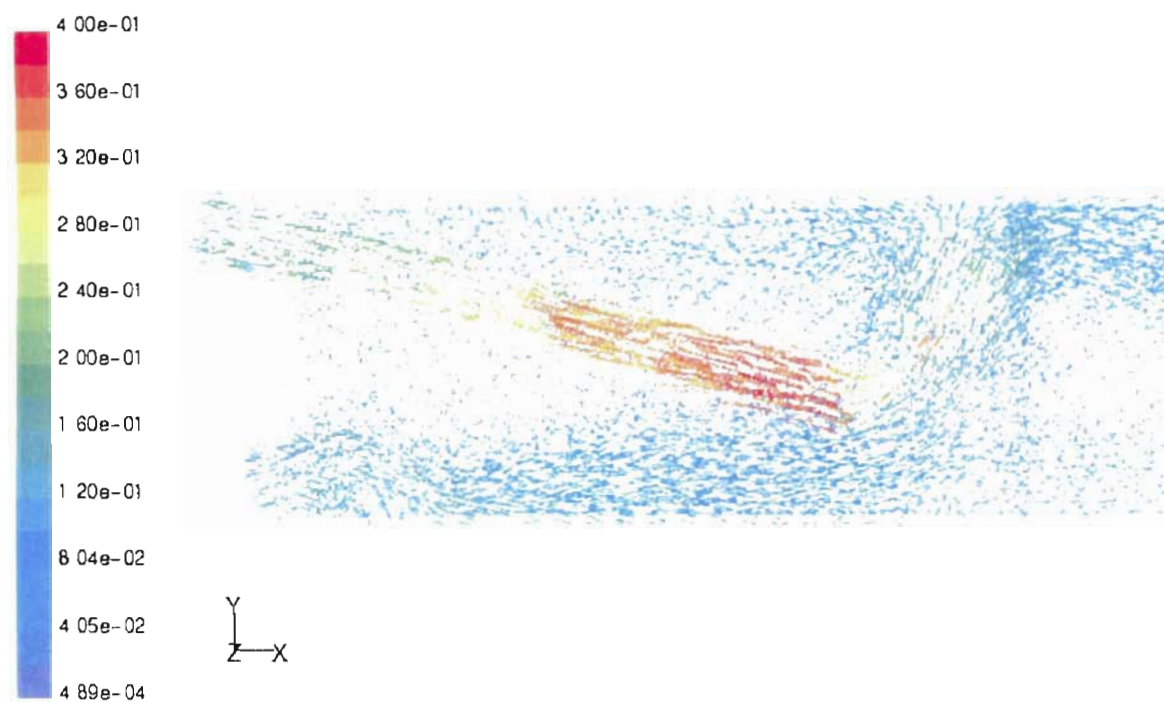


Figure 5-4. Reactor Inlet Affected by Laminar Flow (Velocity Magnitude, m/s)



toward the top of the reactor for zinc inlet species. These effects are shown in Figure 5-4. The difference between no gravity case which is optimal for the convergence of the model and the laminar flow shows the mixing patterns more likely to happen and justifies the known occurrence of the convection rolls at the top of the reactor.

Turbulence model displays the strongest effects of these diffusion forces, especially on the zinc flow inside the reactor, resulting in the almost vertical flow past the inlet. This is shown below in Figure 5-5.

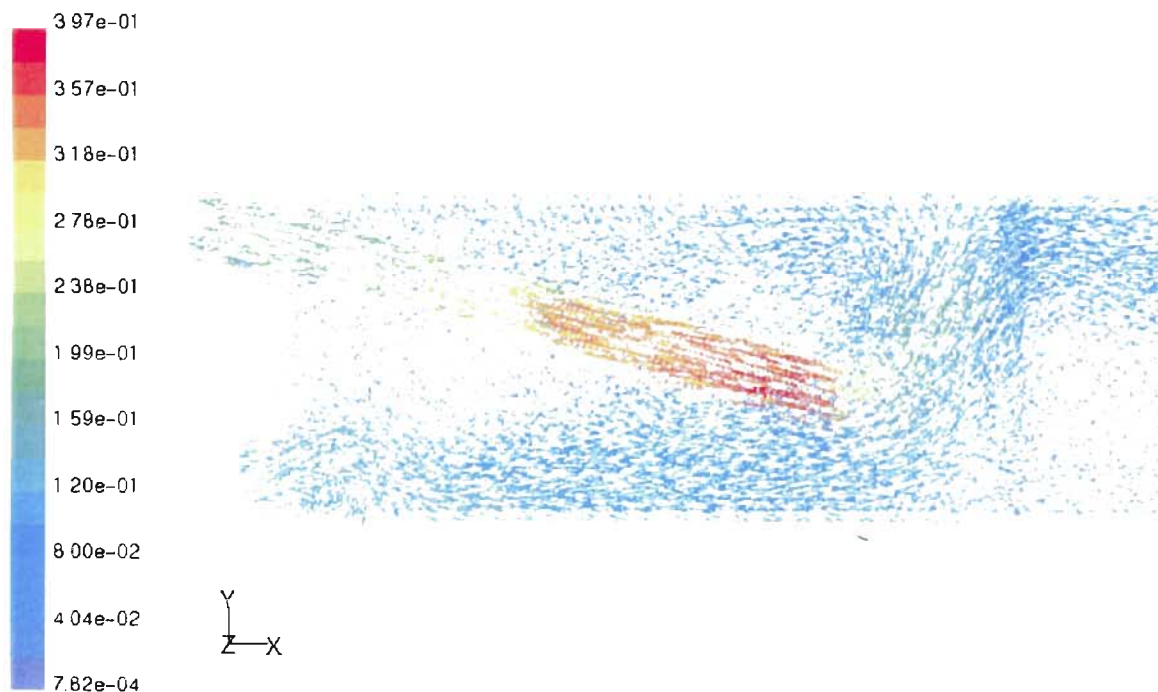


Figure 5-5. Reactor Inlet Effects (Turbulence Model, Velocity Magnitude, m/s)

The difference in results for three different options resulted in difference of yields as well. As it should be expected, poor mixing in the entrance region results in the lower yield. The lower yield is attributed to less contact between molecules inside the reactor,

therefore no gravity run resulting in the lowest yield. Slight difference in the full buoyancy effects available through the RNG model increased yield by less than one percent in comparison with the laminar model and showed that there is a difference between the three. Although one percent was not a significant difference, RNG model was used as the base model since it did not require additional amount of time and resources, but nevertheless it is better representation of the turbulent regions within the reactor. These results are shown in Table 5-3.

Table 5-3. Yield Results for Various Cases

Pre-exponential factor of 5000 for all cases	No Gravity Effects	Laminar	RNG Turbulence
Yield (%)	56.90	59.97	60.72

Effects of buoyancy on  $k$ - $\epsilon$  turbulence models may account for the generation of  $k$  through the term added to the right hand side of the equation 4-6. This term noted as  $G_b$  for ideal gases as is the case is defined as

$$G_b = -g_i \frac{\mu}{\rho Pr_i} \frac{\partial \rho}{\partial x_i} \quad (5-4)$$

where  $Pr_i = 1/\alpha$  and  $\alpha$  is given by equation 4-8. Foster (1999) uses the same model in the 2D solution of the same reactor system and hence the basis for comparison between the two models had to be the similarity in the options used.

After careful consideration of the results of 3D modeling it is concluded that there are certain advantages over a 2D model. Heat conduction in a gas is a process of diffusion, characterized by the wondering of molecules from warmer to colder zones and vice versa, and by the kinetic energy in the collisions of the molecules. These effects are

observed in the entrance region of the reactor where conduction was not confined by the geometry. In the 2D work done by Foster (1999), lack of the third dimension affects the distribution of the reactants inside the front zone of the reactor. Zinc inlet flow is diffused to the upper wall of the reactor where it splits in two directions, one part of the flow going toward the exit of the reactor and the other part of the flow flowing in the opposite direction from where it came from. This back flow causes the concentration of zinc to increase in the top part of the reactor since it is confined to that region by the inlet nozzle wall preventing it to mix with selenium concentration which is at the high level on the other side of this inlet nozzle. The inability to model mixing and therefore reaction in this region has effects on yield, which is the final outcome of the process. This is important because later we will discuss difference in the pre-exponential factor in the Arrhenius law equation for 2D and 3D models to represent the experimental data acquired. One of the reasons for this is the lack of reactions taking place in the front zone of the reactor. Although this particular geometric limitation of a 2D model occurs in the front zone of the reactor, effects are noticeable in the entire reactor through the increased concentration of the reactants, and decreased concentration of products. Since the reaction does not start taking place until both inlet flows get past zinc inlet, concentration of reactants remains higher by the factor of ten when compared to the concentrations of the same in 3D case.

Development of the 3D study started from duplicating the conditions of a 2D base line model. The results obtained were very surprising although the difference between the two was expected. Difference in the yield of the reaction was from 94.84% in 3D case to the 58.3 % given by Foster (1999), given the exact conditions used in 2D work

and applied to this model. The comparison may be seen in Table 5-4 for two different experimental runs.

Table 5-4. Result Comparison with 2D Pre-exponential Factor Value

Case	Experimental Yield (%)	Foster (1999) 2D Model Yield (%)	3D Model Yield (%)
BA 97202	63.1	58.3	94.84
BA 97195	56.9	61.6	95.71

Based on the results from Table 5-4, the only factor that was uncertain in the model input was pre-exponential factor value. This value was calculated from the theoretical formula to obtain the starting point value, which was far too large to be used in modeling. Therefore, the starting point became arbitrary value chosen by Foster (1999) based on the results that were satisfactory for BA 97202 and BA 97195. Information describing the two runs is located in Appendix C. The value obtained by Foster (1999) based on modeling results was 37500. Model developed for 2D case was based on duplicating the experimental results through the adjustment of the Arrhenius rate equation pre-exponential factor and finding the value that can be representation for both cases. This research actually concentrates on this dependence and tries to provide a design tool for the planning of future experiments.

Since the pre-exponential value used in 2D model yielded unreasonable results as far as product yield inside the reactor, some of the parameters had to be adjusted. The first and the only one that has the power of controlling the reaction rate inside the reactor is pre-exponential factor. A study was conducted to shed some insight on its effects on yields. These effects are shown in Figure 5-6.

BA 97202 was used as a baseline model to calculate the first set of data and get a general idea of effects this factor has. Pre-exponential factor values used in the study ranged from 1000 to 100000. In the range of 1000 to 10000 yield appears to be linearly dependant on the pre-exponential factor, while at the higher values it reaches asymptotic value. In order to duplicate experimental results available, pre-exponential factor of 5500 is a match based on the 63.1% yield of products. Second run used from the experimental set was BA 97195. The operating conditions for this case were different in comparison to the baseline model. Temperatures are higher by 100K across the three reactor zones and inlet flow rates are different. Zinc mass flow rate was 25% higher, while the total mass flow rate increase for the zinc inlet was 15.5% with respect to BA 97202. Selenium mass flow rate was also increased by 25%, while total mass flow rate for selenium entrance was 18% greater. Using the same value of pre-exponential factor that yielded exact experimental result for the baseline model, 17% higher yield (74%) resulted from the 3D model. If we look at the results from the other perspective and use a pre-exponential factor of 2700, experimental yield of 56.9% is duplicated for BA 97195, while the same factor results in 16% lower yield (47%) for BA 97202 (baseline model). These results together with the stoichiometric case are shown in Figure 5-6. Stoichiometric case shows virtually no difference from the baseline model, which is to be expected because all of the parameters were the same with the exception of zinc mass flow rate, which was increased by 13.5%. Another important point to notice in Figure 5-6 is the parallel shift in the results of the experimental run for the pre-exponential factor range of 1000 to 10000 in comparison with the baseline model. The result was computational yield of roughly 10%

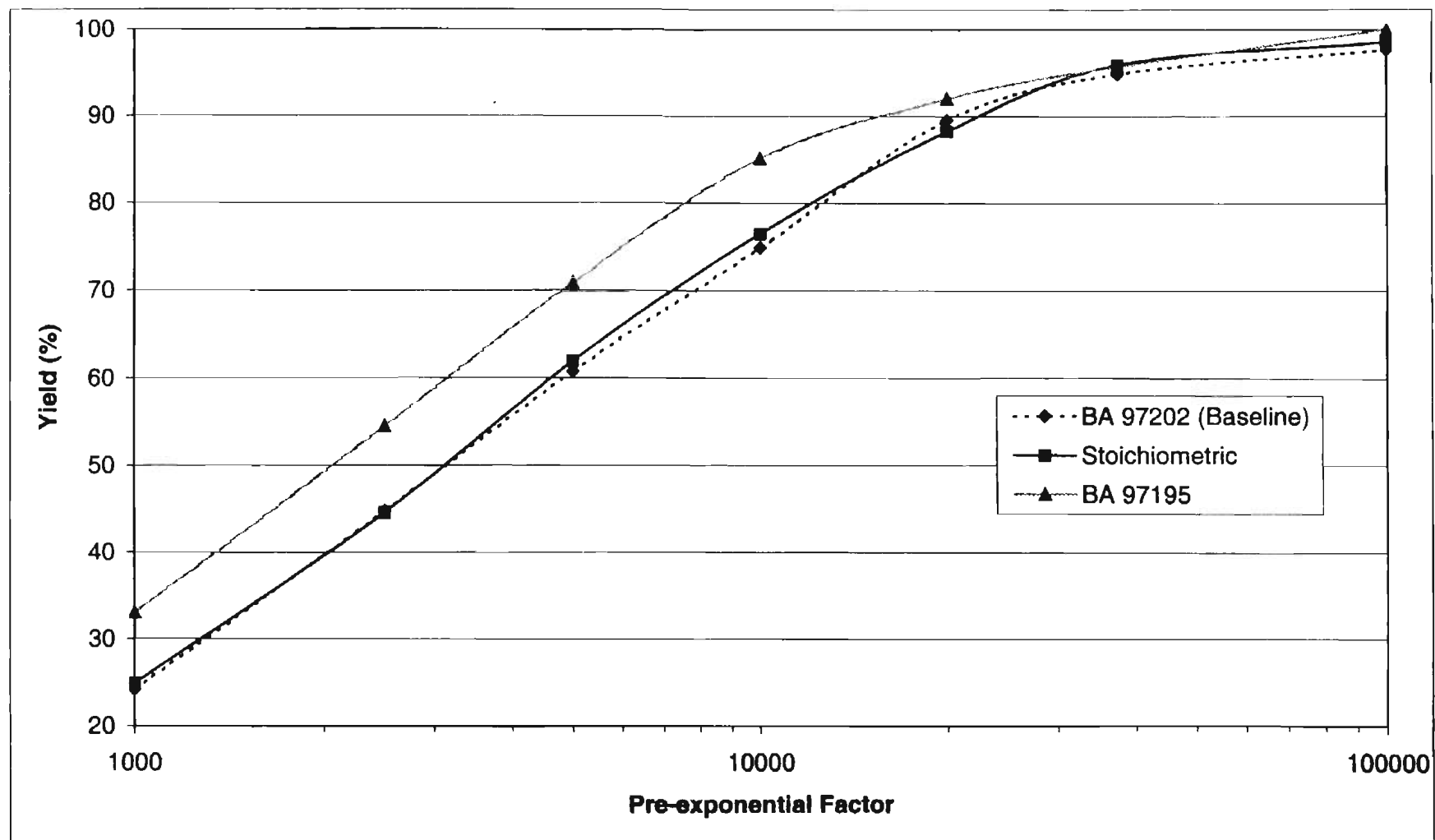


Figure 5-6. Pre-Exponential Factor Variation Effects on Yield

higher for the BA 97195 case. In the region between the two optimum values of 2700 and 5500 for pre-exponential factor, yield results are in the range of 47 to 74% for the computational model.

Foster (1999) conducted several parametric studies in his work that gave insight to the present research and direction to pursue. Reactant species flow rate effects on yield were studied for zinc inlet species and resulted in decreased yield for both higher and lower mass flow rates. This was the only parametric study conducted by Foster (1999) in which yield decreased regardless of whether the parameter was increased or decreased. As a direct result of his study, only total mass flow rates of the inlet species indicate the changes, keeping the reactant species mass flow rates of zinc and selenium the same. The results of this study are shown in Figure 5-7. Again the area of focus was region of pre-exponential factors ranging from 2700 to 5500. In this region, one can see that the decrease or increase of flow rates does not have strong influence on the product yield, resulting in the maximum yield variation of around 5%. Total yield range for this set of pre-exponential factor values was between 45 and 67% yield. Decrease of total mass flow rate of zinc inlet species resulted in longer residence time inside the reactor and more time for diffusion to take place, therefore increasing the yield by about 3%. Increase in these species flow rate resulted in slightly lower yield, around 1% over the entire range. Increase in total mass flow rate of selenium species had negligible effect on yield, which is a reasonable conclusion since excess of selenium already existed inside the reactor. The decrease in selenium species flow rate resulted in negligible difference in the lower part of the range and around 1% in higher part of the range.

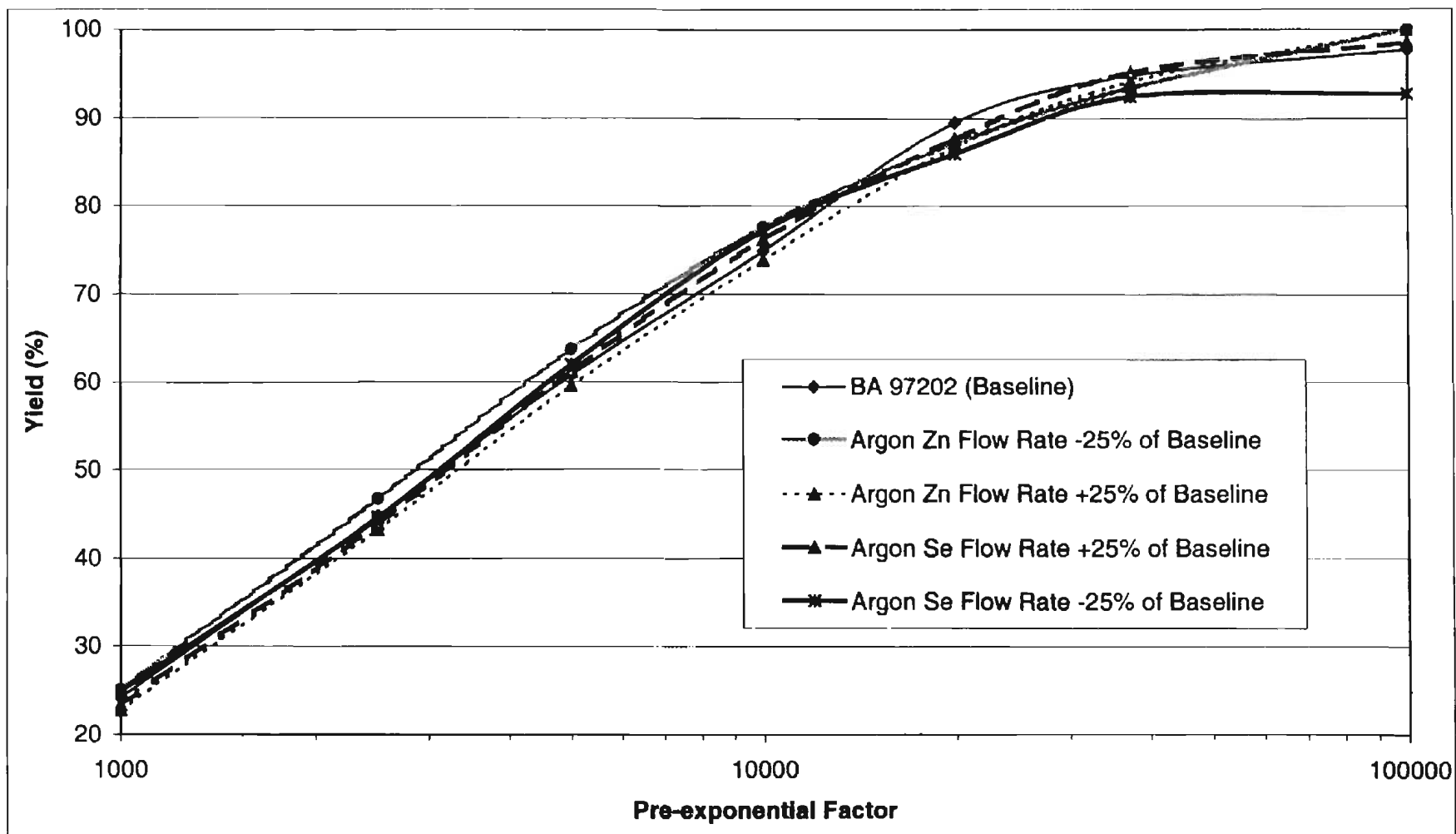


Figure 5-7. Pre-Exponential Factor Variation Effects on Yield (Flow Rate Case)



The last case considered was temperature difference in the middle reactor zone postulating that it has the most effect on the yield since the most reactions happen in this region. Results are shown in Figure 5-8. Middle zone reactor temperature was first lowered by 60K, which resulted in slight decrease of the yield. In the region of interest, this varies from 0 to 2% with respect to the baseline model. Once the temperature was increased to 1320K, which is 60K higher than the baseline model, the yield increase was immediate over the entire range of computational values. This increase varied from 5% at 2700 to 7% at pre-exponential value of 5500.

If we look at the product yield for the two cases discussed in this chapter, a parallel may be drawn between experimental and computational results. Experimental results had yield of 63.1 and 56.9% for runs BA 97202 and BA 97195 respectively. The calculated values for the two cases correspond to two different values of pre-exponential factors. Pre-exponential factor of 5500 gives the same result as experimental run BA 97202 (baseline), while factor of 2700 yields the same experimental result for BA97195. If pre-exponential factor of 5500 is used to calculate the reaction for the conditions of BA97195, yield of 74% is obtained, resulting in +29.8% difference from the experimental result. If the pre-exponential factor of 2700 is used to model conditions of baseline model, 47% yield is obtained resulting in -25.4% difference. These percent differences in the two cases considered are within the uncertainty of the limited experimental data obtained at Eagle-Picher Inc. Difficulties in duplicating data caused limited reliable experimental results, which do not have better uncertainty than the values obtained from the calculated results. One may reduce the uncertainty of the calculated

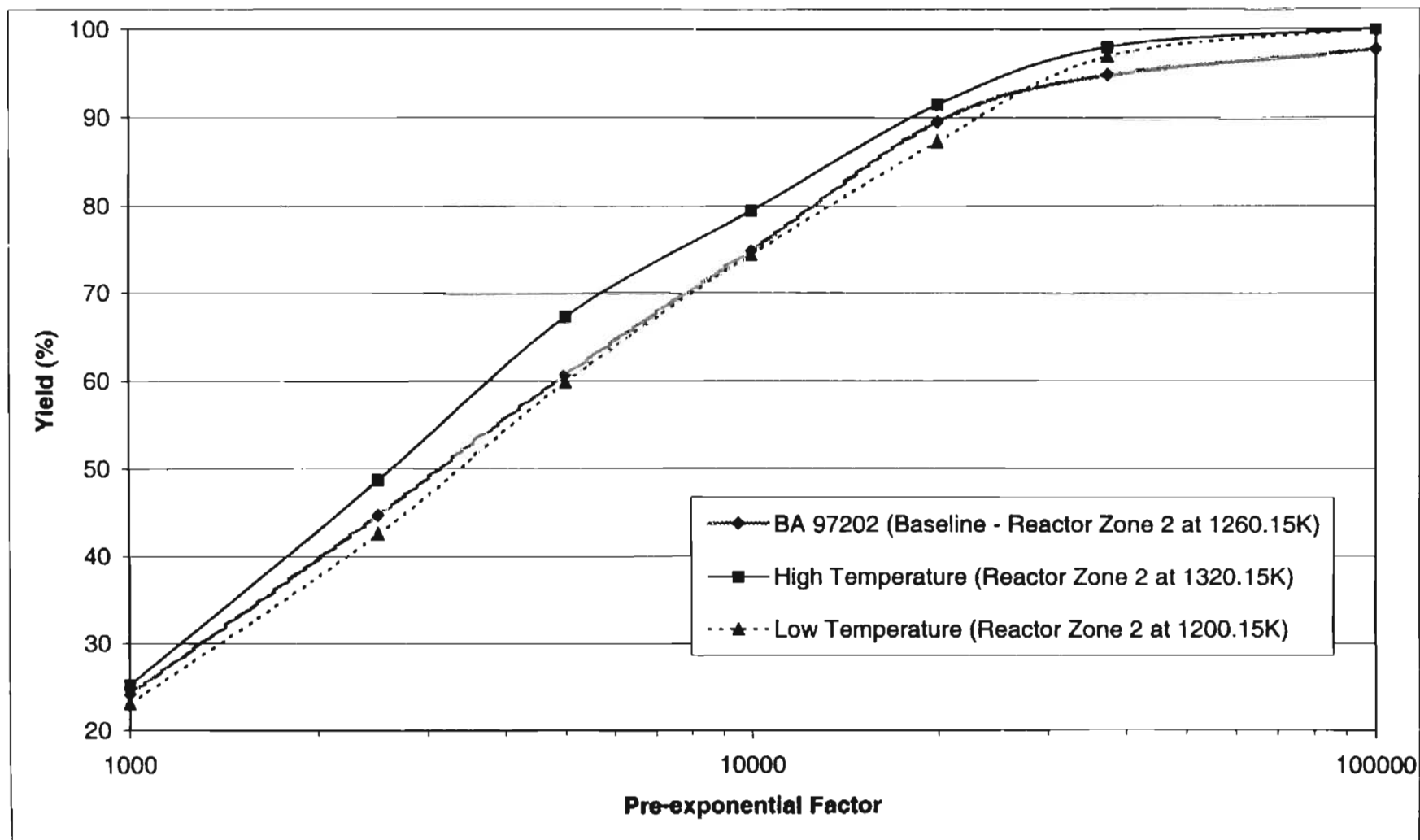


Figure 5-8. Pre-Exponential Factor Variation on Yield (Temperature Case)

values by choosing the pre-exponential factor that is in the middle of the 2700 to 5500 region. The pre-exponential value of 3900 seems to compromise between the two cases. For case BA97202, this factor provides a yield of 55%, or -12.7% difference from the experimental results. BA 97195 computational result using pre-exponential factor of 3900 results in a +14% difference or 65% yield. These uncertainty results are well beyond the uncertainty of the limited and unpredictable experimental data available.

The Arrhenius rate of reaction given by Equation 5-1 shows the exponential function dependency of this term on the temperature of the reaction. When the reaction temperature is increased, exponent raised to the negative power results in smaller values, which is inversely proportional to the rate. Therefore, rate is directly proportional to the temperature increase in the reactor. This can be seen from the results in Figure 5-8. If for example we use the value of 3900 for the pre-exponential factor, baseline model yield is 55%. For the case where the reaction conditions are the same with the exception of the middle zone temperature, which is raised by 60K, the same pre-exponential factor gives a yield of 61.5% or 11.8% increase in the product. In order to obtain the same amount of product, higher temperature case must have a reduced value of pre-exponential factor of 3200.

The key to the increased yields and the amount of products seems to point in the direction of reactor temperature. Foster (1999) concluded that front and rear zone temperature variation had minor effects on the yield, while the middle zone temperature had significant impact. That is a reasonable conclusion because the reactants mix mostly in this region and the majority of reactions take place in this zone. Flow rates are important also, although the values currently used seemed to be near optimum due to the

small change in results. It is important to note that based on the results mentioned in this chapter, one can use the information provided as a good starting point in predicting with certainty the outcome of the computational process.

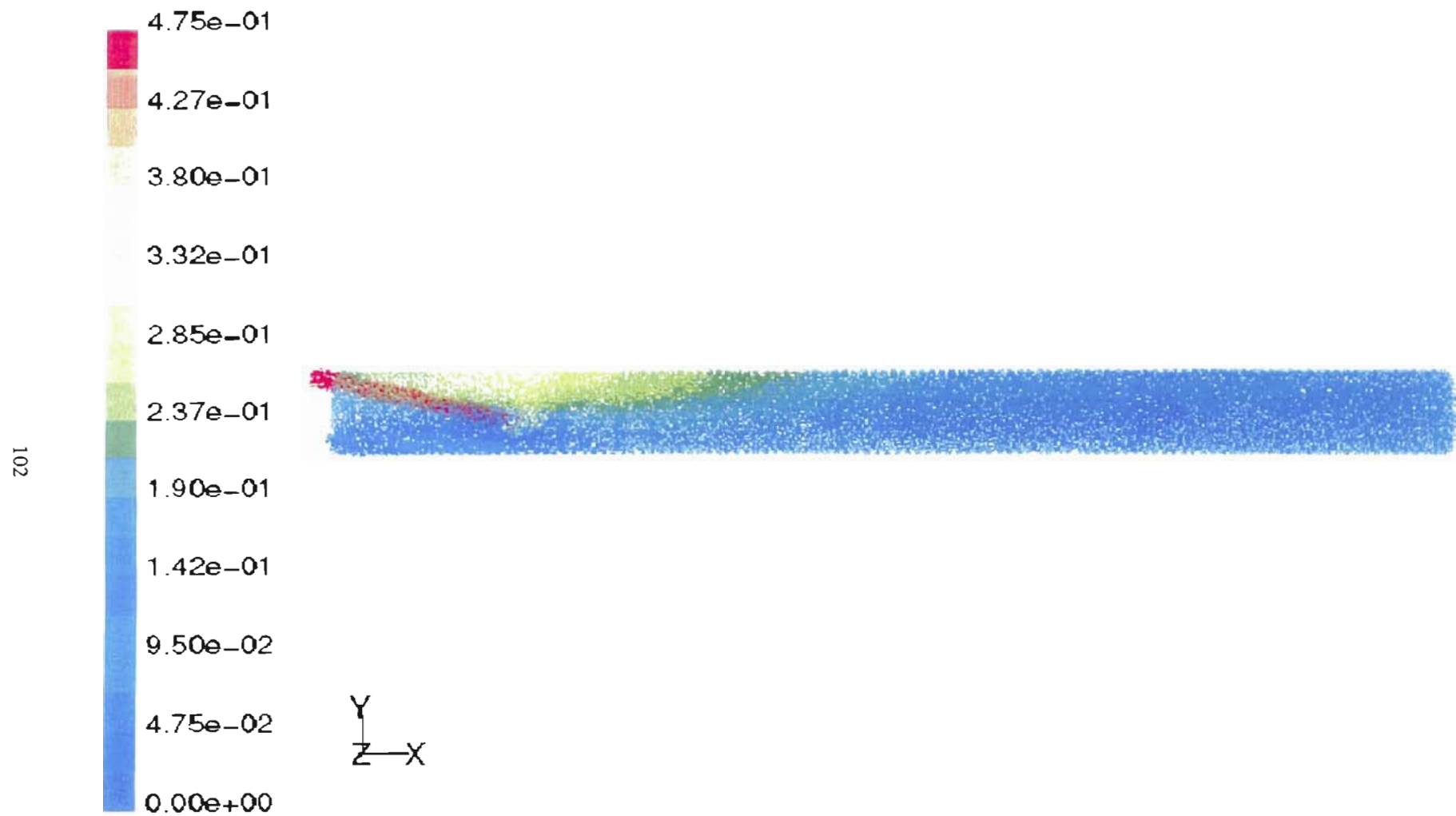


Figure 5-9. Velocity Vectors Colored by Concentration of Zn ( $\text{kg/m}^3$ )

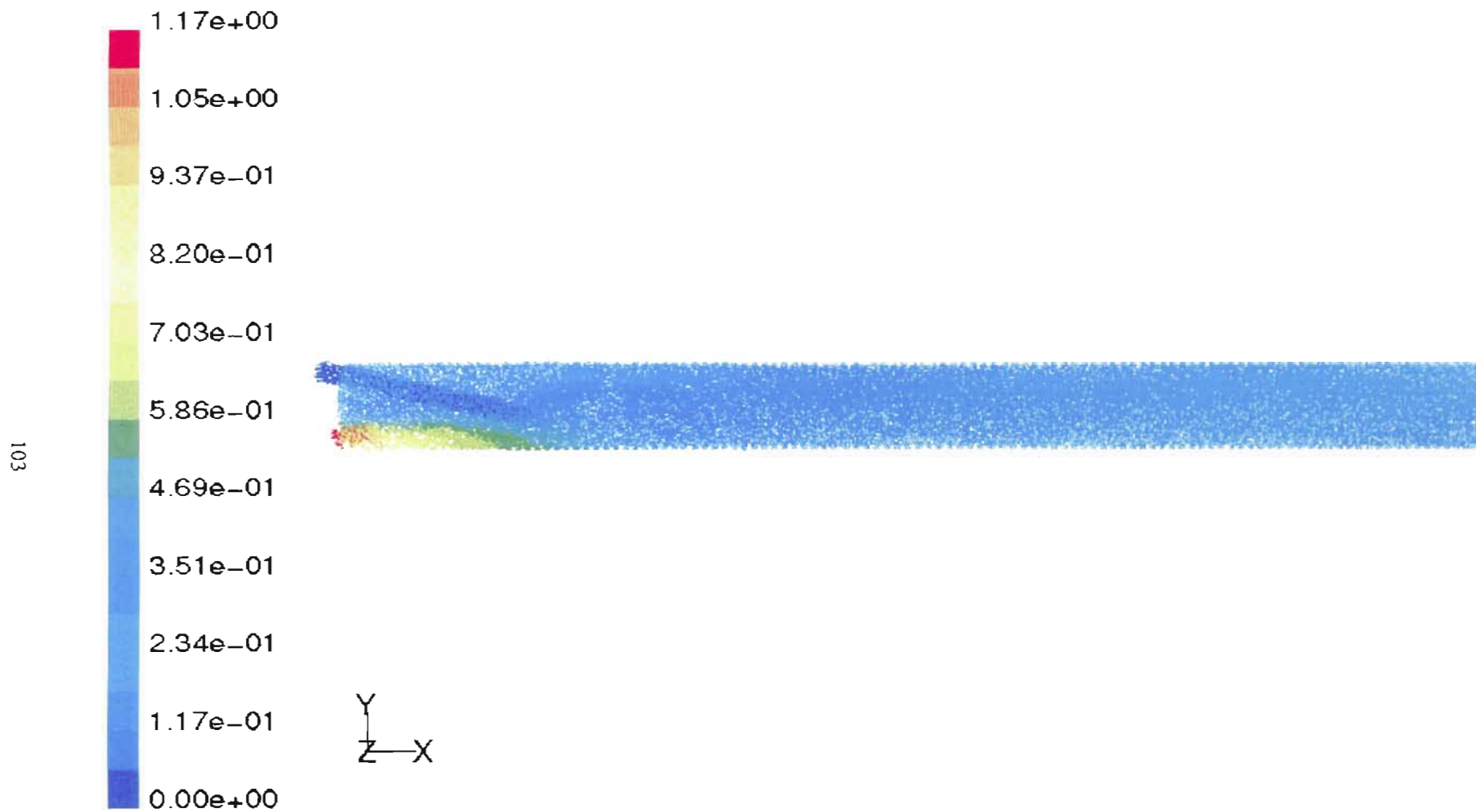


Figure 5-10. Velocity Vectors Colored by Concentration of Se ( $\text{kg/m}^3$ )

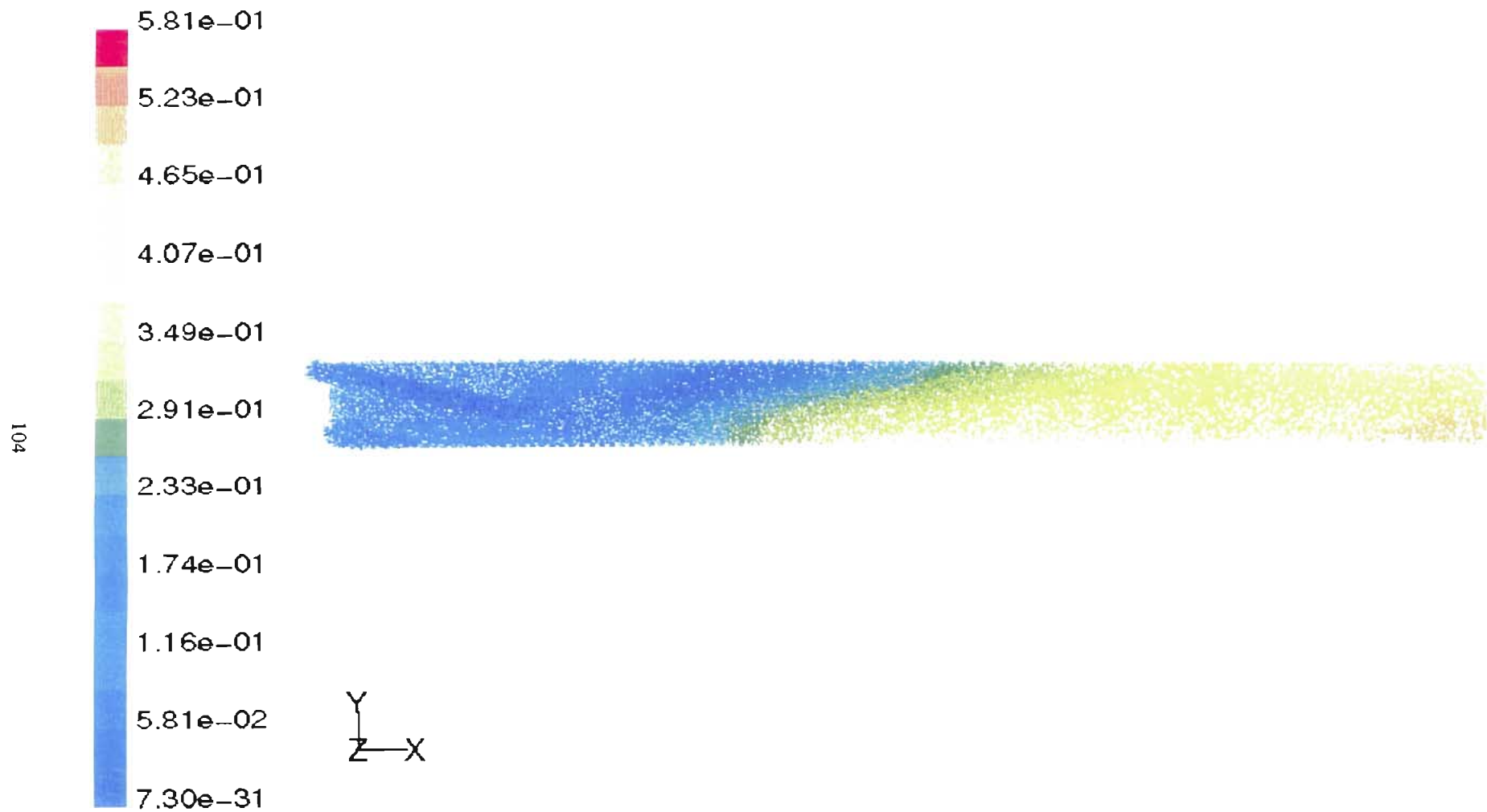


Figure 5-11. Velocity Vectors Colored by Concentration of ZnSe ( $\text{kg/m}^3$ )

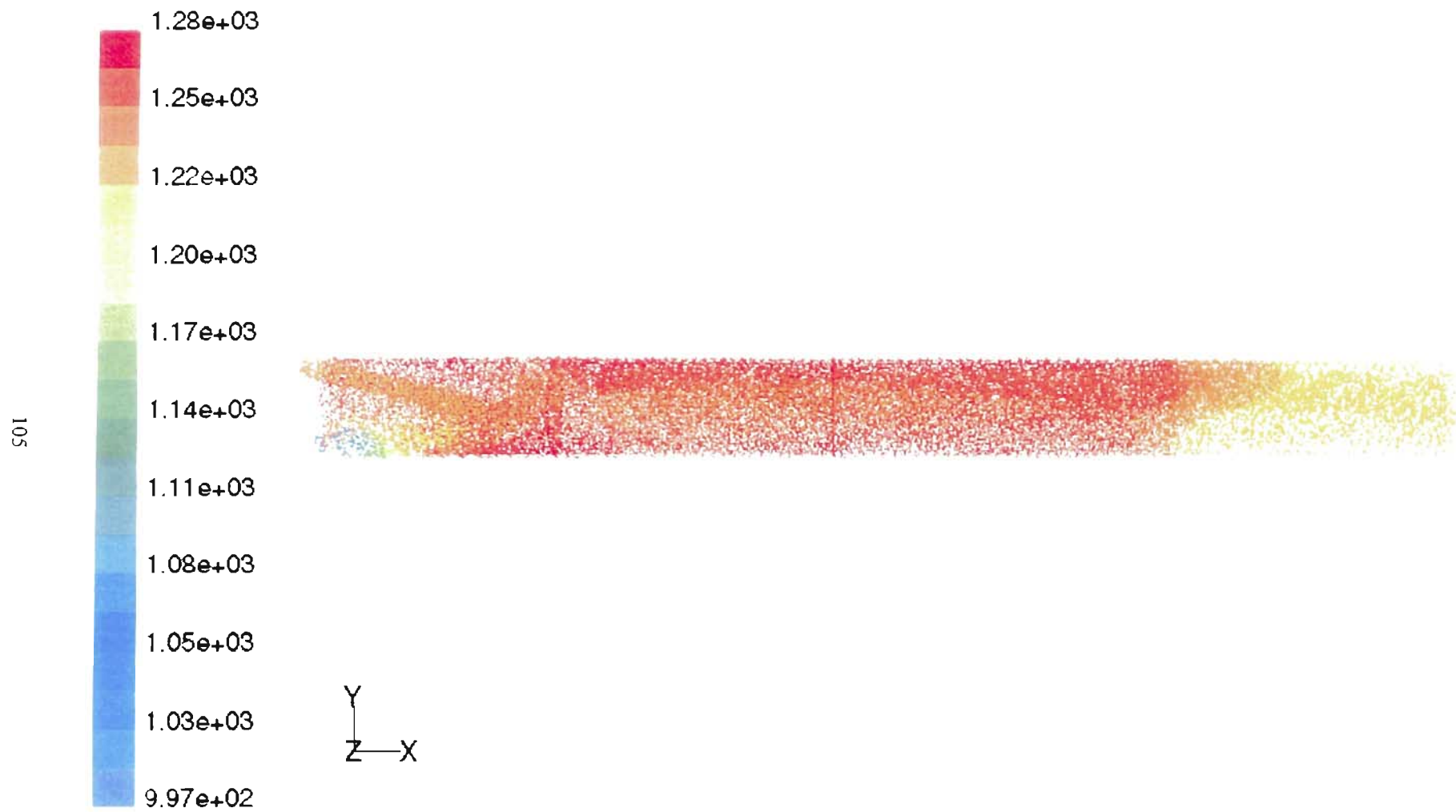


Figure 5-12. Velocity Vectors Colored by Static Temperature (K)



## CHAPTER VI

### CONCLUSIONS AND RECOMMENDATIONS

#### 6.1 Conclusions

Development of computational 3D model was a lengthy process with several obstacles to overcome. Lack of a good 3D starting point reference and changes made within the Fluent commercial code structure were two most challenging difficulties to overcome. The 3D FLUENT 5 model was developed and shown to be the best representation available of the Eagle-Picher Inc. process to date. Extensive documentation to outline the procedures used in the development of the model analyzed in this study is available for reference in Appendix B. This reference should be adequate starting point for future 3D modeling and can be used as a supplement to Fluent Inc. manuals.

With the 2D modeling done and referenced through the work of Foster (1999), Shay (1998) and Morrison (1998), 3D modeling showed further insight into predicting the behavior of species inside the reactor. Stronger visual and computational evidence is presented regarding the flow in the entrance region. In the entrance region of the reactor, flow became confined around inlets because of the limitations of 2D model's geometry. Comparison of a 2D model to the experimental data resulted in pre-exponential factor value of 37500 in the work of Foster (1999). In this study, the range for pre-exponential

factor falls between 2700 and 5500, with factor value of 3900 resulting in a 15% uncertainty of the computational results in comparison to the limited experimental data available.

Yield of reaction for the computational model was related to the pre-exponential factor through region of linear dependency and the region of asymptotic function (Figure 5-6). This relationship is based on the inversely proportional relationship pre-exponential factor has with respect to the reactor temperature. This relationship is seen through the reaction rate equation.

Sensitivity analysis was performed to analyze effects changes in flow rate and temperature in the middle zone of the reactor have on the yield of the ZnSe. Flow rate effects on the yield of the reaction were in the conservative range of up to 4% increase, while the temperature increase showed more significant improvement in yield, in the range of 7%.

The purpose of the material presented in Chapter V was to establish a basis that can be used as a design tool and a starting point for future works with similar criteria. These design basis references are best expressed through the Figures 5-6, 5-7 and 5-8 where the effects of variation of flow rates and middle zone reactor temperatures were considered and their effects on the pre-exponential factor and ZnSe yield were discussed.

## **6.2 Recommendations**

Uncertainty of limited experimental data collected from Eagle-Picher Inc. and difficulty of reproduction of results suggest that the process control needs to be updated and improvements recommended in the works of Morrison (1998), Shay (1998) and

Foster (1999) to be implemented. Once these basic improvements have been made, ideal operating conditions may be obtained by using the 3D model developed for the scope of this study as a starting point and a design tool in predicting some key parameters such as pre-exponential factor, flow rate and temperature influence. Better methods of acquiring flow rate information from the EP system are essential and would eliminate some uncertainty in the experimental and computational results. Failure of experiments and industrial devices to perform as anticipated sometimes may be caused by the unjustified theoretical approximations or because insufficient transport phenomena was considered and therefore further discussion and analysis on these topics would be important.

While 3D model was able to shine the light on several areas 2D model did not have capability to do, further modeling should be considered to provide even more insight into the effects inside the reactor as well as to model the process in its entirety. This focus should mainly include the effects and modeling of phase change taking place and focus on particle flow and heat transfer concerns. There is an abundance of literature available for two-phase study and computation, which could be investigated with advanced models. Also, radiation model should be considered and its impact on the process analyzed. Follow up to this study could be to establish a function relating three reactor zone temperatures to the pre-exponential factor. Using the work done in this thesis as a foundation of 3D computation, these and other improvements may be considered for further explanation.

## REFERENCES

- Alam, M. K., and Graham, G. (1996), "Simulation of SiC Deposition in a Fiber Coating CVD Reactor," *Materials and Manufacturing Processes*, Vol. 11, No. 5, pp. 821-835.
- Angermeier, D., Monna, R., Slaoui, A., and Muller, J. C. (1997), "Modeling and Analysis of the Silicon Epitaxial Growth with  $\text{SiHCl}_3$  in a Horizontal Rapid Thermal Chemical Vapor Deposition Reactor," *Journal of Electrochemical Society*, Vol. 144, No. 9, pp. 3256-3261.
- Babu, K. S. C., Pandey, R. N., and Srivastava, O. N. (1995), "Photoelectrochemical Semiconductor Septum ( $\text{CdSe/Ti}$  and  $\text{TiO}_2/\text{Ti}$ ) Solar cells in Relation to Hydrogen Production," *International Journal of Hydrogen Energy*, Vol. 20, No. 10, pp. 771-775.
- Bailar, J. C. and Trotman-Dickenson, A. F. (1973), "Comprehensive Inorganic Chemistry," Pergamon Press, Oxford.
- Barin, I., Kancke, O., and Kubaschewski, O. (1977), "Thermochemical Properties of Inorganic Substances," Supplement, Springer-Verlag, New York.
- Bathe, K. (1998), "Current Directions in Meshing," *Mechanical Engineering*, Vol. 120, No. 7, pp. 70-72.
- Bird, R. B., Stewart, W. E., and Lightfoot, E. N. (1960), "Transport Phenomena," John Wiley & Sons, New York.
- Bottcher, K., and Hartmann, H. (1995), "Zinc Selenide Single Crystal Growth by Chemical Transport Reactions," *Journal of Crystal Growth*, Vol. 146, pp. 53-58.
- Bottcher, K., Hartmann, H., and Rostel, R. (1996), "Influence of Convection on Zinc Selenide Single Crystal Growth by Chemical Vapour Transport," *Journal of Crystal Growth*, Vol. 159, pp. 161-166.
- Brasoveanu, D., and Gupta, A. K. (1994), "The Effect of Turbulence on Mixing and Flame Characteristics," *Industrial and Environmental Applications of Fluid Mechanics, ASME Fluid Engineering Division*, Vol. 186, No. 8, pp. 95-102.

- Cho, P. S., Ho, P. T., Goldhar, J., and Lee, C. H. (1994), "Photoconductivity in ZnSe Under High Electric Fields," *Journal of Quantum Electronics*, Vol. 30, No. 6, pp. 1489-1497.
- Choudhury, D. (1993), "A Study of Two Benchmark Heat Transfer Problems Using Fluent," *National Heat Transfer Conference*, pp. 21-30.
- Choudhury, D. (1995), "A FLUENT Simulation of Buoyancy-Driven Flow in a Square Enclosure with Variable Viscosity Effects," *Proceedings of the ASME Heat Transfer Division*, Vol. 317, No. Pt. 1, pp. 61-68.
- Cinnela, P. (1996), "Numerical Simulations of Reactive Flows," *ACM Computing Surveys*, Vol. 28, No. 1, pp. 93-98.
- Clark, L., and Woods, J. (1968), "Growth of Single Crystals of Cadmium Sulfide," *Journal of Crystal Growth*, Vol. 3, No. 4, pp. 127-130.
- Collins, D. J., Strojwas, A. J., and White, D. D., Jr. (1994), "A CFD Model for the PECVD of Silicon Nitride," *Semiconductor Manufacturing*, Vol. 7, No. 2, pp. 176-183.
- Detemmerman, T., and Froment, F. (1998), "Three Dimensional Coupled Simulation of Furnaces and Reactor Tubes for the Thermal Cracking of Hydrocarbons," *Revue de l'Institut Francais du Petrole*, Vol. 53, No. 2, pp. 181-194.
- Divis, R. (1997), "CdSe Synthesis," Procedure PS# 00171, Eagle-Picher, Inc., Miami, Oklahoma.
- Durst, F., Kadinski, L., and Schafer, M. (1995), "A Multigrid Solver for Fluid Flow and Mass Transfer Coupled with Grey-Body Surface Radiation for the Numerical Simulation of Chemical Vapor Deposition Process," *Journal of Crystal Growth*, Vol. 146, pp. 202-208.
- Eissler, E. E., and Lynn, K. G. (1995), "Properties of Melt-Grown ZnSe Solid-State Radiation Detectors," *Transactions on Nuclear Science*, Vol. 42, No. 4, pp. 663-667.
- Fluent Inc. (1996a), "Fluent GeoMesh Release 3.0 User's Guide," Vol. 2, March 28, 1996, Lebanon, New Hampshire.
- Fluent Inc. (1996b), "FLUENT/UNS and RAMPANT Release 4.0 User's guide," Vol. 2, March 28, 1996, Lebanon, New Hampshire.
- Fluent Inc. (1996c), "TGrid Release 2.4 User's guide," May 1996, Lebanon, New Hampshire.

- Fluent Inc. (1998), "FLUENT 5 User's guide," Vol. 3, July 27, 1998, Lebanon, New Hampshire.
- Foster, B. L. (1999), "2-D Rendering and Analysis of a Horizontal Zinc Selenide Aerosol Reactor via Computational Fluid Dynamics," M. S. Thesis, Department of Mechanical and Aerospace Engineering, Oklahoma State University, Stillwater, Oklahoma.
- Frerichs, R. (1947), "The Photo-Conductivity of Incomplete Phosphors," *Phys. Rev.*, Vol. 72, pp. 594-547.
- Garibin, E. A., Mironov, I. A., Khoruzhnikov, S. E., and Vorob'ev, A. N. (1996), "Numerical Study of Gasdynamics Influence on Three-Dimensional Transport Phenomena in Vertical Zinc Selenide LPCVD Reactor," *Materials Science and Engineering*, Vol. B39, pp. 8-14.
- Geyling, F., Hill, R., and Krishnan, A. (1996), "CFD Flow Simulations Improve Semiconductor Yield," *The National Engineer*, Vol. 100, No. 4, pp. 18-20.
- Ghajar, A. J., Foutch, G., and Johannes, A. (1996), "OSU-Eagle-Picher, Inc. OCAST Funding Proposal."
- Gobbert, M. K., Merchant, T. P., Borucki, L. J., and Cale, T. S. (1997), "A Multiscale Simulator for Low Pressure Chemical Vapor Deposition," *Journal of Electrochemical Society*, Vol. 144, No.11, pp. 3945-3951.
- Grace, T. M., Lien, S. Schmidl, W., Tse, D., Abdullah, Z., and Salcudean, M. (1998), "Validation of CFD-Based Recovery Furnace Models," *International Chemical Recovery Conference*, Vol. 1, pp. 271-281.
- Greene, L. C., Reynolds, D. C., Czyzak, S. J., and Baker, W. M. (1958), "Method for Growing Large CdS and ZnS Single Crystals," *Journal of Chemical Physics*, Vol. 29, No. 6, pp. 1375-1380.
- Halloin, V. L., and Wajc, S. J. (1996), "Physical and Numerical Simulations of Creeping Flow and Heat Transfer in Forehearths," *Chemical Engineering Comm.*, Vol. 154, pp. 59-85.
- Hamad, F. A., and Khan, M. K. (1998), "Natural Convection Heat Transfer in Horizontal and Inclined Annuli of Different Diameter Ratios," *Energy Convers. Mgmt.*, Vol. 39, No. 8, pp. 797-807.
- Healy, P. D., and Ayers, J. E. (1993), "CdZnSe Ohmic Contacts for II-VI Based Blue-Green Emitters," *Conference Proceedings on Lasers and Electro-Optics Society Annual Meeting*, pp. 650-651.

- Heraeus Amersil (1986), "Price List: Fused Silica, Fused Quartz," Heraeus Amersil Inc., Sayreville, New Jersey.
- Hilgenstock, A., and Ernst, R. (1996), "Analysis of Installation Effects by Means of Computational Fluid Dynamics – CFD vs. Experiments?," *Flow Measurement and Instrumentation*, Vol. 7, No. 3-4, pp. 161-171.
- Huang, C., and Kim, R. H. (1996), "Three-Dimensional Analysis of Partially Open Butterfly Valve Flows," *Journal of Fluids Engineering*, Vol. 118, No. 3, pp. 562-568.
- Huang, Z. C., Wie, C. R., Na, I., Luo, H., Mott, D. B., and Shu, P. K. (1996), "High Performance ZnSe Photoconductors," *IEEE Electronics Letters*, Vol. 32, No. 16, pp. 1507-1509.
- Jensen, K. F. (1987), "Micro-Reaction Engineering Applications of Reaction Engineering to Processing of Electronic and Photonic Materials," *Chemical Engineering Science*, Vol. 42, No. 5, pp. 923-958.
- Jones, A. K. (1997), "Computer Simulation Increases Boiler Capacity," *Power Engineering*, Vol. 101, No. 7, pp. 42-45.
- Kadinski, L., Makarov, Y. N., Schafer, M., Vasil'ev, M. G., and Yuferev, V. S. (1995), "Development of Advanced Mathematical Models for Numerical Calculations of Radiative Heat Transfer in Metalorganic Chemical Vapour Deposition Reactors," *Journal of Crystal Growth*, Vol. 146, pp. 209-213.
- Kelkar, A. S., Mahajan, R. L., and Sani, R. L. (1996), "Real-Time Physiconeural Solutions for MOCVD," *Journal of Heat Transfer*, Vol. 118, No. 11, pp. 814-821.
- Kobayashi, T., and Yoda, M. (1987), "Modified  $\kappa$ - $\epsilon$  Model for Turbulent Swirling Flow in a Straight Pipe," *JSME International Journal*, Vol. 30, No. 259, pp. 66-71.
- Kolpatzik, S. J., Hilgenstock, A., Dietrich, H., and Nath, B. (1998), "The Location of Temperature Sensors in Pipe Flows for Determining the Mean Gas Temperature in Flow Metering Applications," *Flow Measurement and Instrumentation*, Vol. 19, No. 1, pp. 43-57.
- Krishnan, A., and Zhou, N. (1995), "Analysis of Chemical Vapor Deposition in Industrial Reactors," *ASME JSME Thermal Engineering Joint Conference*, Vol. 4, pp. 113-120.
- Krispin, J., Glaz, H. M., and Collins, J. P. (1996), "High-Resolution of Stiff Chemically Reacting Flows," *Journal of Thermophysics and Heat Transfer*, Vol. 10, No. 4, pp. 570-578.
- Kucharczyk, M., and Zabłudowdka, K. (1986), "Review of Methods for Preparation of Zinc and Cadmium Sulfide, Selenide, and Telluride Single Crystals," NASA

- Technical Memorandum, National Aeronautics and Space Administration, Washington D. C. 20546.
- Kurada, S., Rankin, G. W., and Sridhar K. (1997), "A New Particle Image Velocimetry Technique for Three-Dimensional Flows," *Optics and Lasers in Engineering*, Vol. 28, No. 5, pp. 343-376.
- Laidler, K. J. (1965), "Chemical Kinetics," second edition, McGraw-Hill, Inc.
- Leung, R. B., Komplin, N. J., Ellis, A. B., and Tabatabaie (1991), "Photoluminescence Studies of Silver-Exchanged Cadmium Selenide Crystals: Modification of a Chemical Sensor for Aniline Derivatives by Heterojunction Formation," *Journal of Physical Chemistry*, Vol. 95, No. 15, pp. 5918-5924.
- Liu, B., McDaniel, A. H., and Hicks, R. F. (1991), "Modeling of the Coupled Kinetics and Transport in the Organometallic Vapor-Phase Epitaxy of Cadmium Telluride," *Journal of Crystal Growth*, Vol. 112, pp. 192-202.
- Mackowski, D. W., Rao, V. R., and Knight, R. W. (1996), "Effect of Solid Phase Heat Transfer and Wall Deposition on Crystal Growth in Physical Vapor Transport Ampoules," *Journal of Crystal Growth*, Vol. 165, pp. 323-334.
- Mahajan, R. L. (1996), "Transport Phenomena in Chemical Vapor-Deposition Systems," *Advances in Heat Transfer*, Vol. 28, pp. 339-425.
- Min-Yen, Y. (1996), "ZnSe Growth by Ion Laser Assisted Metalorganic Chemical Vapor Deposition," *Semiconductor Electronics, Proceedings*, pp. 101-104.
- Morrison, D. R. (1998), "Analysis and Design of a Laminar Flow Aerosol Reactor for the Production of ZnSe Powder," M. S. Thesis, Department of Chemical Engineering, Oklahoma State University, Stillwater, Oklahoma.
- Murakami, S., Sakachi, Y., Nishino, H., Saito, T., Shinohara, K., and Takigawa, H. (1992), "Compositional Profile of HgCdTe in Metalorganic Chemical Vapor Deposition (MOCVD) System with Multinozzles," *Journal of Crystal Growth*, Vol. 117, pp. 33-36.
- Nami, Z., Misman, O., Erbil, A., and May, G. S. (1997), "Effect of Growth Parameters on TiO<sub>2</sub> Thin Films Deposited Using MOCVD," *Journal of Crystal Growth*, Vol. 179, pp. 522-538.
- Nesmeyanov, A. N. (1963), "Vapour Pressure of the Elements," Academic Press, New York.
- Nietsche, R. (1971), "Crystal Growth and Phase Investigations in Multi-Component Vapour Transport," *Journal of Crystal Growth*, Vol. 9, pp. 238-243.



- Oseid, K., Kim, S., and Choudhury, D. (1994), "Turbulent Heat Transfer in a Backstep Geometry – Benchmark Calculations Using Fluent," *Proceedings of Winter Annual Meeting of the ASME*, pp. 1-10.
- Outokumpu Research Oy (1997), "HSC Chemistry for Windows," Version 3.0, Pori, Finland.
- Patankar, S. V. (1980), "Numerical Heat Transfer and Fluid Flow," Hemisphere, New York.
- Piper, W. W., and Polich, S. J. (1961), "Vapor-Phase Growth of Single Crystals of II-VI Compounds," *Journal of Applied Physics*, Vol. 32, No. 7, pp. 1278-1279.
- Reynolds, D. C., and Czyzak, S. J. (1950), "Single Synthetic Zinc Sulfide Crystals," *Phys. Rev.*, Vol. 79, pp. 543-548.
- Roy, R. P., Agarwal, V., Devasenathipathy, S., He, J., Meier, L., Kim, Y. W., Howe, J., and Ho, K. (1997), "A Study of the Flow Field and Convective Heat Transfer in a Model Rotor-Stator Cavity," *Proceedings of the ASME Heat Transfer Division*, Vol. 353, No. 3, pp. 97-107.
- Saul, A. J., and Svejksky, K. (1994), "Computational Modeling of a Vortex CSO Structure," *Water Science & Technology*, Vol. 30, No. 1, pp. 97-106.
- Sha, Y., Su, C., Palosz, W., Volz, M. P., Gillies, D. C., Szofran, F. R., Lehoczky, S. L., Liu, H., and Brebrick, R. F. (1995), "Mass Flux of ZnSe by Physical Vapor Transport," *Journal of Crystal Growth*, Vol. 146, pp. 42-48.
- Shay, C. (1998), "Design and Optimization of a High Temperature Reactor for the Production of Group II-VI Compounds Via Computer Models and Statistical Experimentation," M. S. Thesis, Department of Chemical Engineering, Oklahoma State University, Stillwater, Oklahoma.
- Smith, J. M. (1970), "Chemical Engineering Kinetics," second edition, McGraw-Hill, Inc.
- Takigawa, H., Nishino, H., Saito, T., Murakami, S., and Shinohara, K. (1992), "Metalorganic Chemical Vapor Deposition Growth of CdTe on GaAs in a Vertical Reactor with Multi-Nozzles," *Journal of Crystal Growth*, Vol. 117, pp. 28-32.
- Tehver, R., Toigo, F., Koplik, J., Banavar, J. R. (1998), "Thermal Walls in Computer Simulations," *Physical Review E*, Vol. 57, No. 1, pp. R17-R19.
- Touloukian, Y. S., and Makita, T. (1970), "Thermophysical Properties of Matter: Specific Heat – Nonmetallic Liquids and Gases," Vol. 6, IFI/Plenum, New York.

- Uehigashi, A., Sugiura, S., Morinishi, K., and Satofuka, N. (1992), "Numerical Investigation Using Compressible Navier-Stokes Equations for Low-Speed Flow in Pipes with Varying Cross Section," *JSME International Journal*, Vol. 35, No. 4, pp. 507-512.
- Vakikilainen, E., Kjaldman, L., Taivassalo, V., Kilpinen, P., and Norstrom, T. (1998), "High Solids Firing in an Operating Recovery Boiler – Comparison of CFD Predictions to Practical Observations in the Furnaces," *International Chemical Recovery Conference*, Vol. 1, pp. 245-256.
- Waliszewski, M. W., Fry, D. L., Kuban, B. D., and Friedman, M. H. (1994), "Calculation of 3-D, Pulsatile Velocity Fields and Endothelial Shear Stress Distributions in an Arterial Organ Support System and Validation by LDA," *Advances in Bioengineering*, Vol. 28, pp. 429-430.
- Wendel, M. W., Chen, N. C. J., and Keith, K. D. (1996), "Computational Fluid Dynamics Tracking of UF<sub>6</sub> Reaction Products Release into a Gaseous Diffusion Plant Cell Housing," *ASME Fluids Engineering*, Vol. 238, No. 3, pp. 529-533.
- Wenisch, H., Schull, K., Behr, T., Hommel, D., Landwehr, G., Siche, D., Rudolph, P., and Hartmann, H. (1996), "(Cd, Zn)Se Multi-quantum-well LEDs: Homoepitaxy on ZnSe Substrates and Heteroepitaxy on (In, Ga)As/GaAs Buffer Layers," *Journal of Crystal Growth*, Vol. 159, pp. 26-31.
- Yu, Z., Ren, J., Sneed, B., Bowers, K., Cook, J. W., Jr., Schetzina, J. F., Hua, G. C., and Otsuka, N. (1992), "Blue Laser Diodes and LEDs Based on II-VI Semiconductor Heterostructures," *IEEE Transactions on Electron Devices*, Vol. 39, No. 11, p. 2653.

## **APPENDIX A**

### **REACTOR DIMENSIONS AND TEMPERATURE DATA**

This Appendix contains drawings of the reactor tube used in the experimental study and computational solution. The drawings of the reactant boilers may be seen in the thesis of Foster (1999).

Temperature data is shown to support the conclusions from Chapter III. This is the data acquired during the experimental study of the system at Eagle-Picher.

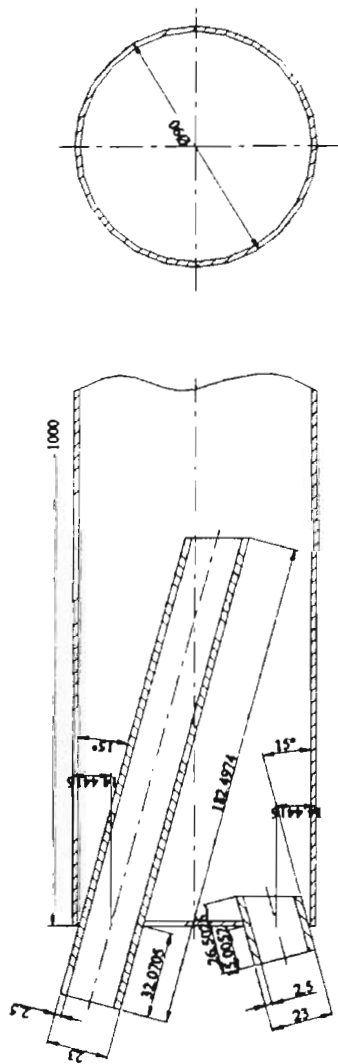


Figure A-1. Reactor Inlet (dimensions are in mm)

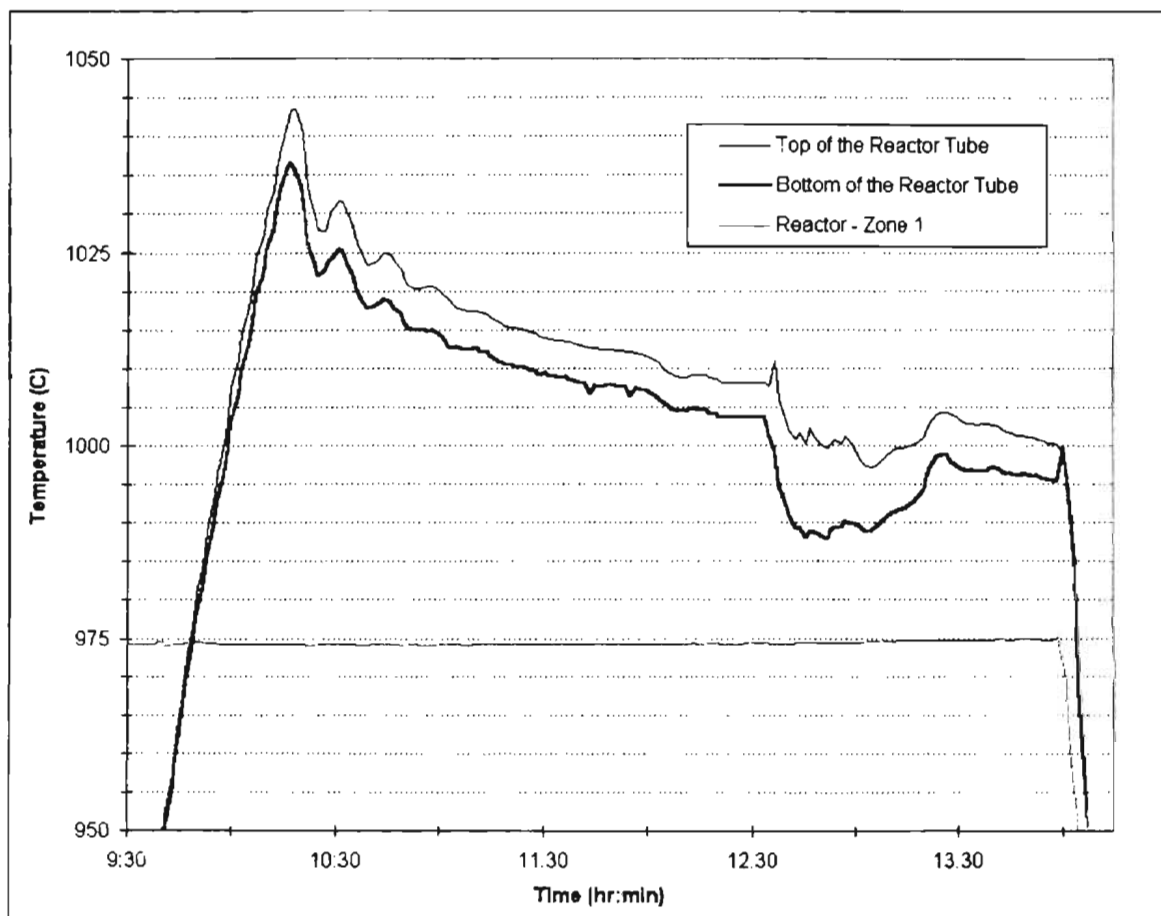


Figure A-2. Thermocouple Collar Readings and Furnace Readings for Reactor Zone 1  
ZnSe Synthesis: Experimental Run 1, July 8, 1997

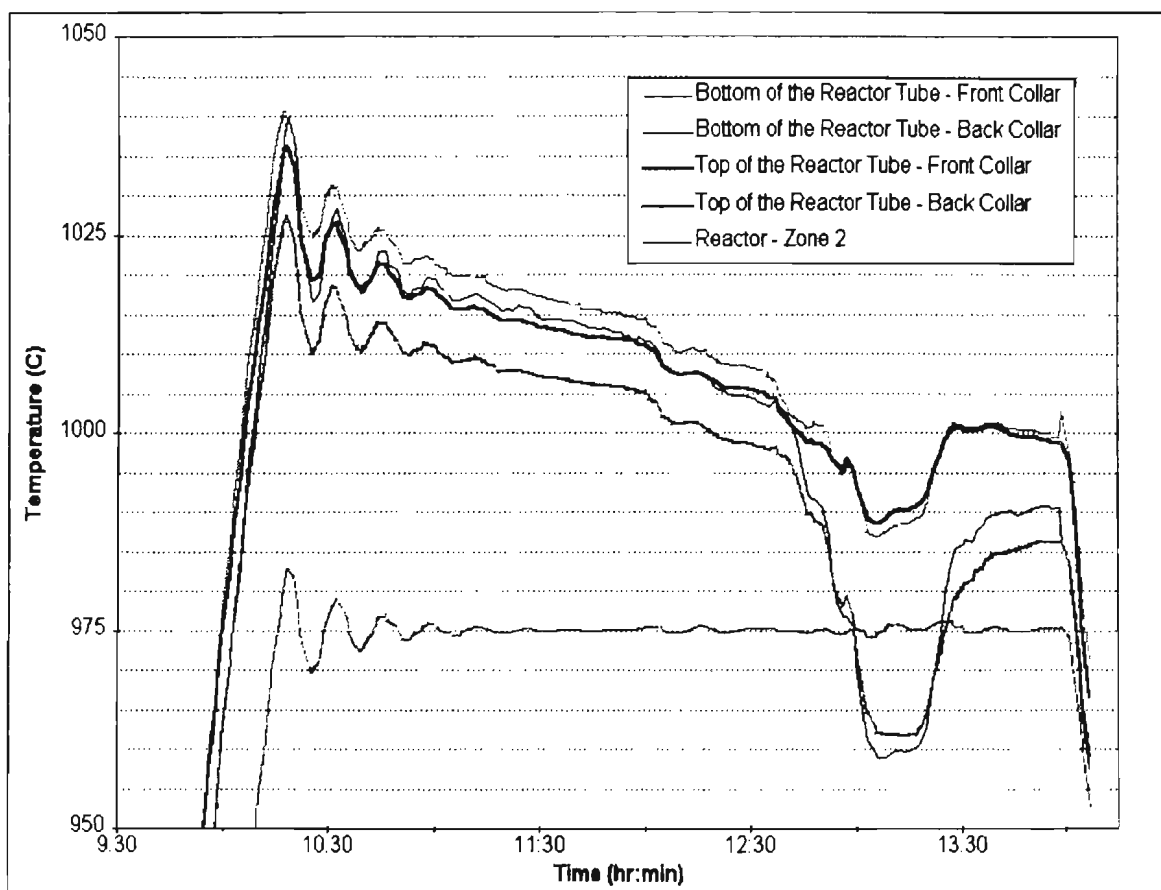


Figure A-3. Thermocouple Collar Readings and Furnace Readings for Reactor Zone 2  
ZnSe Synthesis: Experimental Run 1, July 8, 1997

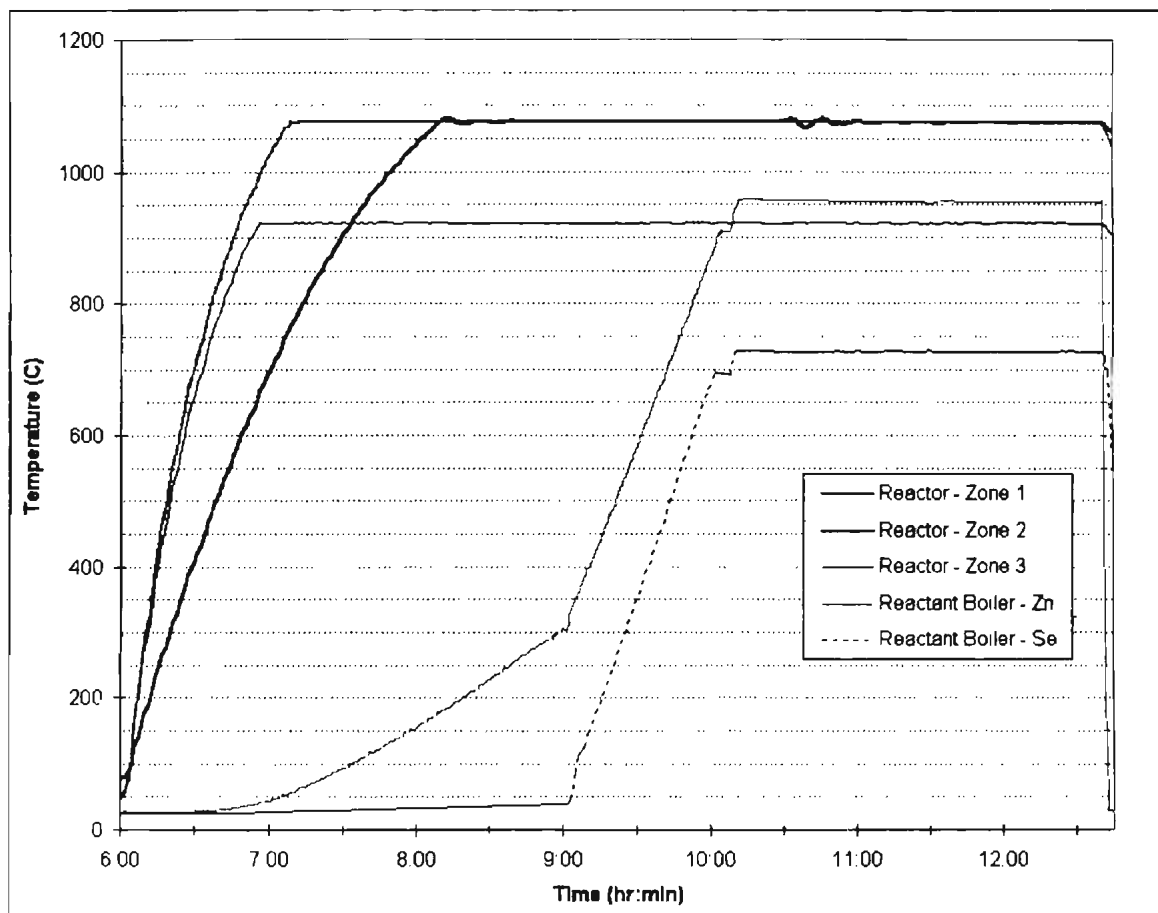


Figure A-4. Furnace and Boiler Temperature Profiles  
ZnSe Synthesis: Experimental Run 2, July 10, 1997

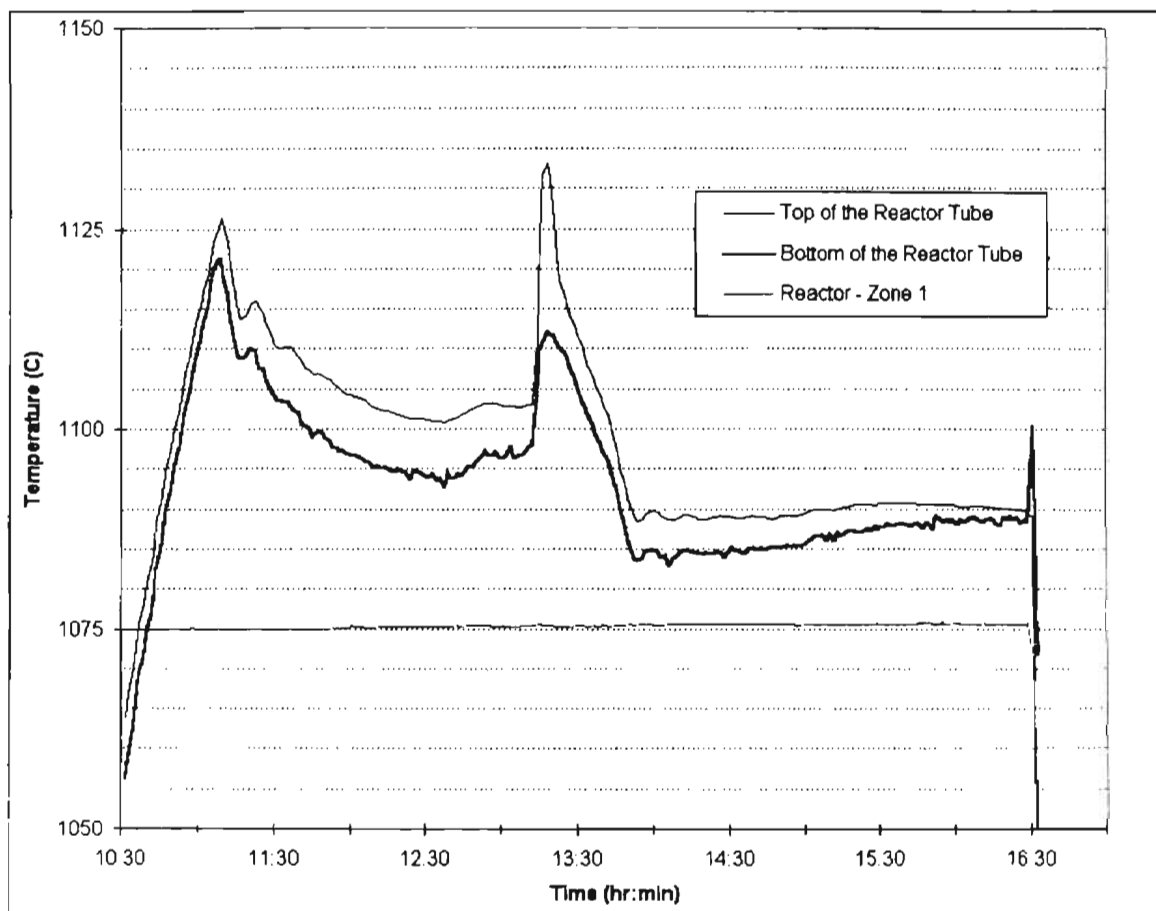


Figure A-5. Thermocouple Collar Readings and Furnace Readings for Reactor Zone 1  
ZnSe Synthesis: Experimental Run 4, July 14, 1997



Table A-1. Tube Dimensions

	Tube A (in)	Tube A (cm)	Tube B (in)	Tube B (cm)
Total Length	45.750	116.205	45.000	114.300
Reactor Length	40.000	101.600	39.500	100.330
Reactor Diameter (OD)	3.750	9.525	3.750	9.525
Zinc Inlet Length	1.969	5.000	1.181	3.000
Zinc Inlet Diameter (ID)	0.787	2.000	0.906	2.300
Zinc Inlet Length Inside the Reactor	7.087	18.000	6.299	16.000
Selenium Inlet (outside section; end of faceplate to center of down tube)	3.346	8.500	2.756	7.000
Selenium Inlet Length (down section)	1.181	3.000	0.787	2.000

## **APPENDIX B**

### **FLUENT COMPUTATIONAL FLUID DYNAMICS MODEL**

#### **DOCUMENTATION**

This appendix describes the process used to create a computational fluid dynamics model using commercial code FLUENT. Although the material in this appendix presents step by step process used for modeling work done in this thesis, for a complete computational model, further guidance is important and may be obtained from the Fluent Inc. (1996) manuals. While initial insight into solution process may be obtained from this appendix, the manuals mentioned should be the cornerstones of any similar work.

The appendix is divided into several parts necessary for the complete computational process. First part contains information on the creation of geometry and domain topology. Next, the mesh generation process is described. Following successful meshing process, process of setting up parameters and methodology used within the solver was introduced. Finally, physical properties used for simulations were tabulated unless their calculation process took place within the solver.

## **B.1 PROCEDURE FOR CREATING THE GEOMETRY**

Geometry creation process consists of several steps. These steps are outlined in the following pages. It is important to follow these steps in the order presented to avoid problems that may otherwise occur.

### **B.1.1 Start GeoMesh**

GeoMesh is a program that enables set up of a 2- or 3-dimensional geometry and creation of a grid associated with that geometry. The grid can be saved in the file and then read into FLUENT, where the problem definition may be completed, solution calculated, and results visualized.

Procedure:

1. Type "geomesh" to start the program at the Unix terminal window.
2. When prompted for a configuration, enter the name you want the configuration to have.
3. Press Enter or click on Okay.

A configuration is a sub-directory in which a copy of the geometry and all meshing-related files will be stored. The configuration name currently being used is displayed in the top left area of the Session Manager. Each meshing project requires a new configuration name. GeoMesh will allow only one grid for each configuration.

### **B.1.2 Start DDN**

DDN is the geometry generator module of GeoMesh. Geometries can be created and modified in DDN even if you have imported IGES file from another CAD system. DDN was used to create a 3-D geometry used for the simulations completed during this research work. To start this geometry generator module, following steps are used:

1. Start DDN from the GeoMesh pull-down menu: Applications → DDN

The Session Manager will prompt for the name of a new part. Part is the location where the geometry is stored within the configuration.

2. Type in the name and press Enter or click on Okay.

### **B.1.3 Create Points**

Geometry is created starting from points. To create points when their coordinates are known, following steps are required:

1. Click on point icon in the upper right hand corner of the DDN window.
2. Select XYZ option.
3. Enter point coordinates in the text interface. Type in the x coordinate, followed by Enter.
4. Type in the y coordinate, followed by Enter.
5. Type in the z coordinate, followed by typing ].

#### **B.1.4 Create a Line Between Two Points**

The lines created will be axes of the cylindrical surfaces that will be created. These lines are created by simply connecting their endpoints created using the above mentioned procedure. Procedure for creating lines is:

1. Click on the line icon at the right hand side of the DDN window, and then on the line with two points as endpoints.
2. Select the two points desired to be endpoints of the line. A straight line will be constructed between the points.
3. Type ] when finished to exit the command.

#### **B.1.5 Create Cylindrical Surface**

In order to create the geometry of the chemical reactor, a cylinder had to be created. This process of creating a circular cylinder can be accomplished by defining the radius and one axis of the cylinder (which are the lines created following the procedure mentioned above). Procedure:

1. Click on the surface icon on the right side of the screen, then choose cylinder picture.
2. Click on 1. AXIS, and then click on 1. EXISTING LINE in the text interface of DDN window, which is located in the lower left corner.
3. Click on the line.
4. Input the radius and then type ]. The surface will be created.
5. Repeat to create the other surfaces.
6. Type ] to exit this command.

### **B.1.6 Create Surface at the Entrance of the Tube**

The above mentioned procedure will create a cylinder that is open on its bases. The reactor simulated is closed at the inlet side and the surface has to be created on that side of the reactor following these steps:

1. Click on the arc icon on the right side of the DDN window. Choose Arc/Circle option.
2. Choose Center-End point option.
3. Select a center point, select an end point with the mouse.
4. Type in the degrees of rotation for the arc (0, 360).
5. Type ] to exit this command.

### **B.1.7 Blank the Points and the Lines**

Blanking is a means of temporarily removing an entity from the display for the primary purpose of removing clutter from the screen. Blanked entity is not deleted from the database. Blanking helps in hiding the entities, which are not important for further development of the geometry using the following procedure:

1. Click on the star shaped pull-down menu, select dot/line/arc symbol.
2. Click on 5. ENTIRE PART in the text interface.
3. Type ] to complete the operation.
4. Type ] again to return to the main menu.

### **B.1.8 Convert the Surfaces to B-Splines Surfaces**

Converting a surface to a B-spline surface refers to approximating the surface with a special kind of surface that has better representation of curves. Procedure for converting the surfaces is as follows:

1. Click on the surface icon on the right side of the screen, then on the B-Spline, and finally on conversion sign.
2. Click on all surfaces and type ].
3. Type in “16” for the order in both u and v directions, and type ]. The conversion will now be performed.
4. Click the middle mouse button several times to return to the main menu or type [.

### **B.1.9 Find the Intersection Between the Surfaces**

Since DDN is a surface modeler one must represent complex boundaries of the geometry with surfaces. When creating surfaces that intersect one another, one must instruct DDN to find the intersection. In order to find the intersection of surfaces at the inlet wall of the reactor, following procedure is used:

1. Click on 3-D icon on the right side of the DDN window, and then on surface-surface intersection symbol.
2. One may intersect one group of surfaces with another group. It does not matter in DDN whether you have one surface or several surfaces in a group. Click on a surface and type ].
3. Click on the other surface and type ]. The intersection will be found.
4. Click on menu item 1. EXIT-SAVE CURVES in the text interface.

5. Click the middle mouse button a few times to return to the main menu or type [.

#### **B.1.10 Create Trimmed Surface**

A trimmed surface is a segmented surface with one or more segments blanked from the display. Trimmed surfaces are useful for removing clutter from the screen. Trimmed surfaces are not necessary for the purpose of the grid generation. When creating trimmed surfaces, one must indicate to DDN what segments of the surface are active, and DDN will blank the segments that are not active. This is important because it was found by trial and error that it is easier to create oversized surfaces and then to trim them to the desired size after the intersection has been found. To trim the surface, do the following:

1. Click on the surface icon on the right side of the DDN window, then on the trimmed sign.
2. Click on the menu item 1. TRIM SURFACE in the text interface.
3. Click on the larger surface.
4. Click on the intersection curve and type ].
5. DDN will prompt for the active regions. Typically, there is one active region. Click on menu item 4. OUTSIDE in the text interface. This instructs DDN to blank part of the surface that is inside the intersection curve (the inactive segment).
6. Click on the menu item 1. TRIM SURFACE in the text interface.
7. Click on the smaller surface.
8. Click on the intersection curve and type ].
9. Click on 1.SCREEN POSITION in the text interface.



10. DDN will prompt INDICATE ACTIVE REGION. Choose the interior of the segment of the surface that you want to remain active using the mouse. DDN will now create the trimmed surface. (Don't click on the edge of the surface, or you will get the message LOCATION OUTSIDE SURFACE BOUNDARY. If you get this message, simply click on 1. SCREEN POSITION, and then click on the interior of the segment you want to remain active.)
11. Click the middle mouse button a few times to return to the main menu or type [.

#### **B.1.11 Save and Exit DDN**

With the geometry creation complete, save the part file and exit DDN.

1. Using the text interface, click on 4. FILE/EXIT.
2. Click on 3. FILE – QUIT SESSION.

### **B.2 DOMAIN TOPOLOGY CREATION STEPS**

P-Cube is the grid generation module of GeoMesh. The creation of the domain topology, specification of the node distribution, setting of boundary condition types and grid interpolation are performed in P-Cube. Geometry created in DDN, using steps mentioned in section B.1, is imported into P-Cube for the surface mesh generation process.

#### **B.2.1 Copy the Part and Start P-Cube**

First, the geometry has to be imported into P-Cube. This is accomplished by following:

1. Click once on the part name, under the heading Geometry Parts in GeoMesh window.

2. Click on Copy part, and then click on Yes to copy the part to the Meshing Parts list.
3. Double-click on the part name under the heading Meshing Parts to start P-Cube.

### **B.2.2 Set the Model Type**

Once the P-Cube is started, type of the model has to be defined, as well as the solver used for the calculation process. These settings can be seen in Figure B-1.

1. In the Startup Modals panel, choose Model type and Analysis code of choice. Click on Apply, and Close the panel.
2. Click on Max at the bottom of the P-Cube window to scale and center the display of the geometry.

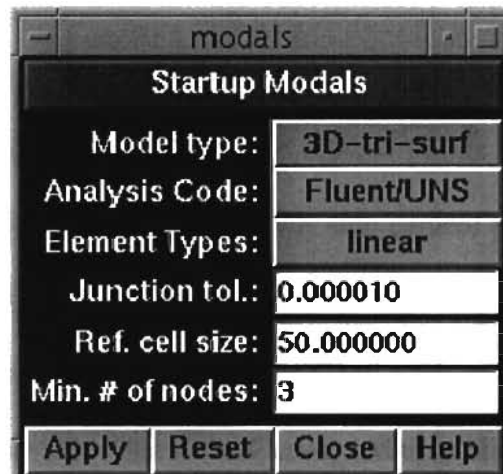


Figure B-1. Startup Modals Panel

### **B.2.3 Create the First Face**

Body-fitted grids are created within the framework of a domain topology. A domain topology is comprised of interconnected mesh areas called faces, which contain quadrilateral or triangular grids. In the P-Cube, surface mesh will be created using faces

on the surfaces of the geometry. Topology represents the manner of how the faces or blocks are connected together. Procedure to create a first face is as follows:

1. Click on the button below word Face, and then click on Create button.
2. Type d on the keyboard, and move the cursor to the right end of the larger cylinder.
3. Position vertex somewhere on the backside of the larger cylinder on the left end, and click the middle mouse button to accept the position of the vertex or type ].
4. Position the vertices on the larger surface. Make sure the face straddles the wall of the reactor. (double click on the vertex to wake it up and reposition it)
5. Click the middle mouse button once more or type ] so the block turns blue and is saved in the database.

#### **B.2.4 Rubberband the Edges to the Cylinder**

An edge is rubberbanded by adding shape control points to the edge, which causes the edge to behave as cubic spline. Adding only one control point will conform the edge to the shape of an arc. This is important to make faces conform to the shape of the reactor walls. Procedure for rubberbanding is as follows:

1. Click on the button below the word Curve, and then click on the Modify button.
2. Click on one of the edges whose ends are constrained to the arc with the left mouse button.
3. Click the middle mouse button or type ] to accept the selection. The edge will be highlighted with its end vertices visible in orange.
4. Move the cursor onto the highlighted edge (not the geometry), and click the right mouse button. Clicking the right mouse button will add a square control point. You

will also see a few yellow lines which are a part of the tool that conforms the edge to the arc.

5. Move the cursor onto the arc between the end vertices of the edge.
6. Click the middle mouse button or type ] to accept the placement of the control point.
7. Click the middle mouse button once more or type ]. The edge will turn blue and will be recorded in the database.
8. Rubberband the other edges to the other arc in the same way.

#### **B.2.5 Create the Sub-Face Inside the Intersection**

The end goal is to create a sub-face inside the intersection for the purpose of building a face from already existing face. In this manner, two faces will be topologically connected, which is a must to insure proper functioning of the simulation. Procedure for creation of a sub-face is the following:

1. Split the face that straddles the intersection using the Misc-Split, Face.
  - (a) Click on Misc-Split and then on the button below the word Face.
  - (b) Click on the edge of the face you want to split, and type ]. Where you click the edge determines where the face will be split. This process is known as splitting a face parametrically.
2. Split the sub-face on the right in the same manner.
3. Add two break points using Edge, Modify on each edge. Attach these break points to the intersection using d tracking.
  - (a) Click on the button below the word Edge and then on the Modify button.

- (b) Click on the edge you want to split at a break point with the left mouse button, and click the middle mouse button or type ] to confirm the selection.
  - (c) Position the tip of the arrowhead of the cursor on the edge, and click the right mouse button. This action will add a break point, which will be attached to the cursor.
  - (d) If not activated, click on the keyboard, and move the cursor onto the intersection and click the middle mouse button to accept the position of the break point or type ] instead. Add another break point in the same manner.
  - (e) Once finished adding break points, click the middle mouse button once more to exit the Modify function or type ]. The edge will turn blue.
4. Split the middle sub-face through two vertices (break points) using Misc-Split.
- (a) Click on Misc-Split and then on the button below the word Vertex.
  - (b) Click on a vertex, and type ]. Click on the opposite vertex, and type ]. This operation will select the vertices. There is no need to click the Select button.
  - (c) After selecting the vertices, make sure the vertices are highlighted in white before splitting the face. Many users fail to accept (by typing ]) the selection of each vertex. If the vertices are not selected, P-Cube will still split the face but not at the intended vertices. This case results in very small sub-edges.
  - (d) Click on the button below the word Face.
  - (e) Click on an edge of the face you want to split, and type ]. This overall process is known as splitting a face through two vertices.
5. Split the lower middle sub-face through the other two break points in the same manner.

6. Rubberband the edges of the circle using Curve, Modify.

### **B.2.6 Pre-Selecting Objects**

When creating objects, you want them to be topologically connected to adjacent objects in your domain topology. If adjacent objects are not topologically connected, nodal information will not be propagated from one domain to the next. To insure that newly created objects will be topologically connected to existing ones, edges must be pre-selected before creating faces. This procedure is as follows:

1. Click the button below the word of the object wanted to pre-select (Edge).
2. Click the Select button. This will choose the first menu item Select: By Type. This means the pre-selected objects will be one at the time and of the type indicated by the highlighted object button.
3. Click on the object until the object of choice is highlighted.
4. Click the middle mouse button or type ]. The object is now pre-selected.

### **B.2.7 Specify a Uniform Node Distribution**

When ready to specify the node distribution, by default, three nodes are assigned per master, which is too coarse in most cases. However, a uniform node distribution can be globally applied on all edges before manually adjusting the number of nodes and distribution on individual edges. A uniform node distribution is applied by setting the reference cell size to an appropriate value, which depends on the dimensions of the geometry. The reference cell size determines the number of nodes on a master edge by dividing length of the master edge by the reference cell size and increasing the number by

one. Specify a value of 10 for the reference cell size in the modal panel shown in Figure B-2 (this means nodes will be spaced roughly 10 units apart) as follows:

1. Open the message window by clicking the Msgs button in the lower left corner of the P-Cube window.
2. Choose Bunch (Tri, Tri-Surf): Reset from the Bunch pull-down menu.
3. Change the value in the numeric field that is to the right of Ref cell to 10.
4. If not active, click the Ref cell button.
5. Click Apply, and Close the panel.

When invoked Bunch (Tri, Tri-Surf): Reset, P-Cube computes connectivity. It determines the number of master and slave edges and the number of nodes thereon. P-Cube chooses edges to be masters and slaves based on the priority being given to the shortest edges. When the slave edge is assigned less than the minimum number of nodes,

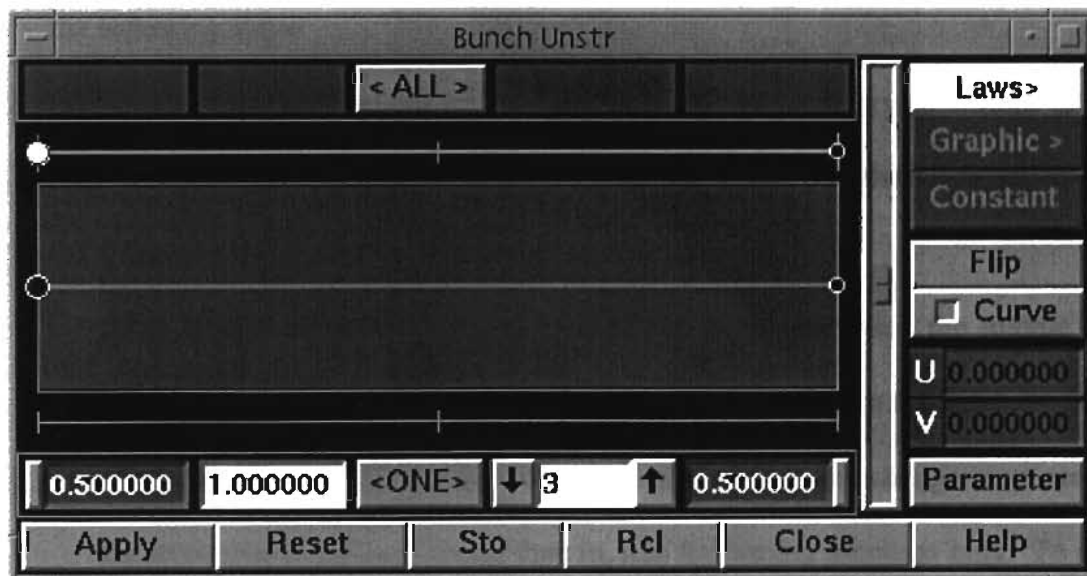


Figure B-2. Bunch Panel

P-Cube makes that edge green. In order to eliminate green edge, increase the number of nodes on the corresponding master edge using the Bunch Panel shown in Figure B-2, or change the green edge to be master using Bunch (Tri, Tri-Surf): Set master.

### **B.2.8 Specify the Boundary Types**

When working on three-dimensional models, boundary types must be set on faces and blocks. The inlets, exits and walls on faces must be denoted. Also, the live (Fluid) and dead (Solid) regions on blocks have to be assigned. This is done in the Boundary Conditions Panel shown in Figure B-3. Using following procedure:

1. Choose B Cond: Set from the B Cond pull-down menu.
2. If not highlighted, click on the button below the word Face. This will allow the boundary conditions to be set on faces.
3. Specify the type of Inlet with Zone 1 on the face at the inlet of the Zinc nozzle. Use the following steps:
  - (a) Click on the face that corresponds to the inlet with boundary conditions to be set, and then click the middle mouse button or type ] to accept the selection.
  - (b) Click on Inlet in the Set Boundary Conditions panel.
  - (c) Click Apply, or move the cursor off of the panel and click the middle mouse button or type ] instead. The specifications will be stored in the database, the face will be deselected, and the icon on the displayed face will change to an arrow. If the arrow points outward rather than in, it is for display purposes only. To reverse the arrow direction, re-select the face, then click the arrow button to the right of the Inlet button in the panel, then click Apply.





Figure B-3. Boundary Conditions Panel

4. Specify the type of Inlet for Selenium nozzle. Repeat the above process for the inlet, but increment the Zone # to 2.

5. Repeat the above process for the exit. Use the Outlet type.
6. Specify the type of boundary conditions for the tube walls.
7. Close the Set Boundary Conditions panel.

#### **B.2.9 Removing Interior Walls**

Since all faces receive the Wall boundary type, the shared faces inside the flow domain are also walls. These walls appear as obstruction to the flow and must be removed. FLUENT does not remove these walls when the grid file is written. One way to solve this problem is to change zone types from Wall to Interior in the Boundary Conditions panel in the solver, since solver detects the walls and changes the zone number to an unused zone number. Easier way to do this is in GeoMesh. Manually it may be done using the following procedure:

1. Click on an edge and type ] once the edge or face of whose Wall boundary type is to be removed.
2. Click the Wall button so that the button is off.
3. Click Apply in the panel. You will no longer see the wall symbol on the edge of the face (Choose B Cond: Clear Interior from the B Cond pull-down menu to remove the internal walls, all at once).

#### **B.2.10 Interpolate the Grid**

After the completion of the set-up process, grid has to be interpolated to complete the generation of the surface mesh and is done using following:

1. Click on the Msgs button in the lower left corner of the window to expand the message window.
2. Choose Mesh: Create from the Mesh pull-down menu. When the message window reports Normal Termination, the grid will be displayed.
3. The grid generation process is now complete. Choose Save & Exit from File pull down menu. You will be returned to the Session Manager.

#### **B.2.11 Load Leo with the Domain Files**

Leo module is where the grid can be displayed, its quality information shown, and modified to improve the quality. Leo can compute diagnostic checks such as skewness and will highlight elements associated within a skewness range. Leo has advantage over P-Cube because it can smooth the grid across block interfaces. Use following procedure to load the domains in Leo:

1. In the Session Manager, choose Leo from Applications pull-down menu.
2. Click Done at the bottom of the Leo Grid Visualizer panel.
3. Click All under the heading of Structured in the Domain selection panel, and then click Done at the bottom of this panel. The two domains correspond to the two blocks you created in P-Cube.

#### **B.2.12 Display a Report of Skewness**

Minimizing grid skew simplifies the governing equations, because cross-derivative terms will be minimized, which is proportional to the grid skew. The result is a more stable numerical solution procedure, which converges more quickly. Also, excessive grid skew

near boundaries, particularly wall boundaries in turbulent flow, can cause the accuracy of boundary condition treatment to deteriorate. Generally skewness should be less than 0.95, and the determinant should be greater than 0. To check skewness, following steps are used:

1. Choose Skewness (Tri, Tri-Surf) or Determinant (Tri, Tri-Surf) from the Diagnostics pull-down menu.
2. Click No to the question of viewing only visible elements found near the lower left corner of the Leo window.
3. Click All and then Done at the bottom of the Diagnostics groups panel.
4. Click on the few bars on the right side of the histogram.
5. Click Highlight at the bottom of the panel. This will show the cells in the “corners” that have the worse skewness. One can use Laplacian smoothing and/or reduce the number of elements on a tube cross-section to help reduce the amount of skewness in these areas.
6. Click on Done in the panel when finished.
7. Click on one of the boxes under the heading I, J, or K.
8. Choose Solid from the Surfaces pull-down menu.
9. Use the narrow buttons as before to step through the various cross sections.

### **B.2.13 Starting Over in P-Cube**

It is very common to start over from scratch in rebuilding the domain topology in P-Cube, because of the learning process. With the first few models it is usually less time-consuming to start over in P-Cube than to try to figure out the problems and solve them.

Starting over is not as simple as deleting the part in the Meshing Parts list and copying over another part because the same domain topology will remain due to the way information is stored in the directory structure. Procedure is as follows:

1. Choose Open Configuration from the Configuration pull-down menu, and open the configuration, which want to abandon. If the part exists in the Meshing Parts list and not in the Geometry Parts list, use Copy Part to copy the part to the Geometry parts.
2. Choose Open Configuration from the Configuration pull-down menu.
3. Enter a new configuration name, and click Okay.
4. Delete the other configuration with Delete Configuration from the Configuration pull-down menu, if desired.
5. Copy the appropriate part from the Geometry Parts list to the Meshing Parts list.
6. Start P-Cube, as usual.

#### **B.2.14 Mouse Button Functions**

Familiarity with the capabilities of the mouse can be very helpful and reduce time required to complete the work. Included is the list of functions each mouse button performs. The left mouse button is used for:

- Selecting icons, buttons, and pull-down menu items
- Selecting text interface menus and commands in DDN
- Selecting geometry and mesh objects
- Rotating the display of your model in the dynamics mode (press and hold button, and move the mouse forward, backward, left, and right)

The middle mouse button is used for:

- Completing operations
- Undoing the last step within a command (press and hold button, and slide mouse to the left)
- Moving up in the DDN menu hierarchy of the text interface ([ or ])
- Accepting the selection of mesh objects
- Translating the display of your model in the dynamics mode (press and hold button, and move the mouse forward, backward, left, and right.)

The right mouse button is used for:

- Adding control points while rubberbanding an edge during Curve, Modify in P-Cube
- Adding break points to split an edge during Edge, Modify in P-cube
- Zooming the display of your model in the dynamics mode (press and hold, and move the mouse only forward and backward.)

### **B.2.15 Function Keys**

Shift + F1	Resizes the window.
F1	Toggles the text interface dialog area.
F2	Toggles the display of the perimeter icons.
F4	Resets the display to the normal projected view (P-Cube only).
F9	Toggles the dynamic mode.
F11	Resets the display to the normal projected view (DDN only).

### **B.2.16 Write out the TGrid Grid File**

When the grid is created in P-Cube, domain files are written for each block or face that is meshed. The grid files for the solvers are written from these domain files as well as the information from the topo and boco files. The topo file contains information about the topology, and the boco file contains information about the boundary types. The overall procedure for writing out a grid file is to specify the name of the grid file and to indicate which domains should be included in the file grid. Domains can be transferred to TGrid using following steps:

1. Choose TGrid from the transfer pull down menu in the GeoMesh window.
2. Since triangular mesh is used, click Unstructured in the panel.
3. Click Done at the bottom of the panel.
4. Click All or select the desired domains under the heading of Unstructured and then click Done in the Domain selection panel.
5. Click Done at the bottom of the TGrid transfer panel. The grid file will be written to the working directory.

### **B.2.17 TGrid**

TGrid is the part of the program that generates interior mesh from the given boundary. The steps used to complete this process include reading the boundary mesh into the TGrid, examining the boundary mesh for possible topology violations and quality, creating volume mesh and then checking the final result for possible problems. Once these steps are accomplished, new output file is created and used to input the information into the solver. Once TGrid is started from the GeoMesh applications pull-down menu,

first step is to read the boundary mesh. This is accomplished from the dialog box invoked using File → Read → Boundary Mesh menu item. After reading the boundary mesh file into Tgrid, one must check the imported mesh. This is done from the panel that appears from Boundary → Nodes menu item and is shown in Figure B-4. Here, the boundary mesh is checked for topologically incorrect entities such as free and multiply connected nodes. It is necessary to merge duplicate nodes if there are any, also unused nodes are counted and specified and can be removed from the grid. Once the imported boundary mesh is checked and existing problems eliminated, interior mesh can be generated. For this project it was generated using automated procedure offered within the TGrid, but should be noted that it can be generated manually using procedures specified in Fluent Inc. (1996c). Automated procedure is activated from the Mesh → Initialize and Refine → Auto menu options in TGrid window. It is important to note that in order to get an interior mesh, it is a must to define general meshing parameter in the Init/Mesh Controls panel shown in Figure B-5. Node Tolerance defines which nodes are duplicates based on calculating the distance between them. If the distance between the nodes is less than specified for tolerance, the nodes will be considered duplicate.

Finally, Non-Fluid Type is where the problems can occur. TGrid uses default specified in this field to define non-fluid cell zone type. By default, this value is set to dead, and therefore there will be only one fluid region and several dead regions. If any other type is specified in this field, after the initialization occurs, all zones will be set to active automatically, which is desired to have a correct calculation domain.



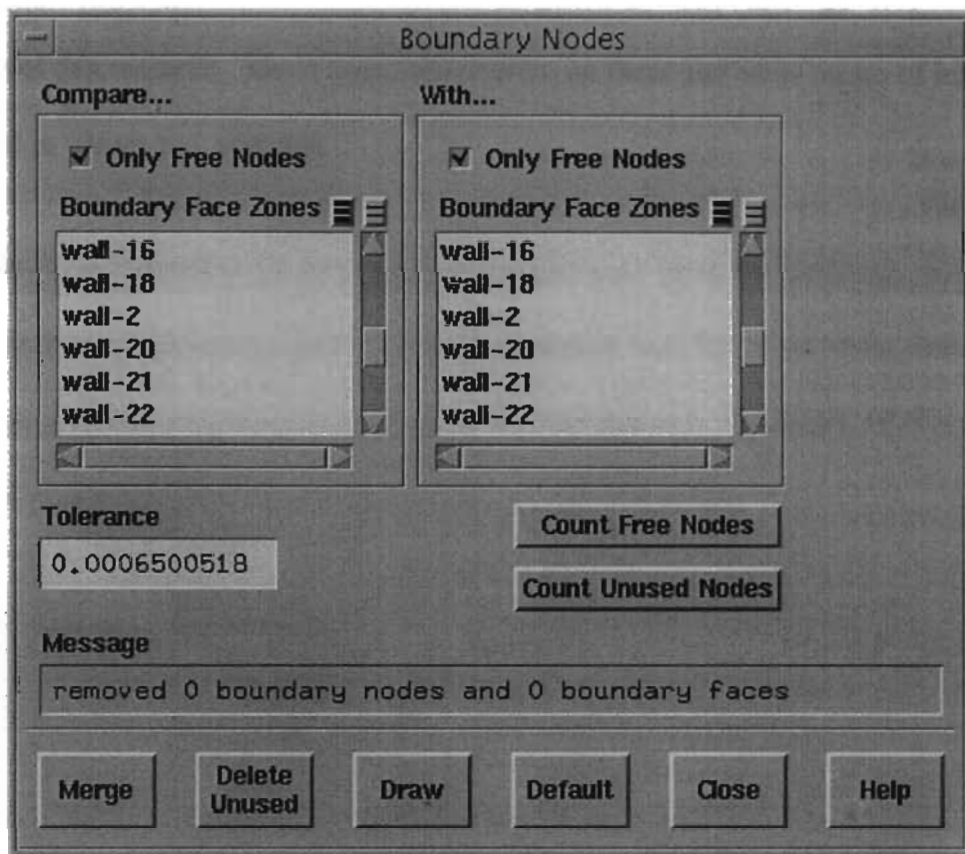


Figure B-4. Boundary Nodes Panel

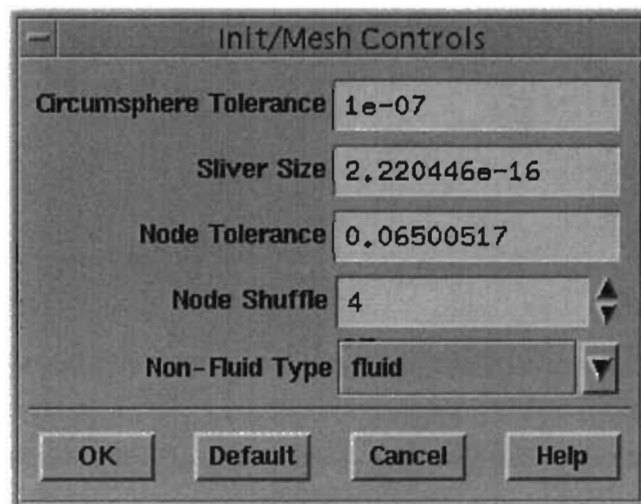


Figure B-5. Init/Mesh Controls Panel

This concludes the discussion of the geometry and topology creation for the purpose of this research. Much more information on these and other topics of interest can be found in Fluent Inc. manuals.

### B.3 GAMBIT GEOMETRY AND TOPOLOGY PROCEDURE

GAMBIT is a software package designed to help analysts and designers build and mesh models for computational fluid dynamics and other scientific applications. Graphical User Interface (GUI) is used to receive user input for building, meshing and assigning zone types to a model. It is very simple to use, but at the same time versatile enough to support wide variety of engineering applications. GAMBIT GUI is shown in Figure B-6.

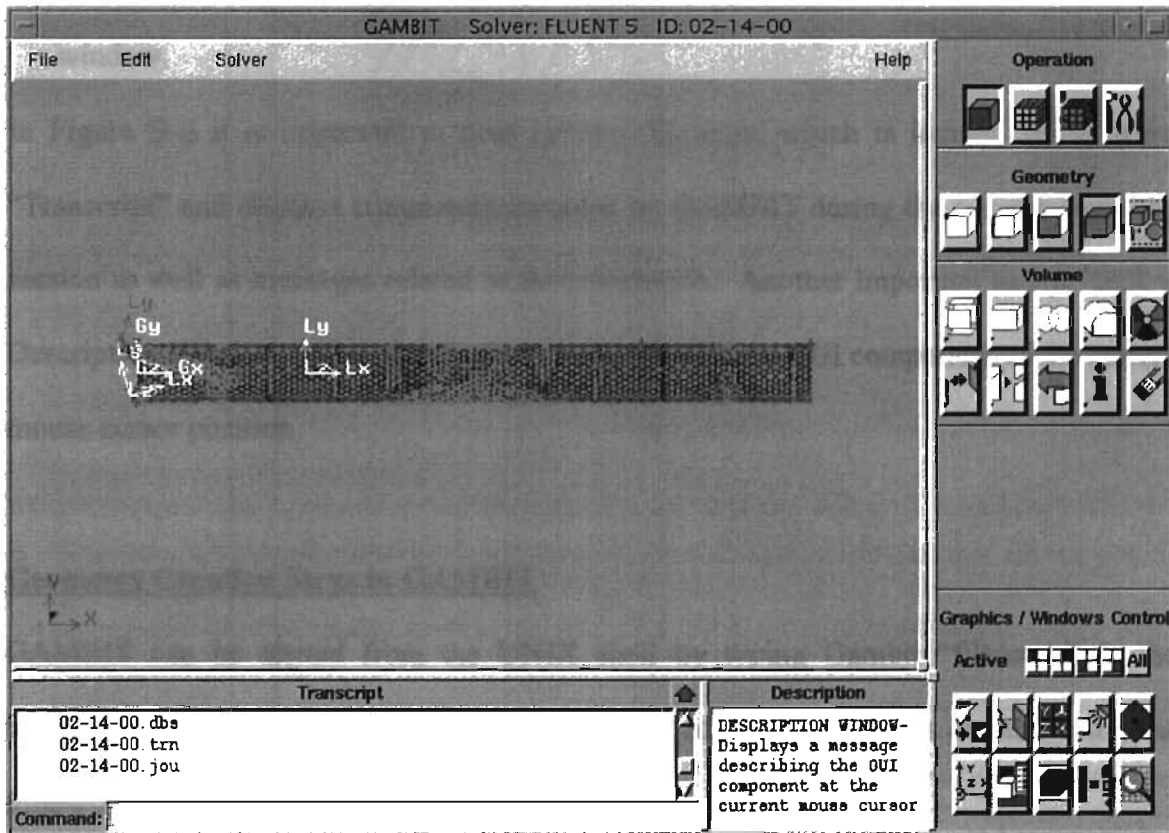


Figure B-6. GAMBIT Graphical User Interface (GUI)

When GAMBIT is started, a modeling session is created. A modeling session in GAMBIT consists of all operations performed in relation to a model considered. Such operations include, but are not limited to the following:

- Import of geometry and mesh information.
- Creation of geometry.
- Creation and refinement of a mesh.
- Assignment of zone types.
- Creation and modification of coordinate systems and grids.
- Changing the appearance and orientation of the model as displayed in the graphics window.

In Figure B-6 it is important to note History Window, which is located below word “Transcript” and displays commands executed by GAMBIT during the current modeling session as well as messages related to the commands. Another important part of GUI is Description Window, which displays a message describing GUI component of the current mouse cursor position.

### **Geometry Creation Steps in GAMBIT**

GAMBIT can be started from the UNIX shell by typing Gambit “filename” in the terminal console. Once the session has been created, the geometry is created using the following steps:

1. Create three relative coordinate systems starting with the **Tools Command Button**, which allows you to create and modify coordinate systems. **Tools Command Button** is located in the upper right corner of the GUI. Click **Coordinate System Command**

**Button**, which will open a subpad related to operations involving coordinate systems.

In coordinate system subpad, click on **Create Coordinate System Button** to display

Create Coordinate System			
Type		Cartesian	
Location and orientation:			
<input checked="" type="radio"/> Offset/Angle		<input type="radio"/> Vertices	
Reference Sys		c_sys.1	
Angle		Offset	
X		X	250
Y		Y	0
Z		Z	0
Label		Reactor-Zone 2	
Apply		Reset	Close

Figure B-7. Create Coordinate System Panel

Create Coordinate System panel, shown in Figure B-7. Three relative coordinate systems are created in this step of the process, one for each inlet in the reactor and one on the interface between Reactor Zones 1 and 2.

2. Next step is to use **Geometry Command Button** to open tools pad that allows you to create and modify model geometry. This button is also located in the upper right corner of GUI. It opens Geometry Command Pad, which is used to create geometry from scratch. To start creating a volume, click on **Volume Command Button** to open a subpad related to operations involving volumes. To create a cylinder, click on **Create Volume Button** with the right button, then select Cylinder and click on it with the left button. As a result, Create Real Cylinder Panel shows. This is how four

cylinders are created, two for inlets and two that will be combined together using Split command to create three Reactor Zones. This panel is shown in Figure B-8.

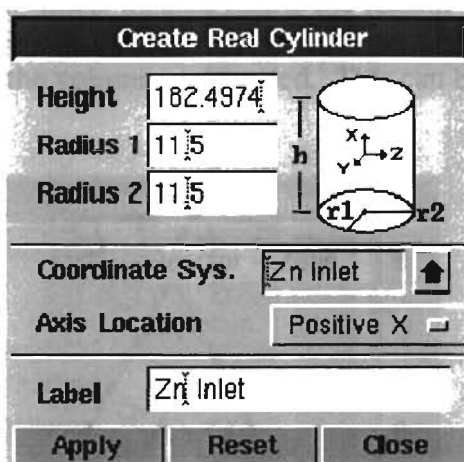


Figure B-8. Create Real Cylinder Panel

- Once the cylinders have been created, choose **Split/Merge Volumes Button** in Volume subpad to connect the inlet nozzles with the main part of the reactor. This is accomplished by splitting the volumes, small inlet cylinders with the large reactor

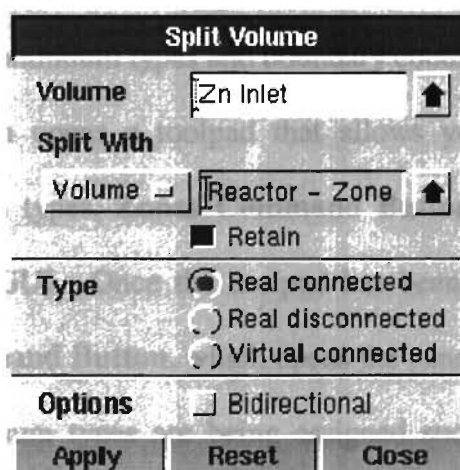


Figure B-9. Split Volume Panel

cylinder, as well as the main reactor cylinder with the shorter one. Split Volume panel is shown in Figure B-9.

4. Once the splitting process has been completed, go to **Boolean Operations Button**, located in the Volume subpad. Select subtraction process by clicking right mouse button to make a choice. Inlets located inside the reactor will be subtracted from the main cylinder retaining the volumes subtracted. This can be seen in Figure B-10.

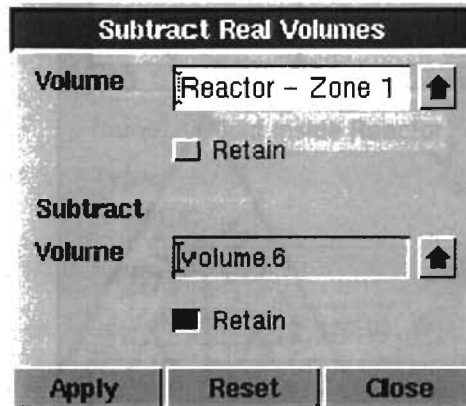


Figure B-10. Subtract Real Volumes Panel

5. This completes the geometry creation process in GAMBIT for the purpose of this research. Next step is to define a solver type from the pull-down menu under “Solver” heading before continuum types and boundary conditions can be defined.
6. **Zones Command Button** opens a toolpad that allows you to specify boundary conditions and continuum types. **Zones Command Button** is also located in the upper left corner of the GUI. Once the toolpad has been opened, select **Specify Continuum Types Command Button**, which opens the panel shown in Figure B-11. This is where the continuum types are being assigned such that each nozzle and reactor interior represents one fluid type. Other types of continuum available are solid or porous types.

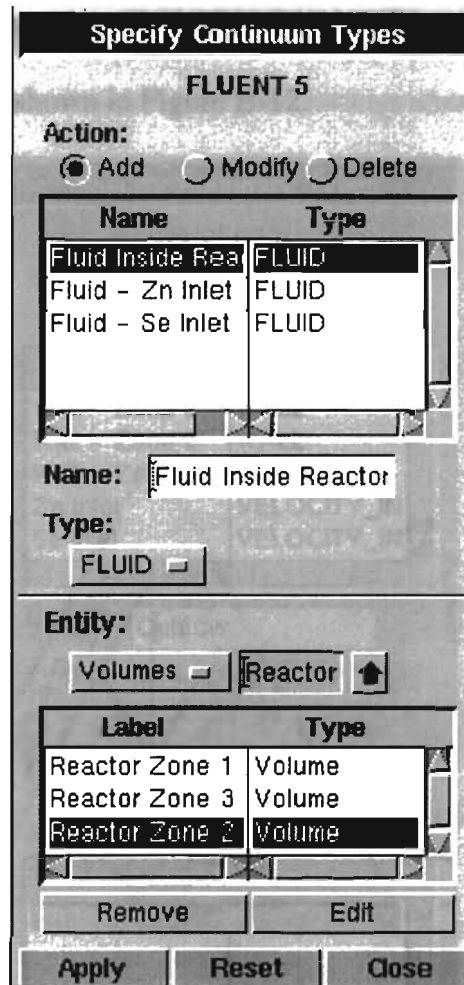


Figure B-11. Specify Continuum Types Panel

7. Following the choice for continuum types, **Specify Boundary Types Command Button** is used to invoke panel where the boundary types are set. Boundary Type definitions are not a secret; each nozzle inlet is defined as velocity inlet, nozzle exits and reactor exit as outflow type boundary conditions, interface between different reactor zones are interior type, and everything else is a wall type boundary condition. It is important to define walls with different boundary conditions as separate entities in order to be able to assign different values. This is accomplished through the careful selection of the faces which make up certain walls. This process is made



easier by the capability to name each face and to visualize it in the GUI. Specify Boundary Types panel is shown in Figure B-12.

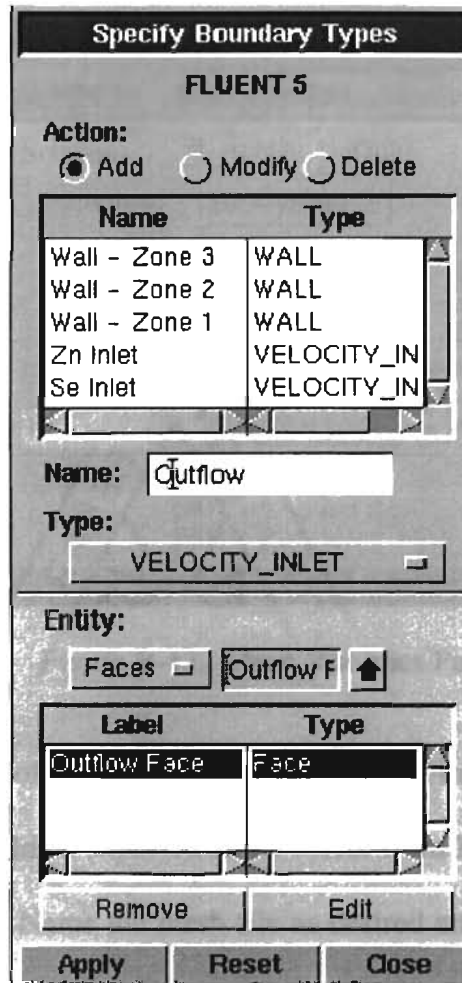


Figure B-12. Specify Boundary Conditions Panel

8. Finally, after the geometry has been created, continuum types and boundary conditions set, **Mesh Command Button** opens a toolpad, which allows creation and modification of the mesh. There are several different options available to generate various types, ranging from surface to volume meshes. Within the Mesh Command pad, select **Volume Command Button**, which will open a subpad related to operations involving volumes. Within this subpad, **Mesh Volumes Button** is used to

invoke Mesh Volume Panel shown in Figure B-13. In this panel, all volumes are selected to create a volume mesh following the settings shown.

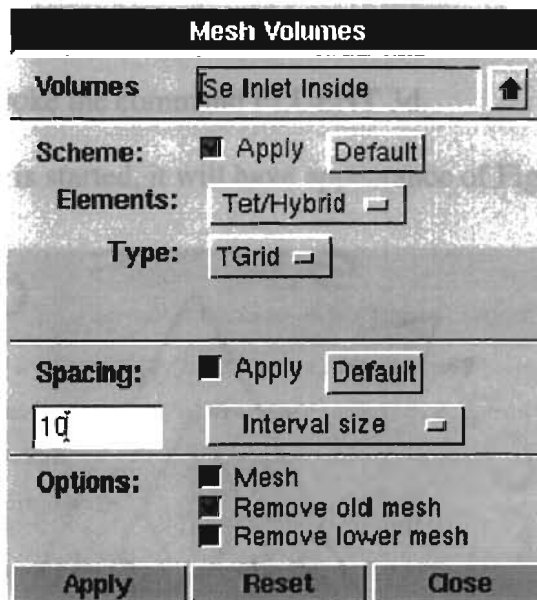


Figure B-13. Mesh Volumes Panel

This completes the process of generating the geometry and mesh in GAMBIT. After the session is saved, mesh should be exported to the solver from File pull-down menu, where export mesh option exists. Name the mesh file as desired and start the solver chosen in GAMBIT. Final mesh used for modeling is shown in Figure B-14.

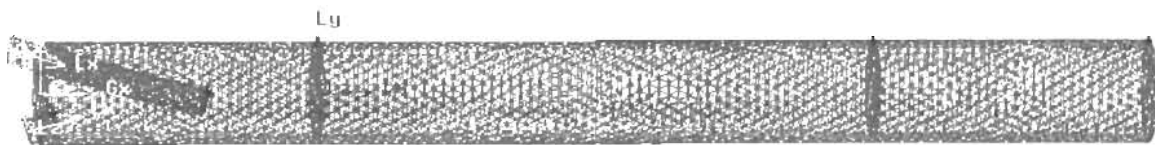


Figure B-14. Final Mesh Imported to FLUENT

## B.4 FLUENT 5 MODEL

### Start FLUENT 5

1. From a Unix shell, invoke the command FLUENT 3d.

Once the FLUENT solver is started, it will have appearance of Figure B-15.

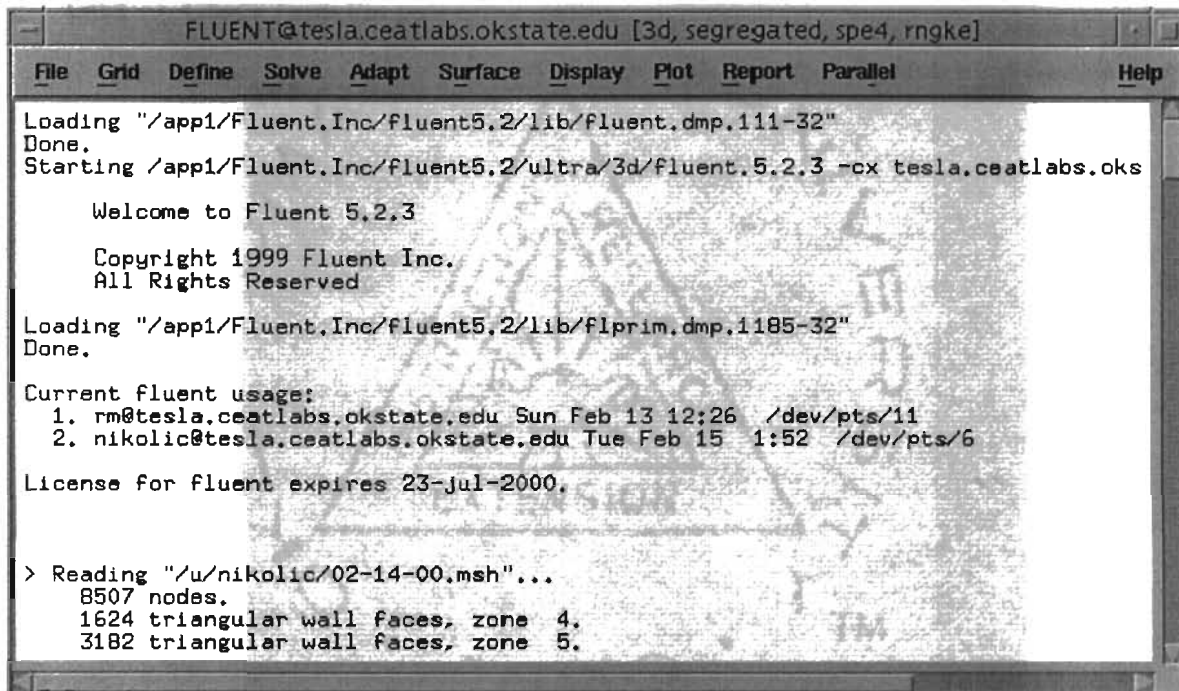


Figure B-15. FLUENT Solver

2. Read the mesh file filename.msh.

File → Read → Case → filename.msh

- (a) Click on filename.msh under heading Files in the panel.
- (b) Click on OK at the bottom of the panel.

### B.4.1 Grid Scale

It is important to check the conversion factors once the mesh file is opened in FLUENT.

Grid generated in geometry subprogram does not carry units, therefore it must be

specified what units were used to create geometry. In order to accomplish this, use following steps:

1. From the Grid heading, select Scale and change the default units to create in mm as shown in Figure B-16.
2. Double check to make sure the grid read in correctly by displaying the grid. Choose Grid → Check from the pull-down menu.

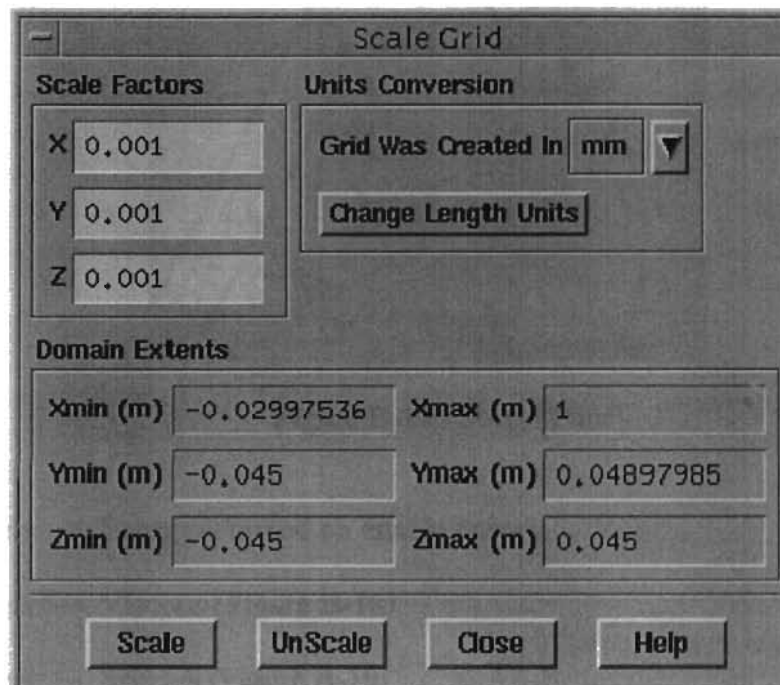


Figure B-16. Scale Grid Panel

#### **B.4.2 FLUENT Settings**

Before the simulation process, heat transfer model and chemical reaction model have to be defined. Arrows indicate selections made from the headings listed in the solver. Once the proper panel is opened, settings are shown in figures where they are available, and where they are not, they are described to the best ability. Therefore, heat transfer model and reaction model were defined through the following steps:

Define → Models → Solver (Figure B-17)

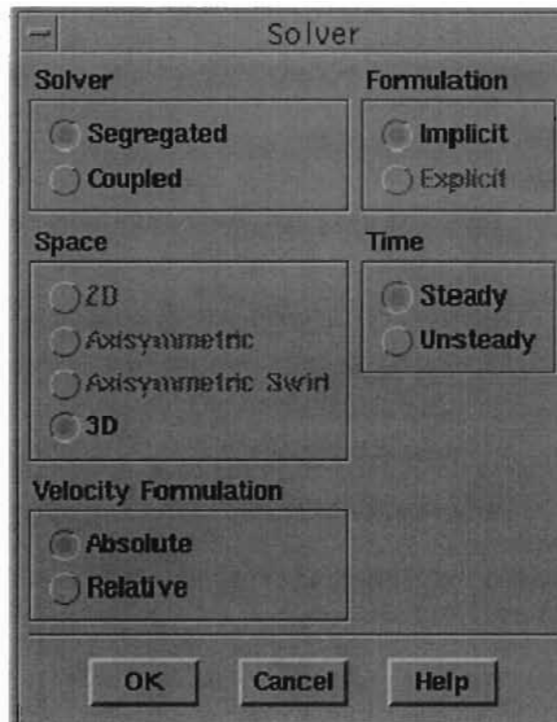


Figure B-17. Solver Panel

Define → Models → Energy – turned on enable energy

Define → Models → Viscous (Figure B-18)

Define → Models → Species (Figure B-19)

Define → Models → Radiation (Figure B-20)

Define → Models → Discrete Phase - Tracking Parameter: Max. Number of Steps 500

Length Scale (m): 0.01

Interaction: None

Stochastic Model: None

Define → Models → Multiphase (Figure B-21)

Define → Models → Pollutants - none

Define → Models → User Defined Scalars – default (zero)

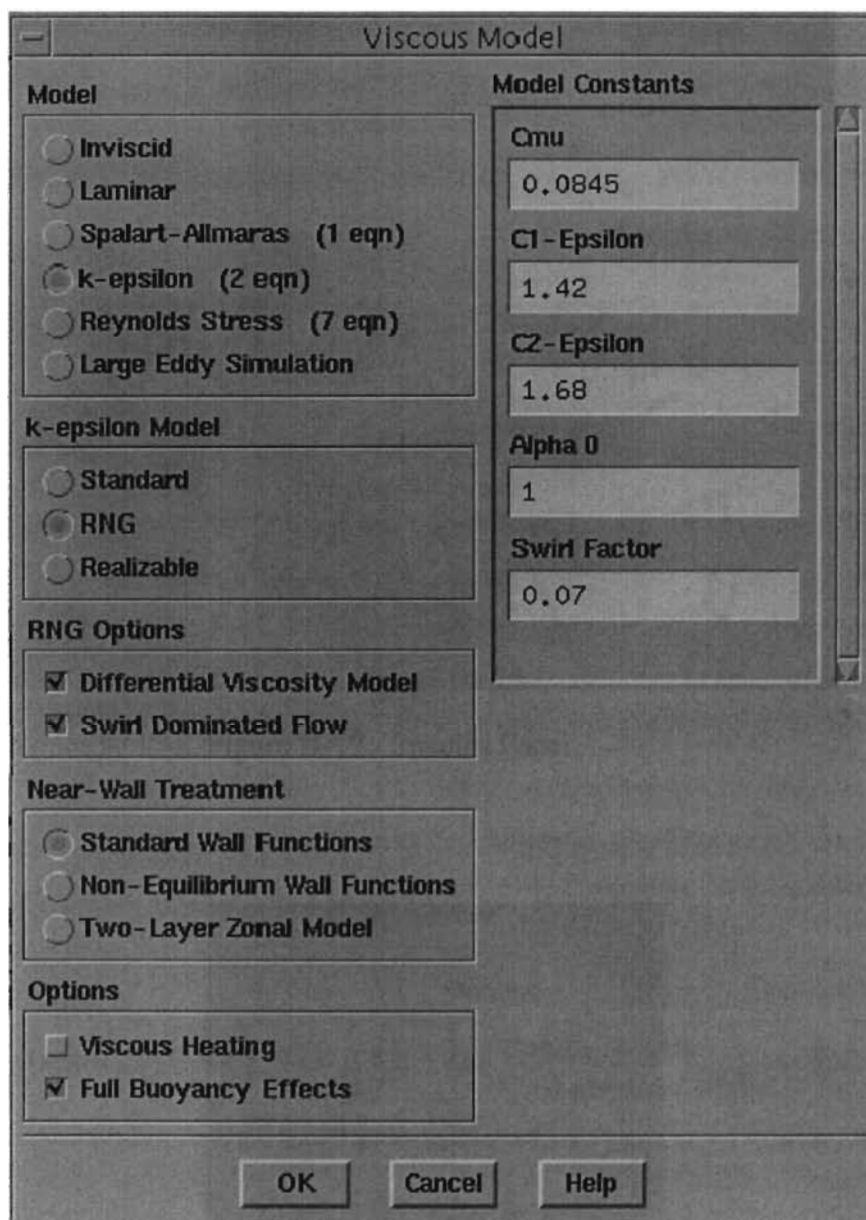


Figure B-18. Viscous Panel

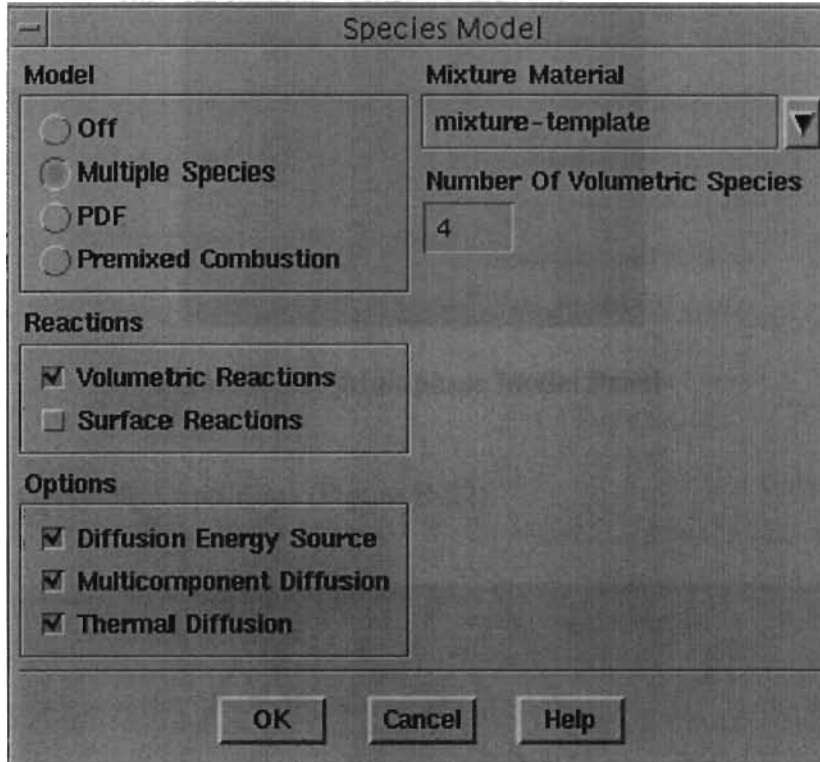


Figure B-19. Species Panel

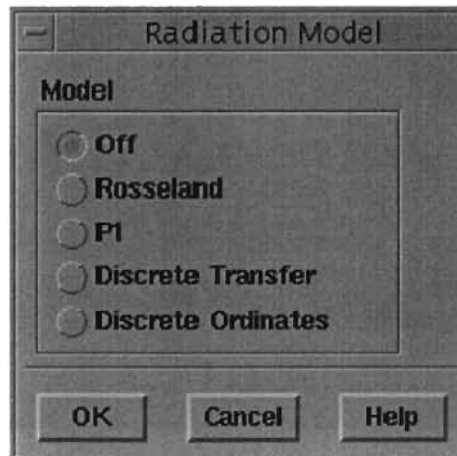


Figure B-20. Radiation Model Panel

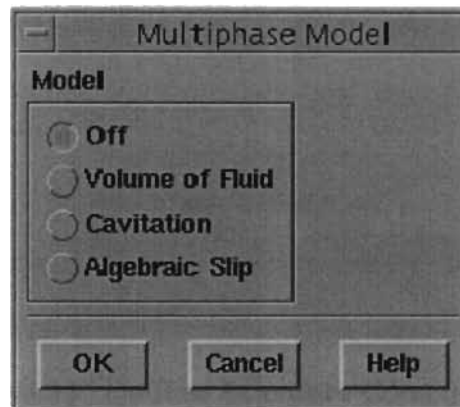


Figure B-21. Multiphase Model Panel

Define → Operating Conditions (Figure B-22)

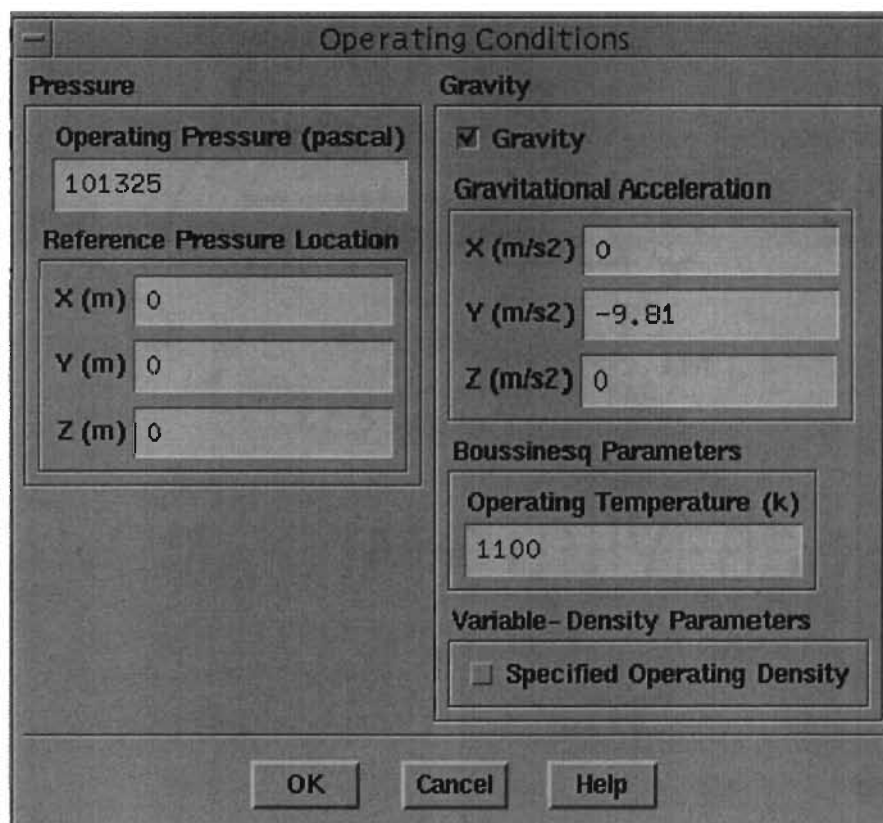


Figure B-22. Operating Conditions Panel

Define → Boundary Conditions → Outflow (Figure B-23)



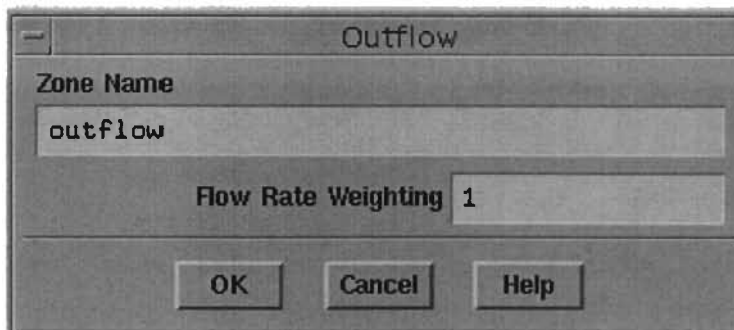


Figure B-23. Outflow Boundary Conditions Panel

Define → Boundary Conditions → Zn Inlet (Figure B-24)

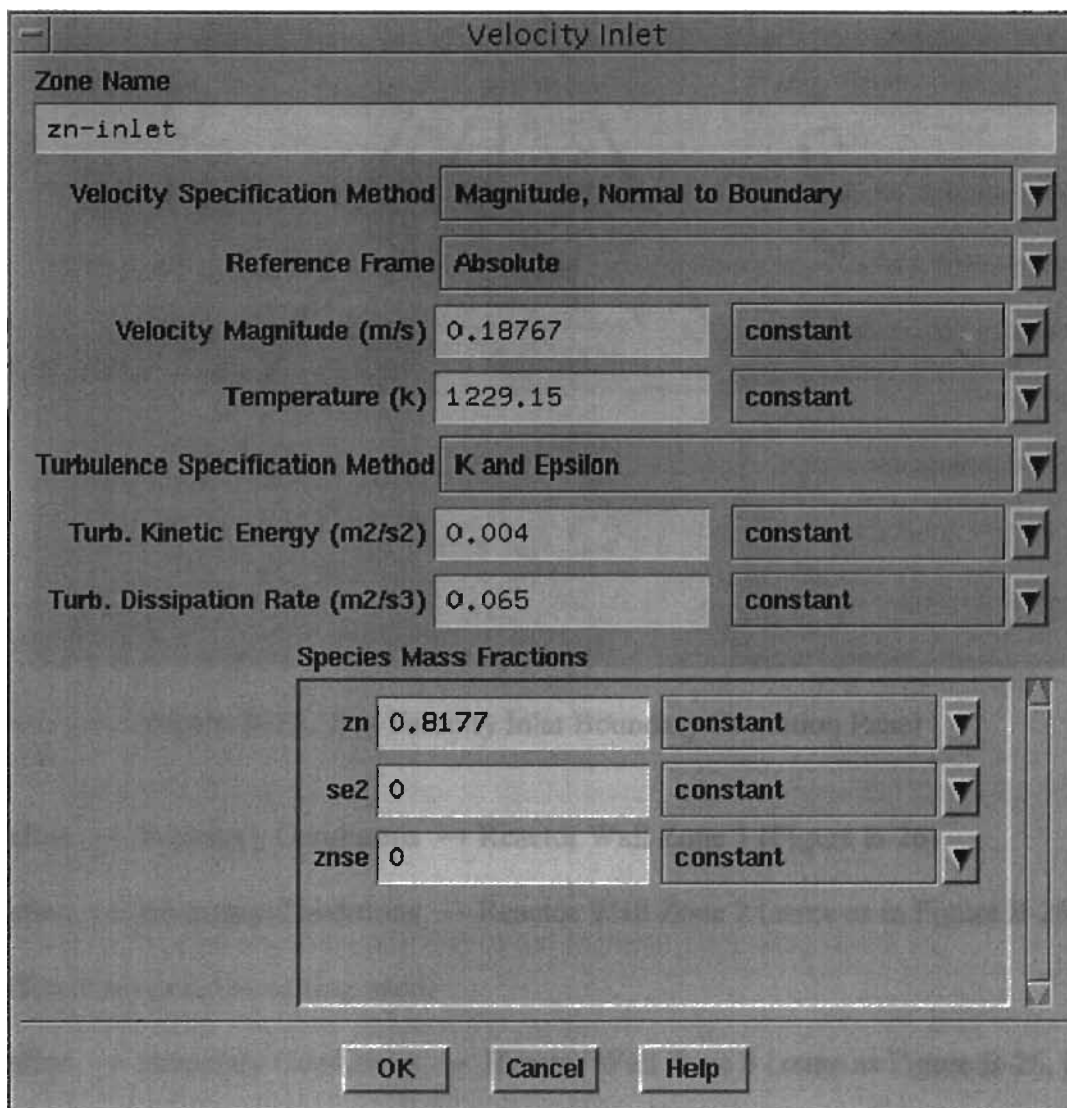
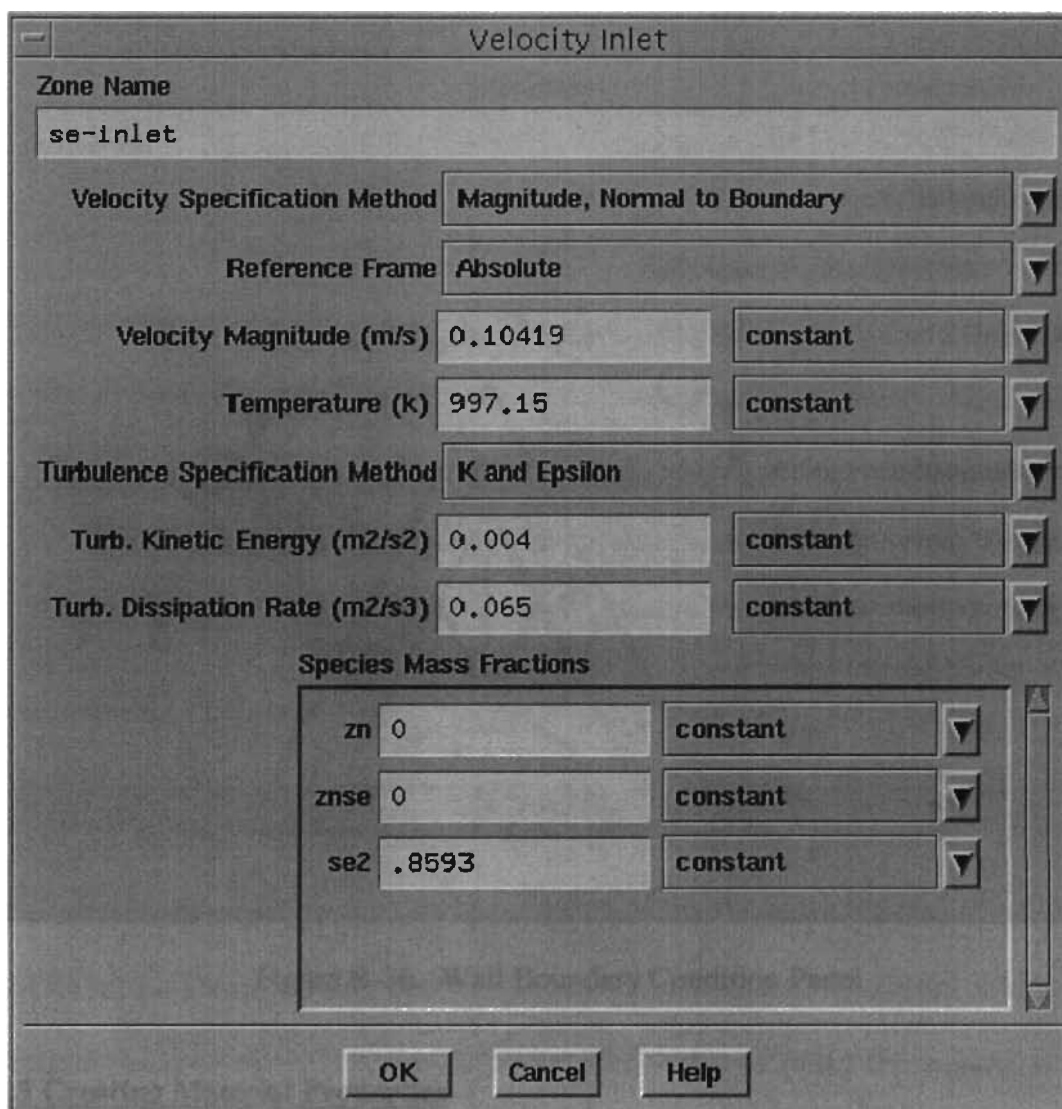


Figure B-24. Zn Velocity Inlet Boundary Condition Panel

Define → Boundary Conditions → Se Inlet (Figure B-25)



The image shows a software dialog box titled "Velocity Inlet". It contains several input fields and dropdown menus for defining boundary conditions. The "Zone Name" field is set to "se-inlet". The "Velocity Specification Method" is set to "Magnitude, Normal to Boundary". The "Reference Frame" is set to "Absolute". The "Velocity Magnitude (m/s)" is set to "0.10419" with a "constant" dropdown. The "Temperature (K)" is set to "997.15" with a "constant" dropdown. The "Turbulence Specification Method" is set to "K and Epsilon". The "Turb. Kinetic Energy (m2/s2)" is set to "0.004" with a "constant" dropdown. The "Turb. Dissipation Rate (m2/s3)" is set to "0.065" with a "constant" dropdown. Below these, there is a section titled "Species Mass Fractions" with three rows: "zn" set to "0" with a "constant" dropdown, "znse" set to "0" with a "constant" dropdown, and "se2" set to ".8593" with a "constant" dropdown. At the bottom are "OK", "Cancel", and "Help" buttons.

Field	Value	Unit	Setting
Zone Name	se-inlet		
Velocity Specification Method	Magnitude, Normal to Boundary		
Reference Frame	Absolute		
Velocity Magnitude (m/s)	0.10419	m/s	constant
Temperature (K)	997.15	K	constant
Turbulence Specification Method	K and Epsilon		
Turb. Kinetic Energy (m2/s2)	0.004	m2/s2	constant
Turb. Dissipation Rate (m2/s3)	0.065	m2/s3	constant
Species Mass Fractions			
zn	0		constant
znse	0		constant
se2	.8593		constant

Figure B-25. Se<sub>2</sub> Velocity Inlet Boundary Condition Panel

Define → Boundary Conditions → Reactor Wall Zone 1 (Figure B-26)

Define → Boundary Conditions → Reactor Wall Zone 2 (same as in Figure B-26, just different temperature setting used)

Define → Boundary Conditions → Reactor Wall Zone 3 (same as Figure B-26, just different temperature setting used)

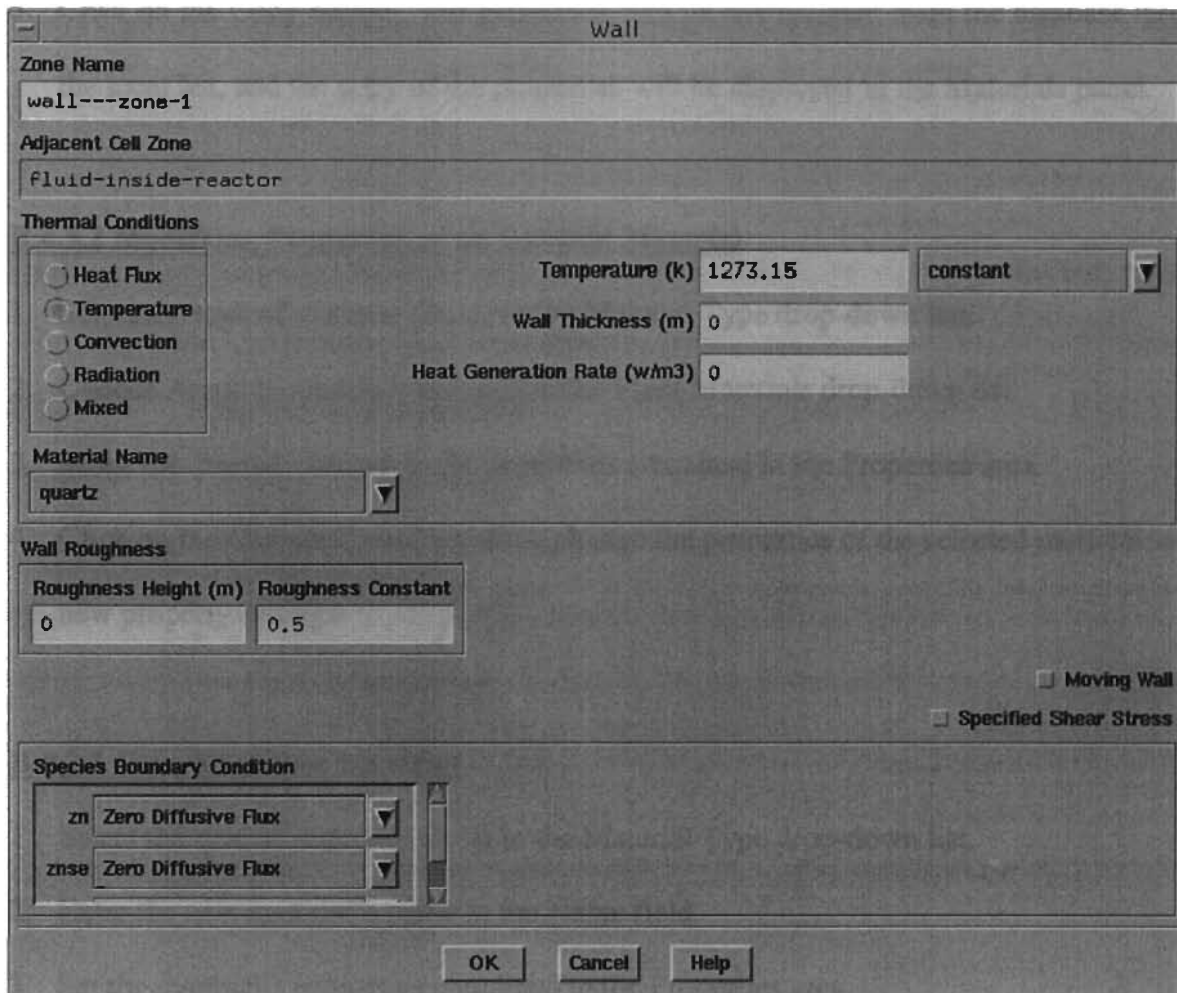


Figure B-26. Wall Boundary Condition Panel

### **B.4.3 Creating Material Properties**

#### **B.4.3.1 Copying a Material from the Database**

1. Click on the Database... button in the Materials panel to open the Database Materials panel.
2. Select the type of material (fluid) in the Material Type drop-down list.
3. Choose Argon to copy in the Fluid Materials drop-down list. Its properties will be displayed in the Properties Area.
4. Make the desired changes to the properties contained in the Properties area.

5. Click on the Copy button. The properties will be downloaded from the database into the local list, and the copy of the properties will be displayed in the Materials panel.

#### **B.4.3.2 Modifying Properties of an Existing Material**

1. Select the type of material (fluid) in the Material Type drop-down list.
2. Choose Argon to modify properties in the Fluid Materials drop-down list.
3. Make the desired changes to the properties contained in the Properties area.
4. Click on the Change/Create button to change the properties of the selected material to new property settings.

#### **B.4.3.3 Creating a New Material**

1. Select the type of material (fluid) in the Material Type drop-down list.
2. Enter the new material's name in the Name field.
3. Set the material's properties contained in the Properties area.
4. Click on the Change/Create button. A Question dialog box will appear, asking if the original material should be overwritten. Click on No to retain the original material and add your new material to the list. The Materials panel will be updated to show the new material name and chemical formula in the Fluid Materials list.

#### **B.4.4 Setting Physical Properties**

Define → Materials: Name: Mixture-Template

Material type: Mixture

Mixture Materials: Mixture-Template

Mixture Species: names (click on names to see Se<sub>2</sub>, Ar, Zn, and ZnSe) shown in Figure B-27; to set the reaction parameters, check Figure B-28.

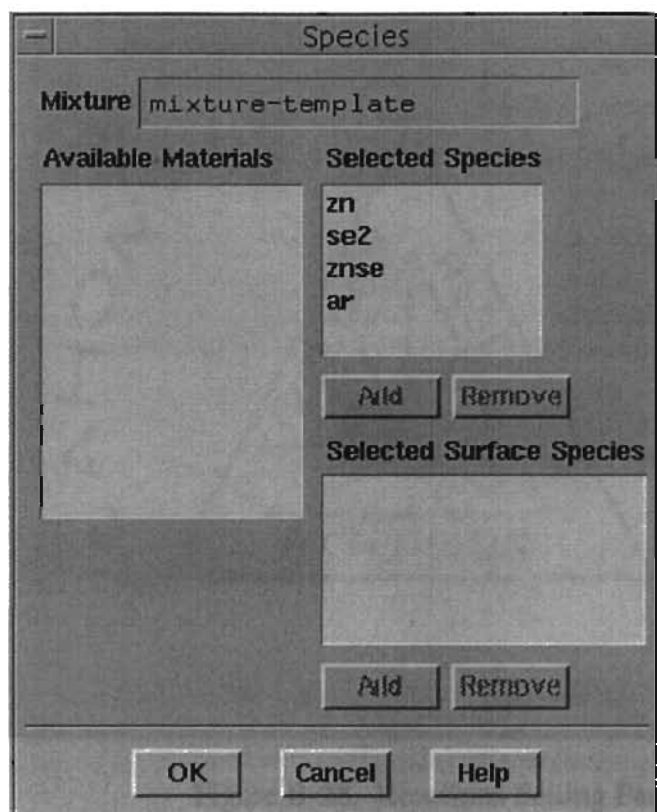


Figure B-27. Species Panel

Density: Incompressible-Ideal Gas

Cp (J/m-K): Mixing Law

Thermal Conductivity (W/m-K): Ideal-Gas-Mixing-Law

Viscosity (kg/m-s): Ideal-Gas-Mixing-Law

Mass Diffusivity (m<sup>2</sup>/s): kinetic-theory

Reactions

Mixture  Total Number of Reactions

Reaction Number

☐ Surface Reaction

Number of Reactants  Number of Products

Species	Stoich. Coefficient	Rate Exponent
zn	2	1
se2	1	1

Species	Stoich. Coefficient	Rate Exponent
znse	2	0

Arrhenius Rate

Pre-exponential Factor

Activation Energy (J/kgmol)

Temperature Exponent

☐ Include Backward Reaction

☐ Third Body Efficiencies

Mixing Rate

A  B

Figure B-28. Reactions Setting Panel

To see properties of components, change Material Type: Fluid

Argon: Cp (J/kg-K): constant: 520.3355

Thermal Conductivity (W/m-K): kinetic-theory

Viscosity (kg/m-s): kinetic-theory

Molecular Weight (kg/kgmol): constant: 39.948

Standard State Enthalpy (J/kgmol): constant: 0

Standard State Entropy (J/kgmol-K): constant: 0

Reference Temperature (K): 298.15

L-J Characteristic Length (angstrom): const.: 3.418

L-J Energy Parameter (K): constant: 124

Selenium:  $C_p$  (J/kg-K): polynomial (Figure B-29)

Polynomial Profile

Define:  $C_p$  In Terms Of: Temperature Coefficients: 6

Coefficients

Order	Coefficient
1	215.9
2	0.2511
3	-0.0004406
4	3.562e-07
5	-1.4e-10
6	2.134e-14
7	
8	

OK Cancel Help

Figure B-29. Polynomial Profile for  $C_p$  for  $\text{Se}_2$

Thermal Conductivity (W/m-K): kinetic-theory

Viscosity (kg/m-s): kinetic-theory

Molecular Weight (kg/kgmol): constant: 157.92

Standard State Enthalpy (J/kgmol):const.:1.388e+08

Standard State Entropy (J/kgmol-K): constant: 0

Reference Temperature (K): 298.15

L-J Characteristic Length (angstrom): const.: 3.576

L-J Energy Parameter (K): constant: 1130

Zinc:  $C_p$  (J/kg-K): constant: 317.8774

Thermal Conductivity (W/m-K): kinetic-theory

Viscosity (kg/m-s): kinetic-theory

Molecular Weight (kg/kgmol): constant: 65.39

Standard State Enthalpy (J/kgmol):const.:1.306e+08

Standard State Entropy (J/kgmol-K): constant: 0

Reference Temperature (K): 298.15

L-J Characteristic Length (angstrom): const.: 2.595

L-J Energy Parameter (K): constant: 1329.89

Zinc Selenide: Cp (J/kg-K): polynomial (Figure B-30)

Polynomial Profile

Define: Cp      In Terms Of: Temperature      Coefficients: 6

Coefficients:

1	227.7	2	0.1267	3	-0.0002086	4	1.691e-07
5	-6.661e-11	6	1.018e-14	7		8	

OK      Cancel      Help

Figure B-30. Polynomial Profile for Cp for ZnSe

Thermal Conductivity (W/m-K): kinetic-theory

Viscosity (kg/m-s): kinetic-theory

Molecular Weight (kg/kgmol): constant: 144.35

Standard State Enthalpy (J/kgmol):const.:2.374e+08

Standard State Entropy (J/kgmol-K): constant: 0

Reference Temperature (K): 298.15

L-J Characteristic Length (angstrom): const.: 3.085

L-J Energy Parameter (K): constant: 3454

Quartz: properties shown in Figure B-31.



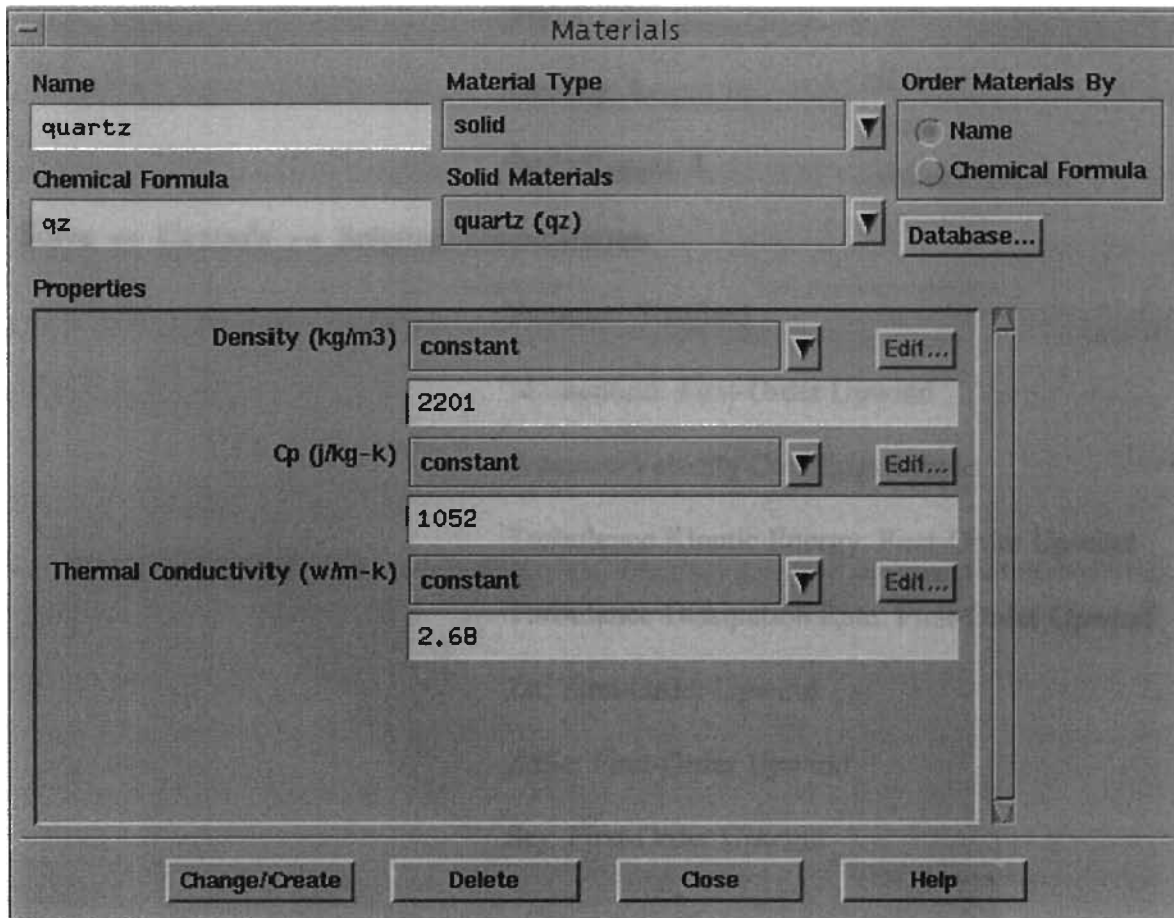


Figure B-31. Quartz Properties Panel

Solve → Controls → Solution: Under Relaxation Factors

Pressure: 0.2

Momentum: 0.5

Energy: 0.8

Turbulence Kinetic Energy: 0.5

Turbulence Dissipation Rate: 0.5

Viscosity: 1

Zn: 1

ZnSc: 1

Se<sub>2</sub>: 1

Density: 1

Body Forces: 1

Solve → Controls → Solution: Discretization

Pressure: Standard

Momentum: First-Order Upwind

Pressure-Velocity Coupling: Simple

Turbulence Kinetic Energy: First-Order Upwind

Turbulence Dissipation Rate: First-Order Upwind

Zn: First-Order Upwind

ZnSe: First-Order Upwind

Se<sub>2</sub>: First-Order Upwind

#### **B.4.5 Initializing and Solving Process**

Before the solution can be obtained, initial values for the solution field must be set.

Following values were used for the purpose of this research:

Solve → Initialize: Gauge Pressure (Pascals): 0.06

X Velocity (m/s): 0.07

Y Velocity (m/s): 0.005

Z Velocity (m/s): 0.002

Temperature (K): 1150

Turbulence Kinetic Energy ( $\text{m}^2/\text{s}^2$ ): 0.004

Turbulence Dissipation Rate ( $\text{m}^2/\text{s}^3$ ): 0.065

Zn Mass Fraction: 0.25

ZnSe Mass Fraction: 0.25

Se<sub>2</sub> Mass Fraction: 0.25

Solve → Monitor (Figure B-32)

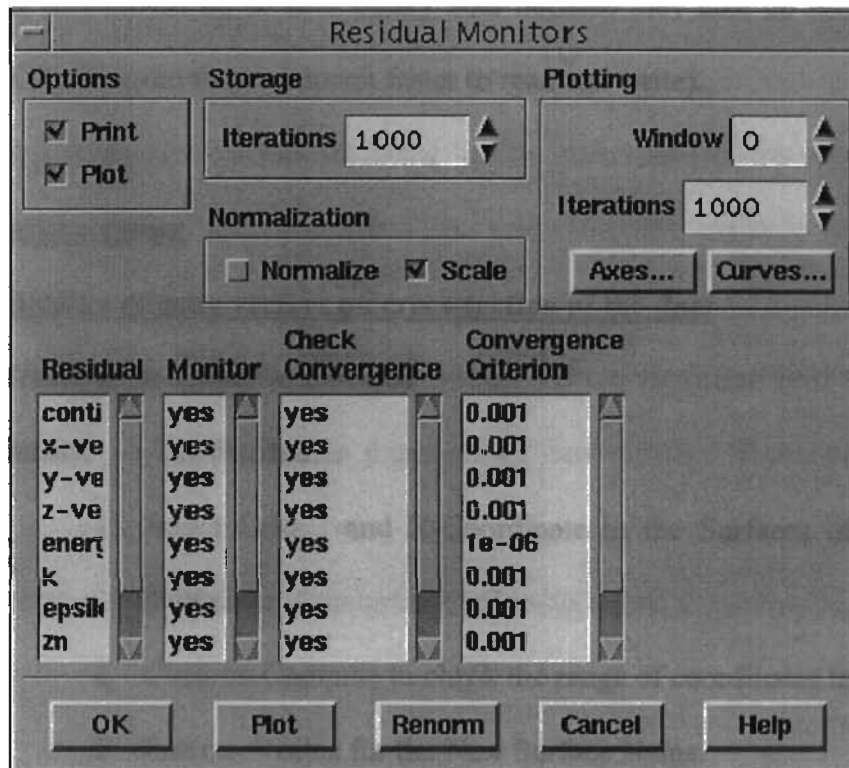


Figure B-32. Residual Monitor Panel

Solve → Iterate; Request the desired number of iterations. (Figure B-33)

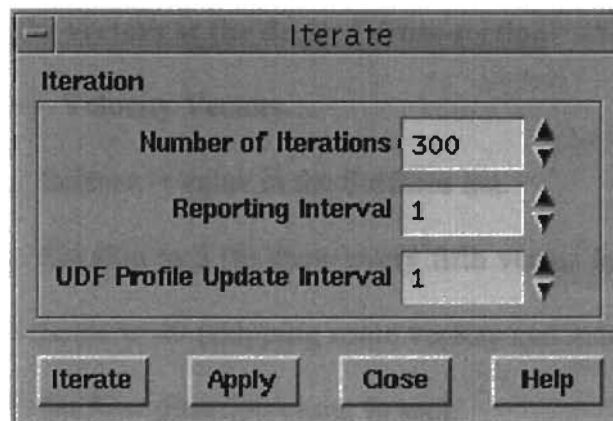


Figure B-33. Iterate Panel

#### **B.4.6 Save the Case and Data Files (run.cas, run.dat)**

File → Write → Case&Data...

Turn on the Write Binary Files option so that a binary file will be written (for 3D problems, one should try to save binary files because they take up less disk space than text (ASCII) files and they are much faster to read and write).

#### **B.4.7 Postprocessing**

##### **B.4.7.1 Display velocity vectors on cross-section of the duct**

Create an isosurface at  $x = \text{value}$

Surface → Iso-Surface...

1. Select Grid... and X-Coordinate in the Surfaces of Constant drop-down list.
2. Click on Compute to check the range of coordinates in the x direction.
3. Enter  $x = \text{value}$  for the New Surface Name.
4. Click on Create to create the new surface.

##### **B.4.7.2 Display the vectors at the desired cross-section**

Display → Velocity Vectors...

1. Select  $x = \text{value}$  in the Surfaces list.
2. Set skip to 5 (to show every fifth vector for example) and change the Scale to 40 (skipping some vectors and increasing their size will make the flow direction easier to see).

3. Click on the Vector Options... button to open Vector Options panel.
4. Enable the In Plane option and select arrow in the Style drop-down list. Click Apply and close the Vector Options panel.
5. Click on the Display button to plot the vectors.

## **B.5 Transport and Physical Properties**

Important part of the modeling is the definition of the physical properties. FLUENT has several built in features that make this task easier to handle. There are several different options to define the properties such as thermal conductivity, viscosity, mass diffusivity, specific heats and densities. When modeling heat transfer, material properties are usually defined as functions of temperature. These properties may be defined as polynomial, piecewise-linear, or piecewise polynomial functions of temperature. Polynomial function has the following form:

$$\phi(T) = A_1 + A_2T + A_3T^2 + \dots \quad (\text{B-1})$$

Piecewise-linear definition of the properties is in the form of:

$$\phi(T) = \phi_n + \frac{\phi_{n+1} - \phi_n}{T_{n+1} - T_n} (T - T_n) \quad (\text{B-2})$$

where  $1 \leq n \leq N$  and  $N$  is the number of segments, while piecewise-polynomial has the following form:

$$\begin{aligned} \text{for } T_{\min,1} < T < T_{\max,1}: \quad \phi(T) &= A_1 + A_2T + A_3T^2 + \dots \\ \text{for } T_{\min,2} < T < T_{\max,2}: \quad \phi(T) &= B_1 + B_2T + B_3T^2 + \dots \end{aligned} \quad (\text{B-3})$$

In three equations mentioned above,  $\phi$  is the physical property being defined. Note that the temperature has to be defined either in degrees Kelvin or degrees Rankine.

Density inputs for materials used were calculated using ideal gas law, which is suggested when pressure variations are small enough that the flow is fully incompressible, but you still want to account for relation between density and temperature. Therefore, density of species was calculated from the following ideal gas law formulation:

$$\rho = \frac{P_{op}}{RT \sum_i \frac{m_i}{M_i}} \quad (\text{B-4})$$

where  $p_{op}$  is 101325 Pa,  $m_i$  is mass fraction of each species and  $M_i$  molecular weight of each species.

Viscosity definition is the start of utilization of FLUENT built in features. The key feature for this modeling process was the application of kinetic theory for property evaluation. Since the ideal gas approach is used, fluid viscosity is defined using kinetic theory as

$$\mu = 2.67 \times 10^{-6} \frac{\sqrt{MT}}{\sigma^2 \Omega_\mu} \quad (\text{B-5})$$

where  $\mu$  is in units of kg/m-s,  $M$  is molecular weight,  $T$  is temperature in Kelvins,  $\sigma$  is characteristic diameter given in meters and  $\Omega_\mu$  is a function of the dimensionless temperature,  $\kappa T/\epsilon$ . In the dimensionless temperature term,  $\kappa$  is the Boltzmann constant and  $\epsilon$  is the characteristic energy of interaction between the molecules (the maximum energy of interaction between a pair of molecules in gas). Note that the viscosity is defined by the same formula via Chapman – Enskog theory (Bird et al., 1960).

The Chapman-Enskog theory relation was used in the work of Foster (1999) and Morrison (1998) to calculate viscosity and then input it in the model using temperature dependent polynomial function.

Parameters  $\sigma$  and  $\epsilon/\kappa$  are known as Lennard-Jones parameters and they are inputs needed to calculate the viscosity using kinetic theory. These parameters were either found in literature or calculated. Values for Lennard-Jones parameters for  $\text{Se}_2$  and Ar were found in the literature. Bird et al. (1960) gives estimate techniques for evaluating these parameters when either the melting point, or boiling point, or critical point is known. When the melting temperature is known, the following relations may be used to evaluate  $\sigma$  and  $\epsilon/\kappa$ :

$$\epsilon/\kappa = 1.92T_m \quad (\text{B-6})$$

$$\sigma = 1.222V_{m,\text{sol}}^{1/3} \quad (\text{B-7})$$

where  $T_m$  is the melting point temperature in Kelvins and  $V_{m,\text{sol}}$  is the molar volume of the solid at the melting point in  $\text{m}^3$ . Using above relationships,  $\epsilon/\kappa$  values were obtained for ZnSe and Zn and  $\sigma$  for Zn. Due to the lack of information available,  $\sigma$  value for ZnSe was estimated as an average of pure species characteristic diameters for Zn and  $\text{Se}_2$  for computational purposes. Their values are shown in Table B-1.

Table B-1. Lennard-Jones Parameters

	Zn	$\text{Se}_2$	ZnSe	Ar
$\sigma$ (Å)	2.594	3.576	3.085	3.418
$\epsilon/\kappa$ (K)	1330	1130	3454	124
Source	calculated	Sha et al., 1995	calculated	Bird et al., 1960

When ideal gas law is used, FLUENT calculates the viscosity of the mixture using kinetic theory (Fluent Inc., 1996b) formulas

$$\mu = \sum_{i'} \frac{X_{i'} \mu_{i'}}{\sum_{i'} X_{i'} \phi_{i'j'}} \quad (\text{B-8})$$

where

$$\phi_{i'j'} = \frac{\left[ 1 + \left( \frac{\mu_{i'}}{\mu_{j'}} \right)^{\frac{1}{2}} \left( \frac{M_{j'}}{M_{i'}} \right)^{\frac{1}{4}} \right]^2}{\left[ 8 \left( 1 + \frac{M_{i'}}{M_{j'}} \right) \right]^{\frac{1}{2}}} \quad (\text{B-9})$$

where  $X_{i'}$  is the mole fraction of species  $i'$ .

Thermal conductivity was also calculated using kinetic theory available in FLUENT. Thermal conductivity was calculated from the following relation:

$$\kappa = \frac{15}{14} \frac{R}{M} \mu \left[ \frac{4}{15} \frac{C_p M}{R} + \frac{1}{3} \right] \quad (\text{B-10})$$

where  $C_p$  is the specific heat,  $\mu$  is viscosity and  $R$  is the universal gas constant. To define a composition-dependent thermal conductivity for mixture, the following equation is evaluated:

$$\kappa = \sum_{i'} \frac{X_{i'} \kappa_{i'}}{\sum_{i'} X_{i'} \phi_{i'j'}} \quad (\text{B-11})$$

where  $\phi_{i'j'}$  is given in Equation B-9.

Diffusion parameters were also calculated using kinetic theory. Bird et al. (1960) gives the relations to calculate Lennard-Jones parameters,  $\sigma_{ij'}$  and  $\varepsilon_{ij'}$ , used for calculating



binary diffusion coefficients as following, same as does built in feature of FLUENT through the use of kinetic theory for binary diffusion coefficients:

$$\sigma_{i,j'} = \frac{1}{2}(\sigma_i + \sigma_{j'}) \quad (\text{B-12})$$

and

$$\varepsilon_{i,j'} = \sqrt{\varepsilon_i \varepsilon_{j'}} \quad (\text{B-13})$$

Based on these values, kinetic theory is used to solve for binary diffusion coefficients using the following relation given in Fluent Inc. (1996b) manual:

$$D_{i,j'} = 0.0188 \frac{\left[ T^3 \left( \frac{1}{M_i} + \frac{1}{M_{j'}} \right) \right]^{\frac{1}{2}}}{p \sigma_{i,j'}^2 \Omega_D} \quad (\text{B-14})$$

where  $p$  was assumed to be 101325 Pa.

Material heat of formation properties are shown in Table B-2. Heat of formation used for modeling purposes of this research were same as the ones used by Foster (1999) in order to facilitate comparison between the two models (2D vs 3D).

Table B-2. Heat of Formation Properties

Species	Molecular Weight	Heat of Formation Foster (1999) (J/kmol)	Heat of Formation Morisson (1998) (J/kmol)	Reference Temperature (K)
Zn(g)	65.39	1.306E+08	1.300E+08	298.15
Se <sub>2</sub> (g)	157.92	1.388E+08	2.271E+08	298.15
ZnSe(g)	144.35	2.374E+08	1.920E+08	298.15
Ar(g)	39.948	0.000E+00	0.000E+00	298.15

Related specific heats  $C_p$  are shown in Table B-3.

Table B-3. Specific Heat Values

Species	Specific Heat (J/kg-K)	Reference	Temperature Range (K)
Zn(g)	317.9	Bailar et al. (1973) Barin et al. (1977)	1180 to 2000
Se <sub>2</sub> (g)	$282.62 - 16.835 \times 10^{-3}T - 15.775 \times 10^{-5}/T^2$	Barin et al. (1977)	298 to 2000
ZnSe(g)	$259.13 + 0.11602 \times 10^{-3}T - 7.4542 \times 10^{-5}/T^2$	Barin et al. (1977)	298 to 2000
Ar(g)	520.7	Touloukian and Makita (1970)	10 to 6000

### Quartz Properties

Table B-4. Quartz Properties for FLUENT (Heraeus Amersil, 1986)

Density (kg/m <sup>3</sup> )	2201
Specific Heat (J/kg-K)	1052
Thermal Conductivity (W/m-K)	2.68

Table B-5. Thermochemical Data for  $\text{Se}_2(\text{g}) + 2\text{Zn}(\text{g}) = 2\text{ZnSe}(\text{g})$   
(Outokumpu Research Oy, 1997)

Se2(g) + 2Zn(g) = 2ZnSe(g)					
T	deltaH	deltaS	deltaG	K	
C	kcal	cal	kcal		
0.000	18.094	-16.209	22.522	9.523E-19	
100.000	17.850	-16.970	24.183	6.845E-15	
200.000	17.609	-17.542	25.909	1.075E-12	
300.000	17.373	-17.995	27.687	2.765E-11	
400.000	17.143	-18.366	29.506	2.629E-10	
500.000	16.918	-18.677	31.358	1.365E-09	
600.000	16.699	-18.943	33.239	4.781E-09	
700.000	16.487	-19.173	35.145	1.278E-08	
800.000	16.281	-19.375	37.073	2.814E-08	
900.000	16.081	-19.553	39.020	5.374E-08	
1000.000	15.887	-19.712	40.983	9.210E-08	
1100.000	15.700	-19.853	42.961	1.451E-07	
1200.000	15.519	-19.980	44.953	2.140E-07	
1300.000	15.345	-20.095	46.957	2.992E-07	
1400.000	15.177	-20.199	48.972	4.006E-07	
1500.000	15.015	-20.292	50.996	5.175E-07	
1600.000	14.860	-20.378	53.030	6.489E-07	
1700.000	14.711	-20.455	55.072	7.937E-07	
1800.000	14.568	-20.526	57.121	9.509E-07	
1900.000	14.432	-20.590	59.177	1.117E-06	
2000.000	14.302	-20.648	61.239	1.294E-06	
Se2(g)		Extrapolated from		2000.000 K	
Zn(g)		Extrapolated from		2000.000 K	
ZnSe(g)		Extrapolated from		2000.000 K	
Formula	FM	Conc.	Amount	Amount	Volume
	g/mol	wt-%	mol	g	l or ml
Se2(g)	157.92	54.704	1	157.92	22.414 l
Zn(g)	65.38	45.296	2	130.76	44.827 l
	g/mol	wt-%	mol	g	l or ml
ZnSe(g)	144.34	100	2	288.68	44.827 l

## **APPENDIX C**

### **RUN DATA**

This Appendix contains description of the two experimental runs used for the study of computational solution. BA 97202 (baseline) and BA 97195 are the data acquired during the experimental study of the system at Eagle-Picher Inc.

Following the description of these two cases, data compiled and used for computational analysis described in Chapter V is documented.

Table C-1. Case BA 97202 Process Characteristics

Experiment Description				
Run Date	Experiment No./ Run No.	Product Lot No.	Amount of Product Collected (kg)	Yield (%)
7/21/97	7/4	BA97202	0.7473	63.10%

Reactor Zone Temperature Data					
Reactor Zone 1 Control Set Temperature (K)	Reactor Zone 1 Actual Temperature (K)	Reactor Zone 2 Control Set Temperature (K)	Reactor Zone 2 Actual Temperature (K)	Reactor Zone 3 Control Set Temperature (K)	Reactor Zone 3 Actual Temperature (K)
1248.15	1273.15	1248.15	1260.15	1198.15	1223.15

Ar Inlet Properties			
Inlet Temperature (K)	Volumetric Flow Rate (m <sup>3</sup> /s)	Mass Flow Rate (kg/s)	Molar Flow Rate (kmol/s)
298.15	5.0574E-06	8.2583E-06	2.0673E-07

Zn Inlet Properties			
Inlet Temperature (K)	Loading (kg)	Mass Flow Rate (kg/s)	Molar Flow Rate (kmol/s)
1229.15	0.5000	3.7037E-05	5.6640E-07

Combined Zn-Ar Inlet Properties					
Combined Temperature (K)	Ar Volumetric Flow Rate (m <sup>3</sup> /s)	Zn Volumetric Flow Rate (m <sup>3</sup> /s)	Combined Volumetric Flow Rate (m <sup>3</sup> /s)	Ar Mass Fraction	Zn Mass Fraction
1229.15	2.0850E-05	5.7125E-05	7.7974E-05	0.1823	0.8177

Ar Density (kg/m <sup>3</sup> )	Zn Density (kg/m <sup>3</sup> )	Cross Sectional Area (m <sup>2</sup> )	Inlet Diameter (m)
0.3961	0.6484	4.1548E-04	0.023

Ar Inlet Properties			
Inlet Temperature (K)	Volumetric Flow Rate (m <sup>3</sup> /s)	Mass Flow Rate (kg/s)	Molar Flow Rate (kmol/s)
298.15	5.0868E-06	8.3063E-06	2.0793E-07

Se Inlet Properties			
Inlet Temperature (K)	Loading (kg)	Mass Flow Rate (kg/s)	Molar Flow Rate (kmol/s)
997.15	0.6847	5.0719E-05	3.2117E-07

Combined Se-Ar Inlet Properties					
Combined Temperature (K)	Ar Volumetric Flow Rate (m <sup>3</sup> /s)	Zn Volumetric Flow Rate (m <sup>3</sup> /s)	Combined Volumetric Flow Rate (m <sup>3</sup> /s)	Ar Mass Fraction	Se <sub>2</sub> Mass Fraction
997.15	1.7013E-05	2.6277E-05	4.3290E-05	0.1407	0.8593

Ar Density (kg/m <sup>3</sup> )	Se <sub>2</sub> Density (kg/m <sup>3</sup> )	Cross Sectional Area (m <sup>2</sup> )	Inlet Diameter (m)
0.4882	1.9301	4.1548E-04	0.023

Table C-2. Case BA 97195 Process Characteristics

Experiment Description				
Run Date	Experiment No./ Run No.	Product Lot No.	Amount of Product Collected (kg)	Yield (%)
7/14/97	4/5	BA97202	0.6747	56.90%

Reactor Zone Temperature Data					
Reactor Zone 1 Control Set Temperature (K)	Reactor Zone 1 Actual Temperature (K)	Reactor Zone 2 Control Set Temperature (K)	Reactor Zone 2 Actual Temperature (K)	Reactor Zone 3 Control Set Temperature (K)	Reactor Zone 3 Actual Temperature (K)
1348.15	1373.15	1348.15	1360.15	1198.15	1313.15

Ar Inlet Properties			
Inlet Temperature (K)	Volumetric Flow Rate (m <sup>3</sup> /s)	Mass Flow Rate (kg/s)	Molar Flow Rate (kmol/s)
298.15	3.6447E-06	5.9514E-06	1.4898E-07

Zn Inlet Properties			
Inlet Temperature (K)	Loading (kg)	Mass Flow Rate (kg/s)	Molar Flow Rate (kmol/s)
1223.15	0.5007	4.6361E-05	7.0899E-07

Combined Zn-Ar Inlet Properties					
Combined Temperature (K)	Ar Volumetric Flow Rate (m <sup>3</sup> /s)	Zn Volumetric Flow Rate (m <sup>3</sup> /s)	Combined Volumetric Flow Rate (m <sup>3</sup> /s)	Ar Mass Fraction	Zn Mass Fraction
1223.15	1.4952E-05	7.1157E-05	8.6109E-05	0.1138	0.8862

Ar Density (kg/m <sup>3</sup> )	Zn Density (kg/m <sup>3</sup> )	Cross Sectional Area (m <sup>2</sup> )	Inlet Diameter (m)
0.398	0.6515	4.1548E-04	0.023

Ar Inlet Properties			
Inlet Temperature (K)	Volumetric Flow Rate (m <sup>3</sup> /s)	Mass Flow Rate (kg/s)	Molar Flow Rate (kmol/s)
298.15	3.7494E-06	6.1225E-06	1.5326E-07

Se Inlet Properties			
Inlet Temperature (K)	Loading (kg)	Mass Flow Rate (kg/s)	Molar Flow Rate (kmol/s)
991.15	0.6845	6.3380E-05	4.0134E-07

Combined Se-Ar Inlet Properties					
Combined Temperature (K)	Ar Volumetric Flow Rate (m <sup>3</sup> /s)	Zn Volumetric Flow Rate (m <sup>3</sup> /s)	Combined Volumetric Flow Rate (m <sup>3</sup> /s)	Ar Mass Fraction	Se <sub>2</sub> Mass Fraction
991.15	1.2464E-05	3.2640E-05	4.5104E-05	0.0881	0.9119

Ar Density (kg/m <sup>3</sup> )	Se <sub>2</sub> Density (kg/m <sup>3</sup> )	Cross Sectional Area (m <sup>2</sup> )	Inlet Diameter (m)
0.4882	1.9301	4.1548E-04	0.023

Table C-3. Computational Study Data

RUN	Description	Zn Inlet Properties								
		Reactor Zone 1 Temperature (K)	Reactor Zone 2 Temperature (K)	Reactor Zone 3 Temperature (K)	Zn Inlet Temperature (K)	Zn Mass Flow Rate (kg/s)	Ar Mass Flow Rate (kg/s)	Total Mass Flow Rate Zn Inlet (kg/s)	Zn Mass Fraction	Zn Inlet Velocity (m/s)
1	BA97202 (laminar effects only, pef 5000)	1273.15	1260.15	1223.15	1229.15	3.7037E-05	8.2583E-06	4.5295E-05	0.8177	0.18767
2	BA97202 (gravity effects excluded, pef 5000)	1273.15	1260.15	1223.15	1229.15	3.7037E-05	8.2583E-06	4.5295E-05	0.8177	0.18767
3	BA97202 (preexponential factor of 1000)	1273.15	1260.15	1223.15	1229.15	3.7037E-05	8.2583E-06	4.5295E-05	0.8177	0.18767
4	BA97202 (preexponential factor of 2500)	1273.15	1260.15	1223.15	1229.15	3.7037E-05	8.2583E-06	4.5295E-05	0.8177	0.18767
5	BA97202 (preexponential factor of 5000)	1273.15	1260.15	1223.15	1229.15	3.7037E-05	8.2583E-06	4.5295E-05	0.8177	0.18767
6	BA97202 (preexponential factor of 10000)	1273.15	1260.15	1223.15	1229.15	3.7037E-05	8.2583E-06	4.5295E-05	0.8177	0.18767
7	BA97202 (preexponential factor of 20000)	1273.15	1260.15	1223.15	1229.15	3.7037E-05	8.2583E-06	4.5295E-05	0.8177	0.18767
8	BA97202 (preexponential factor of 37500)	1273.15	1260.15	1223.15	1229.15	3.7037E-05	8.2583E-06	4.5295E-05	0.8177	0.18767
9	BA97202 (preexponential factor of 100000)	1273.15	1263.15	1223.15	1229.15	3.7037E-05	8.2583E-06	4.5295E-05	0.8177	0.18767
10	BA97195 (preexponential factor of 1000)	1373.15	1368.15	1293.15	1223.15	4.6361E-05	5.9514E-06	5.2312E-05	0.8862	0.20725
11	BA97195 (preexponential factor of 2500)	1373.15	1368.15	1293.15	1223.15	4.6361E-05	5.9514E-06	5.2312E-05	0.8862	0.20725
12	BA97195 (preexponential factor of 5000)	1373.15	1368.15	1293.15	1223.15	4.6361E-05	5.9514E-06	5.2312E-05	0.8862	0.20725
13	BA97195 (preexponential factor of 10000)	1373.15	1368.15	1293.15	1223.15	4.6361E-05	5.9514E-06	5.2312E-05	0.8862	0.20725
14	BA97195 (preexponential factor of 20000)	1373.15	1368.15	1293.15	1223.15	4.6361E-05	5.9514E-06	5.2312E-05	0.8862	0.20725
15	BA97195 (preexponential factor of 37500)	1373.15	1368.15	1293.15	1223.15	4.6361E-05	5.9514E-06	5.2312E-05	0.8862	0.20725
16	BA97195 (preexponential factor of 100000)	1373.15	1368.15	1293.15	1223.15	4.6361E-05	5.9514E-06	5.2312E-05	0.8862	0.20725
17	Low Temperature-Zone 2 (preexponential factor of 1000)	1273.15	1200.15	1223.15	1229.15	3.7037E-05	8.2583E-06	4.5295E-05	0.8177	0.18767
18	Low Temperature-Zone 2 (preexponential factor of 2500)	1273.15	1200.15	1223.15	1229.15	3.7037E-05	8.2583E-06	4.5295E-05	0.8177	0.18767
19	Low Temperature-Zone 2 (preexponential factor of 5000)	1273.15	1200.15	1223.15	1229.15	3.7037E-05	8.2583E-06	4.5295E-05	0.8177	0.18767
20	Low Temperature-Zone 2 (preexponential factor of 10000)	1273.15	1200.15	1223.15	1229.15	3.7037E-05	8.2583E-06	4.5295E-05	0.8177	0.18767
21	Low Temperature-Zone 2 (preexponential factor of 20000)	1273.15	1200.15	1223.15	1229.15	3.7037E-05	8.2583E-06	4.5295E-05	0.8177	0.18767
22	Low Temperature-Zone 2 (preexponential factor of 37500)	1273.15	1200.15	1223.15	1229.15	3.7037E-05	8.2583E-06	4.5295E-05	0.8177	0.18767
23	Low Temperature-Zone 2 (preexponential factor of 100000)	1273.15	1200.15	1223.15	1229.15	3.7037E-05	8.2583E-06	4.5295E-05	0.8177	0.18767
24	High Temperature-Zone 2 (preexponential factor of 1000)	1273.15	1320.15	1223.15	1229.15	3.7037E-05	8.2583E-06	4.5295E-05	0.8177	0.18767
25	High Temperature-Zone 2 (preexponential factor of 2500)	1273.15	1320.15	1223.15	1229.15	3.7037E-05	8.2583E-06	4.5295E-05	0.8177	0.18767
26	High Temperature-Zone 2 (preexponential factor of 5000)	1273.15	1320.15	1223.15	1229.15	3.7037E-05	8.2583E-06	4.5295E-05	0.8177	0.18767
27	High Temperature-Zone 2 (preexponential factor of 10000)	1273.15	1320.15	1223.15	1229.15	3.7037E-05	8.2583E-06	4.5295E-05	0.8177	0.18767
28	High Temperature-Zone 2 (preexponential factor of 20000)	1273.15	1320.15	1223.15	1229.15	3.7037E-05	8.2583E-06	4.5295E-05	0.8177	0.18767
29	High Temperature-Zone 2 (preexponential factor of 37500)	1273.15	1320.15	1223.15	1229.15	3.7037E-05	8.2583E-06	4.5295E-05	0.8177	0.18767
30	High Temperature-Zone 2 (preexponential factor of 100000)	1273.15	1320.15	1223.15	1229.15	3.7037E-05	8.2583E-06	4.5295E-05	0.8177	0.18767

RUN	Se <sub>2</sub> Inlet Properties						Mass Flow Rate Ratio	FLUENT Zn Outflow Concentration (kg/m <sup>3</sup> )	FLUENT Se <sub>2</sub> Outflow Concentration (kg/m <sup>3</sup> )	FLUENT ZnSe Outflow Concentration (kg/m <sup>3</sup> )	Yield (%)
	Se <sub>2</sub> Inlet Temperature (K)	Se <sub>2</sub> Mass Flow Rate (kg/s)	Ar Mass Flow Rate (kg/s)	Total Mass Flow Rate Se <sub>2</sub> Inlet (kg/s)	Se <sub>2</sub> Mass Fraction	Se <sub>2</sub> Inlet Velocity (m/s)					
1	997.15	5.0719E-05	8.3063E-06	5.9025E-05	0.8593	0.10419	0.7674	0.11875	0.17575	0.44412	60.13
2	997.15	5.0719E-05	8.3063E-06	5.9025E-05	0.8593	0.10419	0.7674	0.19000	0.11717	0.40554	56.90
3	997.15	5.0719E-05	8.3063E-06	5.9025E-05	0.8593	0.10419	0.7674	0.29291	0.22958	0.16617	24.13
4	997.15	5.0719E-05	8.3063E-06	5.9025E-05	0.8593	0.10419	0.7674	0.17416	0.22455	0.70422	44.74
5	997.15	5.0719E-05	8.3063E-06	5.9025E-05	0.8593	0.10419	0.7674	0.17575	0.11875	0.45532	60.72
6	997.15	5.0719E-05	8.3063E-06	5.9025E-05	0.8593	0.10419	0.7674	0.07125	0.11717	0.56231	74.90
7	997.15	5.0719E-05	8.3063E-06	5.9025E-05	0.8593	0.10419	0.7674	0.02375	0.05858	0.70422	89.53
8	997.15	5.0719E-05	8.3063E-06	5.9025E-05	0.8593	0.10419	0.7674	0.01021	0.03499	0.77325	94.84
9	997.15	5.0719E-05	8.3063E-06	5.9025E-05	0.8593	0.10419	0.7674	0.00000	0.01953	0.81306	97.65
10	997.15	6.3380E-05	6.1225E-06	6.9503E-05	0.9119	0.10856	0.7527	0.22856	0.28089	0.25136	33.04
11	997.15	6.3380E-05	6.1225E-06	6.9503E-05	0.9119	1.10856	0.7527	0.16134	0.21067	0.44474	54.45
12	997.15	6.3380E-05	6.1225E-06	6.9503E-05	0.9119	2.10856	0.7527	0.10352	0.14044	0.59484	70.92
13	997.15	6.3380E-05	6.1225E-06	6.9503E-05	0.9119	3.10856	0.7527	0.05378	0.07022	0.70643	85.07
14	997.15	6.3380E-05	6.1225E-06	6.9503E-05	0.9119	4.10856	0.7527	0.02689	0.03511	0.72420	92.11
15	997.15	6.3380E-05	6.1225E-06	6.9503E-05	0.9119	5.10856	0.7527	0.00000	0.03511	0.78353	95.71
16	997.15	6.3380E-05	6.1225E-06	6.9503E-05	0.9119	6.10856	0.7527	0.00000	0.00000	0.91550	100.00
17	997.15	5.0719E-05	8.3063E-06	5.9025E-05	0.8593	0.10419	0.7674	0.24176	0.29291	0.17906	23.02
18	997.15	5.0719E-05	8.3063E-06	5.9025E-05	0.8593	0.10419	0.7674	0.17814	0.21676	0.34627	42.58
19	997.15	5.0719E-05	8.3063E-06	5.9025E-05	0.8593	0.10419	0.7674	0.12724	0.14939	0.48487	59.85
20	997.15	5.0719E-05	8.3063E-06	5.9025E-05	0.8593	0.10419	0.7674	0.08907	0.09080	0.62251	74.42
21	997.15	5.0719E-05	8.3063E-06	5.9025E-05	0.8593	0.10419	0.7674	0.04835	0.05858	0.72641	87.30
22	997.15	5.0719E-05	8.3063E-06	5.9025E-05	0.8593	0.10419	0.7674	0.02163	0.02929	0.73018	96.92
23	997.15	5.0719E-05	8.3063E-06	5.9025E-05	0.8593	0.10419	0.7674	0.00000	0.00000	0.85828	100.00
24	997.15	5.0719E-05	8.3063E-06	5.9025E-05	0.8593	0.10419	0.7674	0.23037	0.26671	0.15149	25.21
25	997.15	5.0719E-05	8.3063E-06	5.9025E-05	0.8593	0.10419	0.7674	0.17812	0.19470	0.29192	48.70
26	997.15	5.0719E-05	8.3063E-06	5.9025E-05	0.8593	0.10419	0.7674	0.13775	0.13336	0.42687	67.24
27	997.15	5.0719E-05	8.3063E-06	5.9025E-05	0.8593	0.10419	0.7674	0.09381	0.08001	0.55624	79.47
28	997.15	5.0719E-05	8.3063E-06	5.9025E-05	0.8593	0.10419	0.7674	0.05462	0.03734	0.65346	91.50
29	997.15	5.0719E-05	8.3063E-06	5.9025E-05	0.8593	0.10419	0.7674	0.03562	0.00000	0.70380	98.00
30	997.15	5.0719E-05	8.3063E-06	5.9025E-05	0.8593	0.10419	0.7674	0.01187	0.00000	0.75569	100.00



RUN	Description	Reactor Zone 1 Temperature (K)	Reactor Zone 2 Temperature (K)	Reactor Zone 3 Temperature (K)	Zn Inlet Properties					
					Zn Inlet Temperature (K)	Zn Mass Flow Rate (kg/s)	Ar Mass Flow Rate (kg/s)	Total Mass Flow Rate Zn Inlet (kg/s)	Zn Mass Fraction	Zn Inlet Velocity (m/s)
31	Argon Zn Inlet -25% (preexponential factor of 2500)	1273.15	1260.15	1223.15	1229.15	3.7037E-05	6.1937E-06	4.3231E-05	0.8567	0.17513
32	Argon Zn Inlet -25% (preexponential factor of 5000)	1273.15	1260.15	1223.15	1229.15	3.7037E-05	6.1937E-06	4.3231E-05	0.8567	0.17513
33	Argon Zn Inlet -25% (preexponential factor of 10000)	1273.15	1260.15	1223.15	1229.15	3.7037E-05	6.1937E-06	4.3231E-05	0.8567	0.17513
34	Argon Zn Inlet -25% (preexponential factor of 20000)	1273.15	1260.15	1223.15	1229.15	3.7037E-05	6.1937E-06	4.3231E-05	0.8567	0.17513
35	Argon Zn Inlet -25% (preexponential factor of 37500)	1273.15	1260.15	1223.15	1229.15	3.7037E-05	6.1937E-06	4.3231E-05	0.8567	0.17513
36	Argon Zn Inlet -25% (preexponential factor of 100000)	1273.15	1260.15	1223.15	1229.15	3.7037E-05	6.1937E-06	4.3231E-05	0.8567	0.17513
37	Argon Zn Inlet +25% (preexponential factor of 1000)	1273.15	1260.15	1223.15	1229.15	3.7037E-05	1.0323E-05	4.7360E-05	0.7820	0.20022
38	Argon Zn Inlet +25% (preexponential factor of 2500)	1273.15	1260.15	1223.15	1229.15	3.7037E-05	1.0323E-05	4.7360E-05	0.7820	0.20022
39	Argon Zn Inlet +25% (preexponential factor of 5000)	1273.15	1260.15	1223.15	1229.15	3.7037E-05	1.0323E-05	4.7360E-05	0.7820	0.20022
40	Argon Zn Inlet +25% (preexponential factor of 10000)	1273.15	1260.15	1223.15	1229.15	3.7037E-05	1.0323E-05	4.7360E-05	0.7820	0.20022
41	Argon Zn Inlet +25% (preexponential factor of 20000)	1273.15	1260.15	1223.15	1229.15	3.7037E-05	1.0323E-05	4.7360E-05	0.7820	0.20022
42	Argon Zn Inlet +25% (preexponential factor of 37500)	1273.15	1260.15	1223.15	1229.15	3.7037E-05	1.0323E-05	4.7360E-05	0.7820	0.20022
43	Argon Zn Inlet +25% (preexponential factor of 100000)	1273.15	1260.15	1223.15	1229.15	3.7037E-05	1.0323E-05	4.7360E-05	0.7820	0.20022
44	Argon Se <sub>2</sub> Inlet -25% (preexponential factor of 1000)	1273.15	1260.15	1223.15	1229.15	3.7037E-05	8.2583E-06	4.5295E-05	0.8177	0.18767
45	Argon Se <sub>2</sub> Inlet -25% (preexponential factor of 2500)	1273.15	1260.15	1223.15	1229.15	3.7037E-05	8.2583E-06	4.5295E-05	0.8177	0.18767
46	Argon Se <sub>2</sub> Inlet -25% (preexponential factor of 5000)	1273.15	1260.15	1223.15	1229.15	3.7037E-05	8.2583E-06	4.5295E-05	0.8177	0.18767
47	Argon Se <sub>2</sub> Inlet -25% (preexponential factor of 10000)	1273.15	1260.15	1223.15	1229.15	3.7037E-05	8.2583E-06	4.5295E-05	0.8177	0.18767
48	Argon Se <sub>2</sub> Inlet -25% (preexponential factor of 20000)	1273.15	1260.15	1223.15	1229.15	3.7037E-05	8.2583E-06	4.5295E-05	0.8177	0.18767
49	Argon Se <sub>2</sub> Inlet -25% (preexponential factor of 37500)	1273.15	1260.15	1223.15	1229.15	3.7037E-05	8.2583E-06	4.5295E-05	0.8177	0.18767
50	Argon Se <sub>2</sub> Inlet -25% (preexponential factor of 100000)	1273.15	1260.15	1223.15	1229.15	3.7037E-05	8.2583E-06	4.5295E-05	0.8177	0.18767
51	Argon Se <sub>2</sub> Inlet +25% (preexponential factor of 1000)	1273.15	1260.15	1223.15	1229.15	3.7037E-05	8.2583E-06	4.5295E-05	0.8177	0.18767
52	Argon Se <sub>2</sub> Inlet +25% (preexponential factor of 2500)	1273.15	1260.15	1223.15	1229.15	3.7037E-05	8.2583E-06	4.5295E-05	0.8177	0.18767
53	Argon Se <sub>2</sub> Inlet +25% (preexponential factor of 5000)	1273.15	1260.15	1223.15	1229.15	3.7037E-05	8.2583E-06	4.5295E-05	0.8177	0.18767
54	Argon Se <sub>2</sub> Inlet +25% (preexponential factor of 10000)	1273.15	1260.15	1223.15	1229.15	3.7037E-05	8.2583E-06	4.5295E-05	0.8177	0.18767
55	Argon Se <sub>2</sub> Inlet +25% (preexponential factor of 20000)	1273.15	1260.15	1223.15	1229.15	3.7037E-05	8.2583E-06	4.5295E-05	0.8177	0.18767
56	Argon Se <sub>2</sub> Inlet +25% (preexponential factor of 37500)	1273.15	1260.15	1223.15	1229.15	3.7037E-05	8.2583E-06	4.5295E-05	0.8177	0.18767
57	Argon Se <sub>2</sub> Inlet +25% (preexponential factor of 100000)	1273.15	1260.15	1223.15	1229.15	3.7037E-05	8.2583E-06	4.5295E-05	0.8177	0.18767
58	Stoichiometric (preexponential factor of 1000)	1273.15	1260.15	1223.15	1229.15	4.2040E-05	8.3063E-06	5.0346E-05	0.8350	0.20887
59	Stoichiometric (preexponential factor of 2500)	1273.15	1260.15	1223.15	1229.15	4.2040E-05	8.3063E-06	5.0346E-05	0.8350	0.20887
60	Stoichiometric (preexponential factor of 5000)	1273.15	1260.15	1223.15	1229.15	4.2040E-05	8.3063E-06	5.0346E-05	0.8350	0.20887
61	Stoichiometric (preexponential factor of 10000)	1273.15	1260.15	1223.15	1229.15	4.2040E-05	8.3063E-06	5.0346E-05	0.8350	0.20887
62	Stoichiometric (preexponential factor of 20000)	1273.15	1260.15	1223.15	1229.15	4.2040E-05	8.3063E-06	5.0346E-05	0.8350	0.20887
63	Stoichiometric (preexponential factor of 37500)	1273.15	1260.15	1223.15	1229.15	4.2040E-05	8.3063E-06	5.0346E-05	0.8350	0.20887
64	Stoichiometric (preexponential factor of 100000)	1273.15	1260.15	1223.15	1229.15	4.2040E-05	8.3063E-06	5.0346E-05	0.8350	0.20887

Se <sub>2</sub> Inlet Properties											
RUN	Se <sub>2</sub> Inlet Temperature (K)	Se <sub>2</sub> Mass Flow Rate (kg/s)	Ar Mass Flow Rate (kg/s)	Total Mass Flow Rate Se <sub>2</sub> Inlet (kg/s)	Se <sub>2</sub> Mass Fraction	Se <sub>2</sub> Inlet Velocity (m/s)	Mass Flow Rate Ratio	FLUENT Zn Outflow Concentration (kg/m <sup>3</sup> )	FLUENT Se <sub>2</sub> Outflow Concentration (kg/m <sup>3</sup> )	FLUENT ZnSe Outflow Concentration (kg/m <sup>3</sup> )	Yield (%)
31	997.15	5.0719E-05	8.3063E-06	5.9025E-05	0.8593	0.10419	0.7324	0.17814	0.21676	0.34627	46.72
32	997.15	5.0719E-05	8.3063E-06	5.9025E-05	0.8593	0.10419	0.7324	0.12724	0.14939	0.48487	63.67
33	997.15	5.0719E-05	8.3063E-06	5.9025E-05	0.8593	0.10419	0.7324	0.08907	0.09080	0.62251	77.58
34	997.15	5.0719E-05	8.3063E-06	5.9025E-05	0.8593	0.10419	0.7324	0.04835	0.05858	0.72641	87.17
35	997.15	5.0719E-05	8.3063E-06	5.9025E-05	0.8593	0.10419	0.7324	0.02163	0.02929	0.73018	93.48
36	997.15	5.0719E-05	8.3063E-06	5.9025E-05	0.8593	0.10419	0.7324	0.00000	0.00000	0.85828	100.00
37	997.15	5.0719E-05	8.3063E-06	5.9025E-05	0.8593	0.10419	0.8024	0.22259	0.28852	0.15069	22.77
38	997.15	5.0719E-05	8.3063E-06	5.9025E-05	0.8593	0.10419	0.8024	0.16694	0.21090	0.28813	43.26
39	997.15	5.0719E-05	8.3063E-06	5.9025E-05	0.8593	0.10419	0.8024	0.12243	0.16696	0.42549	59.52
40	997.15	5.0719E-05	8.3063E-06	5.9025E-05	0.8593	0.10419	0.8024	0.07791	0.11717	0.55129	73.86
41	997.15	5.0719E-05	8.3063E-06	5.9025E-05	0.8593	0.10419	0.8024	0.04174	0.05858	0.65618	86.74
42	997.15	5.0719E-05	8.3063E-06	5.9025E-05	0.8593	0.10419	0.8024	0.01503	0.02929	0.71827	94.19
43	997.15	5.0719E-05	8.3063E-06	5.9025E-05	0.8593	0.10419	0.8024	0.00000	0.00000	0.77031	100.00
44	997.15	5.0719E-05	6.2297E-06	5.6949E-05	0.8906	0.093956	0.7954	0.23037	0.32479	0.18372	24.86
45	997.15	5.0719E-05	6.2297E-06	5.6949E-05	0.8906	0.093956	0.7954	0.16625	0.25983	0.34315	44.61
46	997.15	5.0719E-05	6.2297E-06	5.6949E-05	0.8906	0.093956	0.7954	0.10984	0.18488	0.49612	61.95
47	997.15	5.0719E-05	6.2297E-06	5.6949E-05	0.8906	0.093956	0.7954	0.05819	0.12992	0.63683	77.20
48	997.15	5.0719E-05	6.2297E-06	5.6949E-05	0.8906	0.093956	0.7954	0.02375	0.09744	0.74098	85.94
49	997.15	5.0719E-05	6.2297E-06	5.6949E-05	0.8906	0.093956	0.7954	0.00000	0.06496	0.79917	92.48
50	997.15	5.0719E-05	6.2297E-06	5.6949E-05	0.8906	0.093956	0.7954	0.00000	0.06496	0.82920	92.74
51	997.15	5.0719E-05	1.0383E-05	6.1102E-05	0.8301	0.11443	0.7413	0.23037	0.26671	0.15149	23.36
52	997.15	5.0719E-05	1.0383E-05	6.1102E-05	0.8301	0.11443	0.7413	0.17812	0.19470	0.29192	43.91
53	997.15	5.0719E-05	1.0383E-05	6.1102E-05	0.8301	0.11443	0.7413	0.13775	0.13336	0.42687	61.16
54	997.15	5.0719E-05	1.0383E-05	6.1102E-05	0.8301	0.11443	0.7413	0.09381	0.08001	0.55624	76.19
55	997.15	5.0719E-05	1.0383E-05	6.1102E-05	0.8301	0.11443	0.7413	0.05462	0.03734	0.65346	87.66
56	997.15	5.0719E-05	1.0383E-05	6.1102E-05	0.8301	0.11443	0.7413	0.03562	0.00000	0.70360	95.18
57	997.15	5.0719E-05	1.0383E-05	6.1102E-05	0.8301	0.11443	0.7413	0.01187	0.00000	0.75569	98.45
58	997.15	5.0719E-05	8.3063E-06	5.9025E-05	0.8593	0.10419	0.8530	0.24494	0.26362	0.16849	24.89
59	997.15	5.0719E-05	8.3063E-06	5.9025E-05	0.8593	1.10419	0.8530	0.19105	0.20504	0.31858	44.58
60	997.15	5.0719E-05	8.3063E-06	5.9025E-05	0.8593	2.10419	0.8530	0.14084	0.14646	0.46716	61.92
61	997.15	5.0719E-05	8.3063E-06	5.9025E-05	0.8593	3.10419	0.8530	0.09491	0.08787	0.59560	76.52
62	997.15	5.0719E-05	8.3063E-06	5.9025E-05	0.8593	4.10419	0.8530	0.05685	0.03661	0.69959	88.20
63	997.15	5.0719E-05	8.3063E-06	5.9025E-05	0.8593	5.10419	0.8530	0.03123	0.00000	0.73528	95.93
64	997.15	5.0719E-05	8.3063E-06	5.9025E-05	0.8593	6.10419	0.8530	0.01225	0.00000	0.82727	98.54

## VITA

Zeljko Nikolic

Candidate for the Degree of

Master of Science

Thesis: THREE-DIMENSIONAL ANALYSIS OF A REACTOR FOR THE PRODUCTION OF II-VI MATERIALS USING CFD COMMERCIAL CODE FLUENT

Major Field: Mechanical Engineering

### Biographical:

Personal Data: Born in Pancevo, Yugoslavia, On March 17, 1973, the son of Laza and Gordana Nikolic.

Education: Graduated from Deer Creek-Lamont High School, Lamont, Oklahoma in May 1991; received Bachelor of Science degree in Mechanical Engineering from Oklahoma State University, Stillwater, Oklahoma in May 1997. Completed the requirements for the Master of Science degree with a major in Mechanical Engineering at Oklahoma State University in May 2000.

Experience: Raised on the streets of Pancevo, Yugoslavia; foreign exchange student on a farm in Lamont, Oklahoma in 1990/1991; enjoyed working as a farm and oil field help during summers; employed by Oklahoma State University, Residential Life as a Resident Assistant, 1995 to 1998, employed by Eagle-Picher Inc., Miami, Oklahoma as a Research Assistant, summer 1997; Department of Mechanical Engineering as an undergraduate and graduate Teaching and Research Assistant; 1995 to present.

Professional Membership: American Society of Mechanical Engineers.